Forschungszentrum Jülich

Institut für Schicht- und Ionentechnik

Amorphous Silicon Solar Cells

Comparison of p-i-n and n-i-p Structures with Zinc-Oxide Frontcontact

Stephan Wieder

Jül-3721

Amorphous Silicon Solar Cells

Comparison of p-i-n and n-i-p Structures with Zinc-Oxide Frontcontact

Stephan Wieder

Berichte des Forschungszentrums Jülich ; 3721
ISSN 0944-2952
Institut für Schicht- und Ionentechnik Jül-3721
D82 (Diss. RWTH Aachen, 1999)

Zu beziehen durch: Forschungszentrum Jülich GmbH · Zentralbibliothek
D-52425 Jülich · Bundesrepublik Deutschland
☎ 02461/61-6102 · Telefax: 02461/61-6103 · e-mail: zb-publikation@fz-juelich.de

Vergleich von p-i-n and n-i-p Strukturen mit Zink-Oxid Frontkontakt

Kurzfassung: Diese Arbeit vergleicht die p-i-n und n-i-p Struktur von Solarzellen aus amorphem hydrogenisierten Silizium. In beiden Strukturen wurde gesputtertes Zink-Oxid (ZnO) als transparenter Frontkontakt (TCO) verwendet. Im Rahmen der Arbeit wurden glatte, hochleitfähige ZnO Filme mit hoher Transparenz hergestellt. Mit einem anschließenden naßchemischen Ätzschritt in verdünnter HCl-Lösung wurde die für die Lichteinkopplung notwendige Oberflächentextur erzeugt. In beiden Solarzellenstrukturen bildet sich an der amorph-p/ZnO-Grenzfläche eine Kontaktbarriere aus. Deren negative Auswirkungen auf die elektrischen Eigenschaften der Solarzelle ließen sich in beiden Fällen durch das Einfügen einer hochleitfähigen mikrokristallinen p-Schicht (μc-p) vermeiden, deren Abscheidung sowohl mit RF- wie auch mit VHF-Plasmaanregungsfrequenz gelang. Es ließ sich klar herausarbeiten, daß die ideale p-Schicht für a-Si:H Solarzellen mit ZnO Frontkontakt eine amorph/mikrokristalline Doppel-p-Schicht ist: Durch die μc-p-Schicht läßt sich ein niederohmiger p/TCO Kontakt realisieren, während die amorphe Schicht für eine hohe offenen Klemmenspannung von entscheidender Bedeutung ist. In beiden Strukturen führte die optische Optimierung zu einer hohen spektralen Ausbeute, wobei sich – bedingt durch die Ausführung des Frontkontaktes als Anti-Reflexschicht – ein Vorteil für die n-i-p Struktur im Labor zeigte. Es konnten Literaturberichte bestätigt werden, wonach der Einsatz von Absorbermaterial oberhalb von 200 °C in p-i-n Zellen zu einem Spannungseinbruch führt, während in der n-i-p der Spannungsabfall mit der Abnahme der optischen Bandlücke des Materials korreliert. Der Einsatz der entwickelten Materialien in Solarzellen führte zu einer hocheffizienten a-Si:H/a-Si:H Stapelzelle in der p-i-n Struktur auf einem gesputterten ZnO Substrat mit 9,2 % stabilem Wirkungsgrad nach 900 h Lichtalterung. Die Übertragung der erzielten Resultate in die Modulproduktion wird im Rahmen eines Industrieverbundprojektes verfolgt.

Amorphous Silicon Solar Cells
Comparison of p-i-n and n-i-p Structures with Zinc-Oxide Frontcontact

Abstract: This work compares amorphous silicon solar cells in the p-i-n and n-i-p structure. In both cell structures, sputtered Zinc-Oxide (ZnO) films were established as front contact. We developed smooth TCO films with high conductivity and high transparency. The required surface texture is achieved by a post deposition wet chemical etching step in diluted HCl. In both cell structures, a contact barrier emerges at the amorphous-p/ZnO interface. In both cases, the negative effects of the barrier on the electrical properties of the solar cell are avoided by the application of highly conductive, microcrystalline p-layers (μc-p), which were developed with the RF as well as the VHF deposition technique. We were able to clearly show that the optimum p-layer structure for a-Si:H solar cells with ZnO frontcontact is an amorphous/microcrystalline double-layer: The thin μc-p-layer provides a low-ohmic ZnO/p-contact, while an amorphous phase is essential in order to build up a high open-circuit voltage (V_{OC}). The optical optimization led to high quantum efficiencies in both cell types and showed an advantage of the n-i-p structure in the laboratory caused by the possible antireflection design of the frontcontact in this structure. We confirmed literature reports asserting a drop in the V_{oc} of p-i-n cells when using elevated substrate temperatures during deposition of the i-layer material, while the decrease in V_{oc} for the n-i-p cells simply correlates with the decrease of the band gap of the absorber material. The implementation of the developed materials led to a highly efficient a-Si:H/a-Si:H tandem cell in the p-i-n structure on sputtered ZnO with 9.2 % stable efficiency after 900 h of light soaking. The transfer of the achieved results to module production is performed in an joint venture between research and industry.

Contents

List of Figures

List of Tables

Chapter 1

Introduction

Solar cells offer the possibility of environmentally friendly production of electric energy based on an inexhaustible source – the sun. There is a variety of concepts using monocrystalline, polycrystalline, amorphous and even liquid materials to convert this solar energy. Reviews on the state of the art of the different technologies are given in the proceedings of the international photovoltaic conferences [1–3]. The main factor which prevents solar cells from winning significant market share are still the high cost of the photovoltaic technology. Since they have a big cost reduction potential, thin film solar cells have reached growing attention in the recent years. The main advantages of thin-film technology are the possibility of large-area in-line processing, the use of a variety of cheap substrate materials, the monolithic series connection and the low material and energy consumption during the manufacturing process. Monolithic means that the series connection is an inherent part of the thin film module design in contrast to the external wire bonding used for crystalline or polycrystalline silicon based modules. The by far most developed type of thin film solar cells is based on hydrogenated amorphous silicon(a-Si:H). The raw materials – silicon and hydrogen – are abundant and ecologically harmless. There are a number of companies around the world already producing modules based on a-Si:H or planning to build new or enlarge existing manufacturing plants.

A detailed review treating amorphous silicon solar cell technology is given by Catalano [4]. Only one year after the announcement of the first solar cell based on amorphous silicon by Carlson and Wronski [5] in 1976, Staebler and Wronski reported the light induced degradation of this material [6]. This so-called Staebler-Wronski-effect (SWE) is still not fully understood and results in a deterioration of the electrical properties of the material after prolonged light exposure. This causes the device to stabilize at lower efficiencies than in the initial state – a severe drawback in a-Si:H solar cell technology. Consequently, concepts were developed to improve the stabilized efficiency of the solar cells: material improvement by the use of high hydrogen dilution during the growth of the intrinsic amorphous films led to improved electronic properties of the material in the initial as well as in the light-soaked state [7–10]. Optimized light trapping schemes by means of textured substrates allow the reduction of the absorber thickness, thereby reducing the amount of degradation in the ma-

terial. Moreover, the use of hydrogenated silicon carbon p-layers [11] or microcrystalline p-layers [12] reduce absorption losses, thereby enhancing the short-circuit current-density. Stacked cells (also called: multi junction cell, tandem or triple cell) emerged as a powerful tool to enhance the stabilized efficiency of a-Si:H solar cells [13–16]. They consist of two or more complete single cells deposited on top of each other. In the thin top cell, a high electric field provides efficient extraction of charge carriers, while in the bottom cell less defects are created due to a lower light intensity. Both effects lead to reduced degradation of the device. Moreover, the use of different band gaps in the component cells provides a better utilization of the solar spectrum [17].

The current world record for a small area solar cell based on amorphous hydrogenated silicon and its alloys containing all mentioned techniques is a 13 % stable a-Si:H/a-Si:H/a-SiGe:H triple cell developed by the United Solar System Corporation [18].

More recently, microcrystalline silicon emerged as a promising new material for thin film solar cells as a non-degrading, low band gap absorber material. The preparation of this material is fully compatible with the existing a-Si:H technology. A stable record efficiency as high as 10.7 % for a small area cell is already reported [19].

1.1 p-i-n and n-i-p Structure – Concepts

Solar cells based on a-Si:H are carried out as PIN junctions. As explained in 2.1.1, the intrinsic layer is necessary to allow separation and collection of the photogenerated carriers. The combination of two facts motivates that almost all solar cells based on a-Si:H developed today are illuminated through the p-layer of the device: firstly, according to Beers' law ($I = I_0 \cdot e^{-\alpha d}$) most of the incident light is absorbed in the front of the illuminated layer. Secondly, the mobility of holes in a-Si:H is lower than for the electrons. Consequently, one wants the holes to have the shortest possible way to their recombination junction in order to get efficiently collected. The labeling "p-i-n" (also: "superstrate") and "n-i-p" (also: "substrate") configuration of an amorphous silicon solar cell in this work corresponds to the deposition order only (p = p-doped layer, i = intrinsic layer, n = n-doped layer). As said, in both cases, the light penetrates the solar cell through the p-layer. There is no fundamental difference in the working principle of the two configurations – in fact, the differences are related to a different growth of the thin films on top of each other. A schematic sketch of both structures is shown in figure 1.1.

A p-i-n device is normally prepared on a glass substrate coated with a transparent conductive oxide (TCO), which has to fulfill a couple of requirements: high transparency, high conductivity and suited surface texture to provide an effective light trapping by scattering the incident light and thereby increasing the optical path length. Ideally, the electrical device performance (fill factor and open-circuit voltage) should not be negatively affected. Common commercial TCO substrates do not fulfill all these requirements at the same time. For laboratory use, optimized fluorine doped tin oxide films (SnO_2:F) prepared off-line by

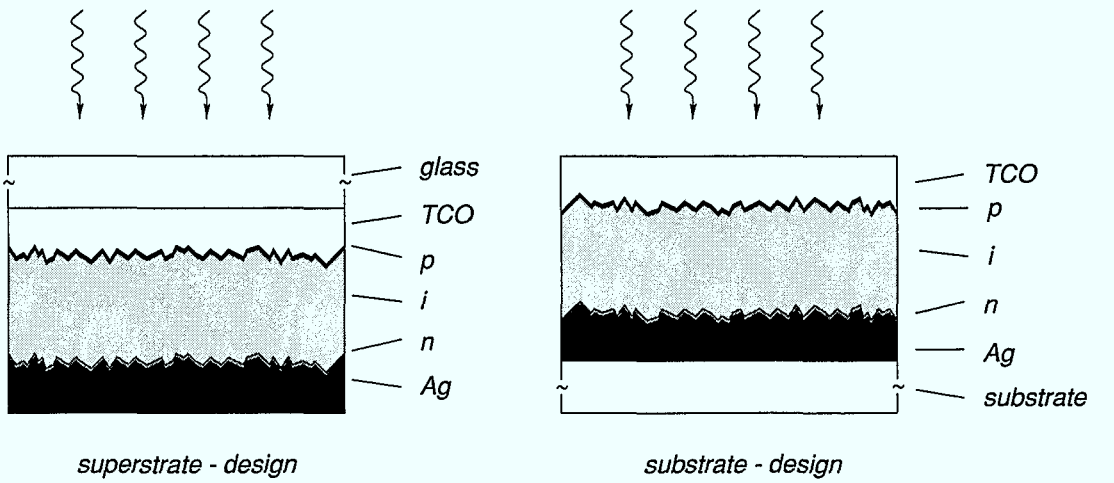

Figure 1.1: *p-i-n and n-i-p structure of a-Si:H based solar cells. In both cases, the device is illuminated from the p-side. The thicknesses are approximately: glass ~1-3 mm, TCO ~ 800 nm, p ~10 nm, i ~400 nm, n ~20 nm, Ag ~800 nm, substrate: arbitrary.*

atmospheric pressure chemical vapor deposition (developed by Asahi glass company [20]) fulfill these requirements to a large extent, and consequently most of the record efficiencies for small area cells or test modules are achieved using this type of substrate. Unfortunately, these optimized TCO coated glass substrates are not yet available on large scale at low costs. The subsequent deposition of the semiconductor layers is commonly done with the plasma enhanced chemical vapor deposition (PECVD) method at moderate temperatures ($\sim 200\,^{\circ}\mathrm{C}$). After the deposition of the solar cell, contacting and encapsulation of the device is performed.

In contrast, a n-i-p device can be deposited on a variety of cheap substrates like glass, aluminium, stainless steel, plastic foil etc. As in the p-i-n case, the back contact is usually provided with ZnO to enhance back reflection of the metal contact. In the n-i-p case, the texture of this metal/ZnO reflector controls the light scattering properties and can be tuned independently of other optical and electrical properties of the film within certain limits. Moreover, the n-i-p configuration is ideally matched to the substrate temperature requirements in a multi-junction device, allowing the fabrication of low band gap bottom cells at high substrate temperatures. The subsequently deposited top cell can be prepared at significant lower substrate temperature leading to higher open-circuit voltages. Next, the front TCO – which can be carried out as an anti reflection layer – is applied. Here, only moderate temperatures are allowed and restrict the variety of deposition techniques and materials, since the underlying n-i-p cell must not be damaged.

1.2 This Work

Up to now, different groups and companies throughout the world have realized amorphous silicon solar cells in the p-i-n as well as the n-i-p structure using a variety of different materials. Although reports are published which discuss the assets or drawbacks of the two structures, so far no comparison of the physical properties of both structures based on the same material system was performed. This lack was one motivation for the work presented here. Under experimental boundary conditions as similar as possible, this work investigates amorphous silicon solar cells in the p-i-n as well as in the n-i-p configuration. The similarity of the boundary conditions extends mainly to the use of identical contact material for the transparent front contact. In both cases, sputtered zinc oxide (ZnO) was used as transparent front contact material. During the mandatory development of a highly conductive and transparent ZnO material which was conducted within an accompanied diploma thesis [21], these films were found to have excellent light trapping properties after a post-deposition wet chemical etching step [22]. Only the development of these textured ZnO coated glass substrates allowed the comparative investigation of the two cell structures.

In the past, our group worked on solar cells in the p-i-n configuration only. For this structure, the present work aimed at the replacement of the commonly used SnO_2 coated glass substrates with our newly developed textured ZnO substrates by means of an adapted p-layer. As said, our group only worked with p-i-n devices before, so solar cells with the n-i-p structure had to be newly developed in order to carry out this study. The motivation to investigate n-i-p solar cells resulted from the potential advantages which are attributed to this cell structure: higher quantum efficiencies can be expected and the deposition order is more adapted to the physical requirements of the tandem cell design. Moreover, in the framework of the European research project NEST[a] our group dealt with the development of an inverted microcrystalline/amorphous silicon tandem cell (microcrystalline silicon is used as a non-degrading low band gap absorber here). The technological goal of this thesis was the development of the amorphous top cell for the inverted micromorph tandem cell. Furthermore, the working n-i-p device was a necessary prerequisite to study low band gap amorphous i-layer materials prepared at high substrate temperatures in solar cells. For both configurations, the TCO/p/i-region plays a crucial role for the performance of the device. Therefore, the development of ZnO-adapted p-layers was the necessary first step in the development of working p-i-n and n-i-p solar cells with ZnO front contact. The structure of the work is as follows:

In **chapter 2** some fundamental aspects of a-Si:H are reviewed. The working principle of solar cells based on a-Si:H is explained. The Staebler-Wronski-effect in a-Si:H as well as the tandem cell concept are discussed briefly. Emphasis will be laid also on the function of the transparent conductive oxide and some particularities of the thin microcrystalline p-layer needed for a low-ohmic p/ZnO contact.

[a]New and Enhanced Silicon Thin Film Solar Cell, funded by the European Commission under contract JOR3-CT97-0145.

Next, **chapter 3** will describe the experimental details. The two routinely used deposition techniques and systems for the preparation of amorphous and microcrystalline material as well as the TCO-films are introduced. The characterization methods will be illustrated in **chapter 4**.

The experimental results obtained in this work are presented in chapters 5 and 6:

Chapter 5 describes the results of the material investigations conducted during this work which serve as a prerequisite for the further solar cell development. Beginning at the front side of the solar cell, the highly conductive and transparent ZnO films are presented first. Here a new post-deposition etching technique to obtain textured ZnO films with a suited structure for implementation in p-i-n solar cells is described. To avoid the contact barrier which occurs at the amorphous p/ZnO interface, the development of microcrystalline p-layers was necessary. The results achieved with two different techniques – RF (radio frequency) and VHF (very high frequency) – will be compared. Finally, the results of the development of intrinsic absorber material with low band gap are presented and discussed.

The implementation of the developed materials into solar cells and the comparison of the p-i-n and the n-i-p structure is presented in **chapter 6**. First, the p-i-n development on ZnO substrates with an adapted p-layer structure is shown. The n-i-p development started with an extensive study of microcrystalline p-layers on a-Si:H presented in this section. In the next part of each section, the requirements and the specific influence of the p-layer structure on the electrical and optical device performance will be investigated. This is followed by the presentation of our efforts in the implementation of the optimized single-cell designs in order to obtain high efficiency tandem cells in the p-i-n and n-i-p configuration.

In **chapter 7**, a comparative discussion of the key findings gained during the solar cell development will be conducted, including technical aspects of the two different cell structures. Emphasis is laid in particular on the ZnO/p/i-region of both cell structures, which plays a dominant role for the device performance. Incorporation of low-gap material prepared at high substrate temperatures in both cell structures completes this section. In **chapter 8**, the results are summarized. Finally, an outlook will be given, discussing how this work can contribute to the future development of silicon thin film solar cell technology.

Chapter 2

Fundamentals

In this chapter, some fundamental aspects of hydrogenated amorphous silicon are described. The principal of operation of amorphous silicon solar cells is explained briefly. The p-i-n and n-i-p structure is sketched. The degradation effect of amorphous silicon with its severe influence on the solar cell performance is described and the tandem cell concept – which is used to reduce this degradation – is introduced. The function and requirements of transparent conductive oxide films in p-i-n and n-i-p solar cells are described. The chapter finishes with a short discussion to the difficulties related to thin microcrystalline doped films.

2.1 Hydrogenated Amorphous Silicon

Detailed surveys on the topic of hydrogenated amorphous silicon which are used here are for example given in the works of Street [23], Luft [24], Madan and Shaw [25], and in volumes 21A – 21D of the Academic Press series "Semiconductors and Semimetals" [26].

The main difference between amorphous and crystalline silicon is the missing long-range order in amorphous silicon. The tetrahedral short-range order in both materials is very similar although bond-angles as well as bond-lengths in amorphous silicon vary slightly. This leads to charge-carrier scattering and broadening of the density of states. The derivation of a strict $E(\vec{k})$-relation based on the periodic structure in crystals is not possible, the conservation of the momentum $\vec{k}$ is not longer granted. This leads to massive changes in the electrical and optical properties of the material. Unsaturated valences (dangling bonds) cause energy states around a mid gap position – these are the only deep defects identified in amorphous silicon so far with a density of about $10^{19}\,\mathrm{cm}^{-3}$. This high density of defects makes it impossible to move the Fermi energy out of mid gap: the material is not dopable. By introducing hydrogen, the technologically interesting *hydrogenated* amorphous silicon

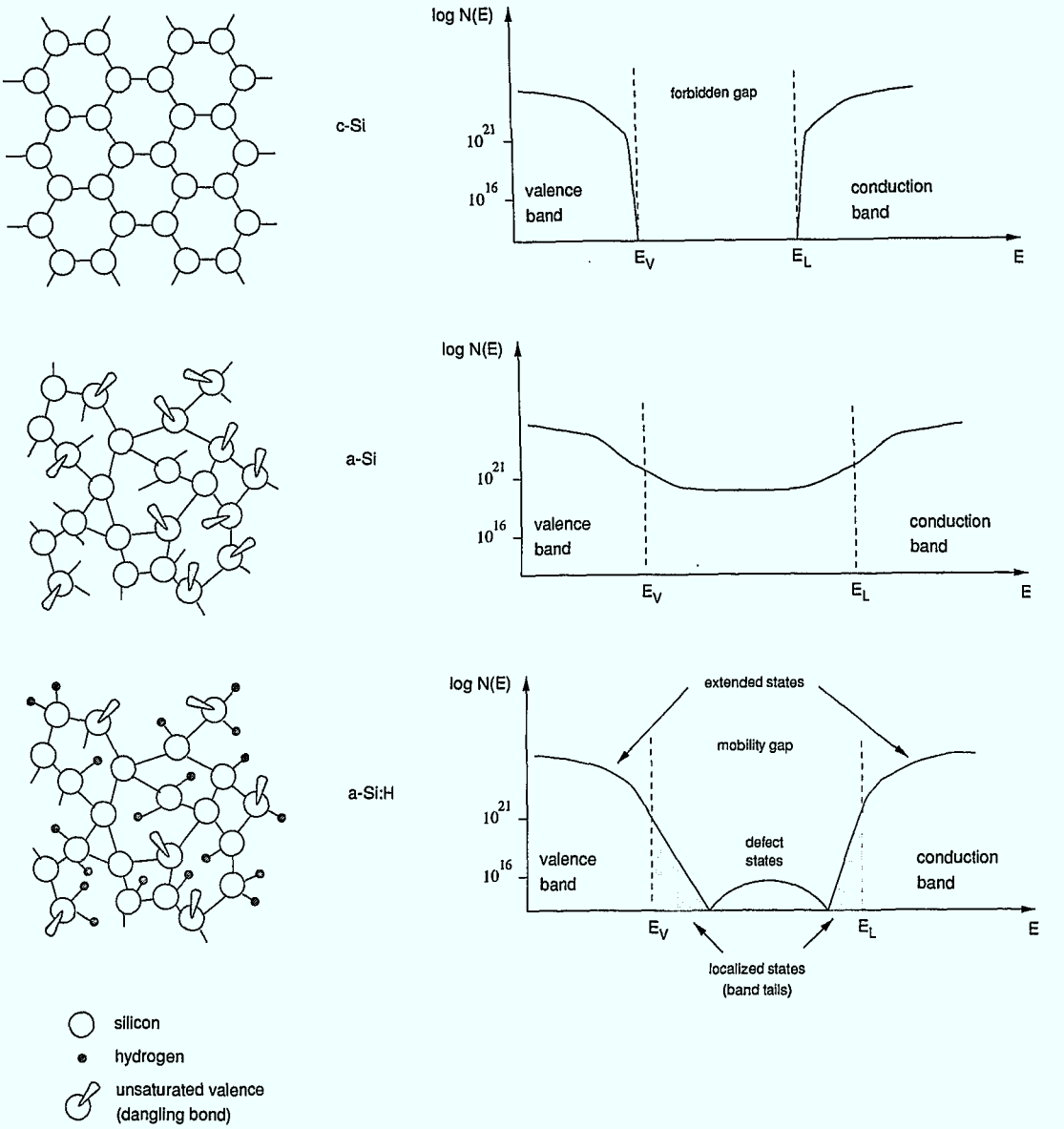

Figure 2.1: *Two-dimensional illustration of the lattice structure (left) and the density of states as function of the energy (right) for c-Si, a-Si, and a-Si:H [27]. In the sketch of the lattice structure, the density of dangling bonds in a-Si:H is strongly exaggerated for clarification.*

(a-Si:H) is produced. The hydrogen saturates most of the dangling bonds and thereby reduces the defect density to an extent where doping becomes possible [28]. However, much more hydrogen than needed for the saturation of all dangling bonds is incorporated in the material. As is generally accepted, hydrogen in high quality amorphous silicon should be present as mono-hydride or Si-H bond, rather than as SiH_2 or SiH_3 bonds. Typically, intrinsic material used as absorber layer in amorphous silicon solar cells contains between 10 and 20 atomic percent hydrogen, justifying the label a-Si:H – a silicon-hydrogen alloy.

The structural disorder leads to the formation of localized "band tail" states. They extend from the band edges into the gap over an energy range of 200 meV (conduction band tail) or 300 – 400 meV (valence band tail) [29]. The rough classification in valence- and conduction band still holds in a-Si:H. But one can observe a smooth merging between extended states of the valence- and the conduction band, respectively, and the localized tail states, whose density decreases exponentially with energy towards the mid gap (see figure 2.1). Since these states are localized between the valence- and the conduction band, it is experimentally (and theoretically) difficult to even define the optical band gap in a-Si:H. Instead, the concept of density of states and a mobility gap is approved in literature: due to the localized nature of the tail states, the mobility of charge carriers sharply drops several orders of magnitude, and one speaks of a *mobility* gap.

Optical properties

Since in a-Si:H the conservation of momentum is not longer granted, the material acts as a direct semiconductor which increases the absorption probability of photons drastically. One striking difference between a-Si:H and crystalline silicon is the absorption coefficient of a-Si:H, which is about a factor of 10 to 100 higher for photon energies above 1.7 eV (730 nm). The incident light is absorbed almost completely in film thicknesses below 1 μm, while c-Si based solar cells need thicknesses around 50 μm, and for handling reasons the wafers even have to be ~200 μm thick. The low material consumption is another advantage of the a-Si:H solar cell technology.

Electrical properties

The electrical properties of a-Si:H are very sensitive to the density and distribution of the localized states. These states determine the devolution of the absorption edge, the carrier transport, the doping ability, the lifetime and diffusion lengths of the charge carriers and the potential distribution in devices. The current transport in the 3 distinguishable zones – extended, localized and defect states – is dependent on the temperature and dominated by one of these. However, at common operating temperatures of solar cell devices, extended state conductivity is dominant and the transport can be estimated to be similar to transport in crystalline semiconductors. The free electrons and holes at the band edge (here and in the following used as synonym for "mobility edge") dominate the transport, while the localized states in the band tails and at mid gap act as trapping and recombination centers.

An important parameter in the characterization of semiconductors is the conductivity σ. The thermally activated dark conductivity can be described by

$$\sigma_d = \sigma_0 \cdot e^{-\frac{E_a}{kT}} \qquad [23].$$

Here, E_a denotes the activation energy as the distance between the Fermi level and the band edge which dominates the transport – in intrinsic a-Si:H, this is the conduction band.

Photoconductivity occurs by optical excitation of charge carriers into conducting states. The charge carrier density n depends on the generation rate G and the lifetime τ of the charge carriers: $\sigma = en\mu = eG\tau\mu$ (μ = mobility). In first approximation, for intrinsic material this gives

$$\sigma_{ph} = eG\left(\mu_e\tau_e + \mu_h\tau_h\right),$$

with $\mu_{e/h}$ and $\tau_{e/h}$ as the mobility and lifetime for electrons and holes, respectively. Time-of-flight experiments show, that in a-Si:H the contribution of holes can be neglected since the mobility of holes is significantly smaller than that for electrons. Hence, for a-Si:H one obtains $\sigma_{ph} = eG\mu_e\tau_e$. Since the charge carriers recombine mainly via defects in the mid gap, photo conductivity experiments can be used as an indirect measure of the defect density (see also 4.1.3).

2.1.1 Solar Cells Based on a-Si:H

The working principle of a crystalline p/n-junction under illumination is as follows: charge carrier pairs are generated by incident photons. The minority charge carriers reach the space charge region by diffusion and are separated by the electric field therein; a photo generated current flows. Crystalline solar cells are so-called diffusion cells, the charge carriers diffuse to the p/n-junction.

In contrast to its crystalline counterpart, in amorphous hydrogenated silicon the diffusion lengths are very short and even shorter in doped a-Si:H; the carriers would recombine long before they reach the space charge region. Hence, an intrinsic (= undoped) a-Si:H layer is inserted between the p- and the n-layer. The doped layers build up the electric field across this i-layer. Figure 1.1 shows two possible structures of a-Si:H based solar cells. As can be seen in the figure, the illuminated side of the cell has to be covered with a transparent electrode; a transparent conductive oxide (TCO) – which is essentially a degenerately n-doped semiconductor with high band gap – fulfills this purpose (see section 2.2). Across the i-layer, a very high electric field is obtained because the i-layer is usually very thin (~400 nm). Charge carriers generated by illumination are driven and separated by the electric field and recombine at "their" junction. Solar cells based on a-Si:H are therefore called drift cells since the charge carriers are driven to their junctions by means of the electric field. The metal back contact can be completed with a ZnO coating between the n-layer and the metal to enhance the reflection of the back contact [30, 31]; this leads to significantly higher current densities due to enhanced absorption of the incoming light.

p-i-n and n-i-p structure

Early structures for solar cells based on a-Si:H comprised Schottky barriers and PIN junctions. Meanwhile, the PIN junction turned out to be the most promising one. In terms of deposition order, one distinguishes between two types of junctions, as already described in section 1.1: superstrate or p-i-n structure and substrate or n-i-p structure, respectively.

The requirements for the material are high: the glass substrate (in the p-i-n case) as well as the TCO have to be highly transparent. Furthermore, the TCO has to be highly conductive to avoid ohmic losses. Another important function of the TCO in the superstrate configuration is to provide a suited surface structure for efficient "light trapping". This means that by scattering of the incident light, the effective path length of the light through the absorbing i-layer material is enhanced, thereby increasing the current delivered by the cell significantly. In the n-i-p case, this must be achieved by optimizing the substrate surface texture. The electron-hole pairs generated in the p-layer do (almost) not contribute to the photocurrent, as they are lost by recombination processes. Hence, the p-layer should be as thin as possible and exhibit a wide band gap in order to avoid absorption losses, but has to be thick enough to build up an efficient electric field across the i-layer. This is usually achieved by amorphous silicon carbide (a-SiC:H) or microcrystalline silicon films. The n-layer as the counterpart to the p-layer should also have a low perpendicular series resistance and a low absorption. The i-layer should show a high charge carrier mobility μ together with a long lifetime τ (low defect density) in order to provide efficient collection of the generated carriers. To gain as much current as possible, the absorption coefficient together with the i-layer thickness must be tuned to allow high currents without deteriorating the fill factor *after* degradation.

2.1.2 Degradation

Already at the beginning of the development of a-Si:H, it became evident that the electronic properties of this new material degrade significantly when illuminated; of course, this is especially undesirable for the application in solar cells. The primary impact of this important effect is the decreasing photo conductivity due to an increase of the defect density. The created defects are metastable [6]: the effect can be reversed by application of moderate temperatures below 200°C.

One attempt to explain the effect – which is not fully understood yet – is the "weak bond – dangling bond conversion"–model by Stutzmann et al. [32]. Due to the strained a-Si:H lattice, some of the Si-Si bonds are weak enough to be broken up by bimolecular recombination of electron-hole-pairs. Neighboring hydrogen atoms may occupy the released bonds and prevent the back reaction: two dangling bonds are created, which represent future recombination centers. Higher temperatures in turn increase the probability of the back reaction, the defects are annealed. In principle, the saturation value of the defect density depends on the intensity of the illumination and the temperature during degradation. This mirrors the dynamic equilibrium between defect generation and defect annealing. An overview of other models is given in the work by Luft and Tsuo [24].

The light induced degradation of a-Si:H based solar cells still represents the most severe physical problem in competition with crystalline or polycrystalline technology. A still open question in this field is the correlation between suited material quality parameters and solar cell degradation behaviour.

2.1.3 Stacked Cell Concept

The most successful concept against the light induced degradation of a-Si:H solar cells is the stacked cell concept: by deposition on top of each other, two or more solar cells are connected in series; in the case of two cells, the label tandem cell has been asserted. The electrons generated in the top cell recombine with the holes generated in the bottom cell at the inner p/n-junction, which should be loss-free in the ideal case (the labels top and bottom cell refers to the illumination side of the cell). To optimize the efficiency of a tandem cell, the so-called current matching is necessary: since the two cells are interconnected in series, the current flowing through the device has to be equal in both individual cells and hence, the total current is limited by the cell generating the lower current. This current matching has to be achieved for the stabilized (light soaked) state of the solar cell.

The stacked cell concept also allows the utilization of different semiconductor materials; for example, microcrystalline silicon can be used as a non-degrading low band gap absorber for the bottom cell as demonstrated recently [33]. Another advantage of stacked cells – which becomes important for module production – is the decrease of ohmic losses (e.g. in the TCO) since the current is lower and the voltage higher. A detailed discussion of the stacked cell concept can be found in [34].

2.2 Transparent Conductive Oxide

The use of textured TCO substrates was a milestone in the development of highly efficient a-Si:H based solar cells. The incident light is scattered and hence, the effective path length in the absorbing film is longer, thereby enhancing the current yield. The enhanced reflection of the metal back contact by an additional thin ZnO film further increases the current. In the ideal case, the surface structure of the TCO together with a highly reflective back contact provides multiple reflections in the semiconductor layer structure – a resonator with light trapping properties is created. Although it is very difficult to even evaluate a suited structure for ideal light trapping, the concept is demonstrated impressively by the current world record efficiencies which all rely on the light trapping concept: in the p-i-n case, rough SnO_2-substrates optimized for the a-Si:H technology from the Asahi company [20] have been the state-of-the-art substrate (at least in the laboratory) for many years now. In the n-i-p case, the USSC group uses a reflector with an optimized stainless steel/Ag/ZnO structure [35] and the development of Kaneka Corporation is based on their STAR structure [36] and, more recently, on the use of light scattering back reflectors [19]. In all cases, the focus on the development of light trapping structures led to significantly improved efficiencies of the solar cell device.

Materials and demands

As already mentioned in section 2.1.1, the TCO material used as front contact has to fulfill several requirements: first of all, it has to be highly transparent in the desired wavelength region. In addition, it should exhibit a conductivity as high as possible. Furthermore, these

properties should be paired with a suited texture allowing a high amount of scattered light when transmitted. The particular technological problem is to achieve all these demands with a single film. Several materials for use as transparent conductive oxide are currently used: fluorine doped tin-oxide (SnO_2:F), tin-doped indium-oxide (In_2O_3:Sn, in short "ITO" for indium tin oxide), and aluminum doped zinc-oxide (ZnO:Al) are the most common ones. All materials can be deposited using a variety of deposition methods, overviews are for example given in [37, 38].

Since the favourable SnO_2:F substrates from the Asahi company are not available for large areas at low cost yet, and commercially available SnO_2:F substrates cause distinct losses in module efficiency due to enhanced absorbance and reduced light scattering properties [39], there is a high demand for alternative TCO substrate materials. ITO contains the rare element indium leading to high cost of the source material. So ZnO:Al offers a promising alternative. Moreover, it is more abundant and ecologically harmless. For a-Si:H based solar cells, it has the additional advantage of high stability against H_2-plasma impact, which usually occurs during the PECVD process.

2.3 The TCO/p Contact

A very sensitive region in the solar cell device is the TCO/p front contact. Here, holes generated within the device recombine with electrons delivered by the TCO.

Unfortunately, with ZnO[a] as TCO substrate material, the fill factor of the solar cells significantly decreases when using an amorphous p-layer. The JV characteristic and the independence of the observed series resistance from the p-layer thickness indicate the interface nature of this problem. Moreover, in the p-i-n case, the plasma conditions during deposition of the p-layer influence the contact behaviour. In the n-i-p case, the ZnO preparation conditions are found to influence the interface, too. This indicates that the electrical properties of the TCO/p interface are strongly influenced by the chemical conditions during deposition of the first few nm of the interface layer.

The problem of a high-ohmic amorphous p/ZnO contact behaviour in p-i-n cells deposited on a ZnO coated substrate has been reported before [15, 40]. It is attributed to an emerging electron accumulation layer in the ZnO surface which is caused by the interaction with atomic hydrogen. This in turn leads to a thicker depletion zone in the p-layer giving rise to an increased series resistance of the contact. One solution of this interface problem was already addressed in previous publications of our group [40–42]: The insertion of a microcrystalline contact layer – which shows much higher doping efficiencies than amorphous material, therefore allowing a thinner depletion zone – leads to improved contact behaviour. Also, microcrystalline p-layers are supposed to provide higher open-circuit voltages than their amorphous pendant [43, 44]. Furthermore, microcrystalline p- and n-doped

[a]Note that here and in the following, ZnO:Al and ZnO are used as synonym for convenience.

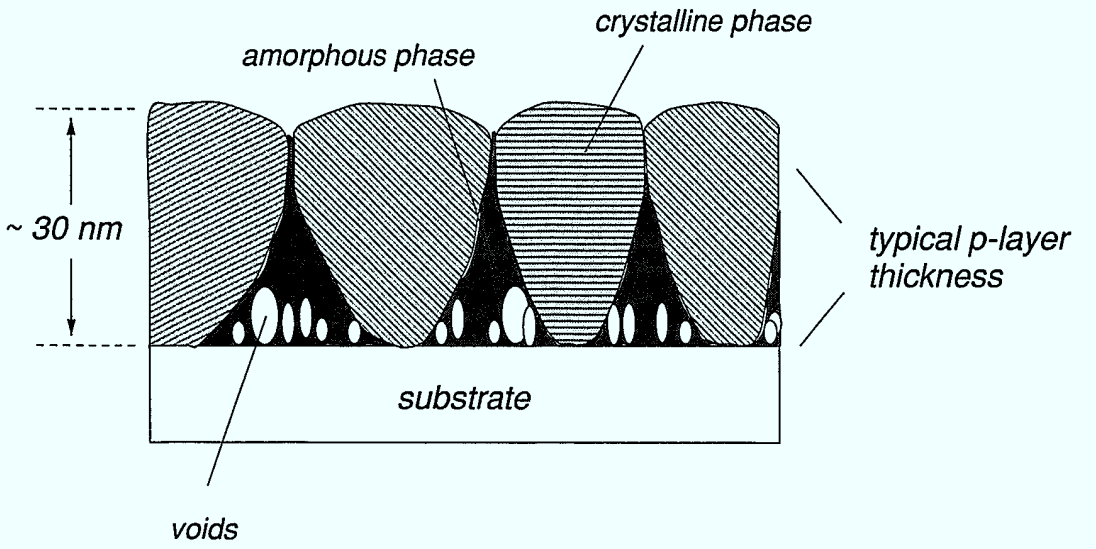

Figure 2.2: *Schematic model for the initial growth of microcrystalline silicon. For comparison, the typical thickness of a microcrystalline p-layer used in a solar cell is indicated also. Draft after [51].*

films serve as contact layers of the optimized low-ohmic inner p/n-junctions in stacked cells [13, 15, 45–47].

Due to the difficult accessibility, it is generally very hard to gain detailed insight into the initial growth mechanism of microcrystalline silicon. In literature, solely the general characteristic of an island-growth model is accepted: in the early stage of growth small amorphous and crystalline islands form. Since there is no coalescence at growth temperatures as low as 200 °C, growth competition of neighbouring islands leads to the typical cone-like shape of crystallites in the early stage of film formation (schematic view see figure 2.2). Depending on the plasma excitation frequency, also void incorporation takes place. Later on, columnar growth in the bulk material is observed. The initial nucleation phase is extremely critical and strongly depends on the substrate (e.g. glass, a-Si:H , or c-Si) and the growth conditions (e.g. H_2-dilution during deposition or doping ratio). For a detailed description see [48–50]; an overview is for example given in [51]. As indicated in the figure, microcrystalline p-layers finally applied to the solar cell usually exhibit thicknesses which are similar or even smaller than the actual film nucleation phase which extends over the first 30 nm. Another difficulty arises since the evaluation of these thin layers is not easy: for the low-ohmic resistance of the TCO/p contact, the contact resistance perpendicular to the substrate is important, but difficult to measure. Moreover, the characteristics of these thin films can be distinctively different from those obtained in the volume of the same material. Up to now, the solar cell itself is the only reliable monitor to evaluate the TCO/p contact behaviour by examination of the light JV characteristic.

Chapter 3

Experimental

In this chapter, the plasma enhanced chemical vapor deposition method is explained briefly; emphasis is laid on the role of hydrogen in the PECVD process. The used deposition system is sketched and the general procedure used to prepare the samples is presented. The sputter technique and the system for the preparation of the transparent conductive oxide films is explained as well. The substrates are described and the cell design for the p-i-n and n-i-p configuration used throughout this work is sketched.

3.1 Plasma Enhanced Chemical Vapour Deposition

Plasma enhanced chemical vapor deposition (PECVD) is a standard deposition method to prepare a-Si:H films in the laboratory as well as on industrial scale. Detailed information about the PECVD method is given in the books by Chapman [52], Haefer [53], or Frey and Kienel [54]. Particularities related to the growth of a-Si:H are treated in the work of Street [23], Luft [24], or Madan and Shaw [25].

To deposit amorphous hydrogenated silicon films, the decomposition of silane gas – SiH_4 – is the most common way. Thermal dissociation of silane starts around 450°C but usually leads to the growth of low quality material. At lower substrate temperatures, the dissociation energy must be supplied by other means. PECVD is a process which provides the necessary energy in a low pressure glow discharge. The plasma is usually created by application of a high frequency field between two parallel electrodes, which allows the preparation of films also on insulating substrates. The independently adjustable substrate temperature is typically around 200 °C. These moderate temperatures offer the possibility to use a variety of substrate materials. Moreover, low energy consumption is provided in an industrial-scale process compared to e.g. crystalline technology, which uses temperatures > 600°C.

By introducing boron- or phosphorus-containing source gases into the reaction, doped films are easily achieved. Band gap tuning is an important means to adjust the optical absorption properties of a-Si:H: by addition of carbon- or oxygen-containing gases, a-Si:H alloys with wide band gap used as so-called "window layers" are prepared, while the addition of germane leads to low band gap alloys used as i-layer absorber material. Another very important source gas is hydrogen, which is used to improve the material quality and control the deposition process within certain limits; the role of hydrogen will be treated later on.

By electron impact, radicals are created in the plasma. Complex secondary reactions including ionization, excitation, quenching, and chemical reactions are possible before a particle contributes to the formation of a film. Moreover, chemical equilibrium processes driven by their chemical potential influence the growth of the film as well as sticking coefficient and surface mobility of the impinging fragments. Despite the simple working principle of the glow discharge process, the variety of physical and chemical process variables controls the growth process of the amorphous films in a rather complex way and the details of the reaction paths leading to the growth process are not fully understood yet. Some important parameters varied in the process are:

- The power density fed into the glow discharge controls the dissociation rate of the inserted gases and thereby to a large extent the growth rate. Typical values: 30 – 300 mW/cm^2

- The excitation frequency used determines the mean energy of the ionized molecules and thereby the collision energies as well as the impact on the growth surface. Typical values: 13.56 MHz – 110 MHz

- The gas flow controls the dwell time of the reactants in the process chamber. At low flow rate-to-power ratios, this leads to a limitation of the growth rate. Typical values: 1 – 200 sccm[a]

- The gas pressure determines the mean free path length of the gas molecules and thereby the collision probability. Typical values: 0.1 – 2 Torr[b] resulting in about $10^{-4} - 10^{-5}$ cm mean free path length.

- The chemical equilibrium on the substrate surface strongly depends on the substrate temperature. Typical value: ~200°C.

- The use of additional source gases, mainly inert gases (e.g. argon, xenon, ...), results in complex effects which affect the quality of the grown film in various ways.

[a] sccm = standard cubic centimeter per minute. By definition of the standard conditions (25 °C and 10^5 Pa) the gas flow corresponds to a fixed number of particles per time unit.

[b] 1 Torr = 133,3 Pa. The instruments used do not display pressure values in standard SI-units. Since conversion is a frequent source of calculation errors and the reproducibility of the used experiment-protocols has to be ensured, here and in the following, conversion to SI-units was omitted.

3.1.1 Hydrogen in the PECVD Process

The important role of hydrogen for amorphous silicon was already pictured in section 2.1. Thus, one important process parameter is the hydrogen dilution $H_2 - dil.$ defined as the hydrogen to silane flow ratio:

$$H_2 - dil. = \frac{H_2\ flow}{SiH_4\ flow}$$

The true hydrogen dilution is also dependent on the pump utilized, since the pumping ratio for silane and hydrogen is usually different and also differs from type to type.

Even when using pure silane as source gas, a certain hydrogen dilution is always present since the decomposition of silane (SiH_4) releases hydrogen into the reaction. Recent studies show that the additional use of hydrogen favours the deposition of high quality a-Si:H films [8–10]. Improved electrical properties of the material and higher stabilized efficiencies testify to this fact.

Very high concentrations of hydrogen in the plasma can cause the film to become crystalline rather than amorphous (see [23] and references therein). Since the size of the crystallites is very small (in the nm-range), this material is termed "microcrystalline". The transition between amorphous and microcrystalline growth is rather abrupt. High power enhances this effect while high frequency of the applied power lower the hydrogen dilution necessary for the formation of microcrystalline films.

However, a detailed understanding of the effect of the hydrogen dilution on the growth of a-Si:H films is still missing and this topic is still treated in current research. Etching of weak Si-Si bonds [55], H_2-induced reconstruction of the strained Si-lattice [56], or enhanced surface mobility caused by hydrogen-coverage of the growing surface [57] are ideas discussed in literature. The initial nucleation of the film on the substrate (e.g. glass or a-Si:H) and the subsequent pattern of growth is strongly dependent on the sticking probability and the surface mobility of the growing species. Low surface mobility, for example, can cause atomic shadowing effects leading to macroscopic inhomogeneities, such as voids, columnar structures or surface roughness.

3.1.2 PECVD System

All depositions made in this work were carried out in a commercial PECVD system manufactured by Glasstech Solar Inc. (supplied by Materials Research Group Inc.). The system consists of four deposition chambers which are interconnected by two transfer chambers; the latter also serve as load locks (see figure 3.1).

Via the loading chambers, a substrate holder containing the substrate is transfered into the desired deposition chamber. In the p- and n-chamber, the boron and phosphorus doped films were deposited, respectively. The i-chamber served for the deposition of the intrinsic

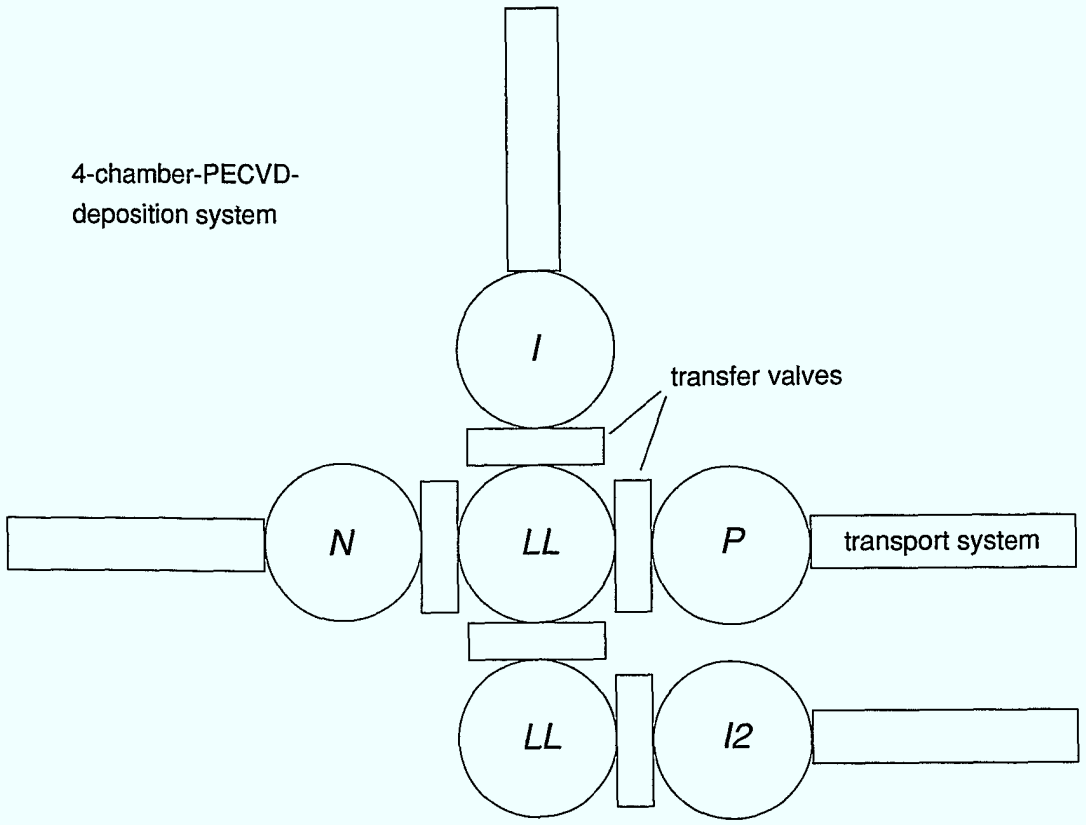

Figure 3.1: *Layout of deposition system (top view) showing the four individual chambers to prepare p-, i-, and n-layers as well as the transfer- and loading chambers (load lock), respectively.*

layers only, since the material quality of these layers strongly depends on contamination (e.g. by boron cross contamination from the p-chamber [58]).

The gas supply and pumping scheme is sketched in figure 3.2. Each chamber is equipped with a manual flow controller in the Argon purge line. All other gas lines are equipped with automatic mass-flow-controllers. During deposition, each chamber is pumped with a wide-range turbo pump via a pressure-controlled butterfly-valve. The pumps are running with nitrogen-gas ballast to prevent the pump bearings from being contaminated by the toxic waste gases. In addition, each turbo pump has a rotary-pump providing a pre-vacuum.

The layout of a single chamber is shown in figure 3.3. The substrate holder is heated indirectly via the heater system; according to calibration measurements, the substrate temperature T_S is about two thirds of the heater temperature. The substrate holder consists of a frame holding the substrate and a heavy metal plate fixing the position of this substrate by its weight. Riding on a grounded track-system, the substrate holder serves as a counter electrode during deposition. The circular electrode has a diameter of 13.5 cm and is surrounded by a shield confining the plasma. The high frequency (HF)

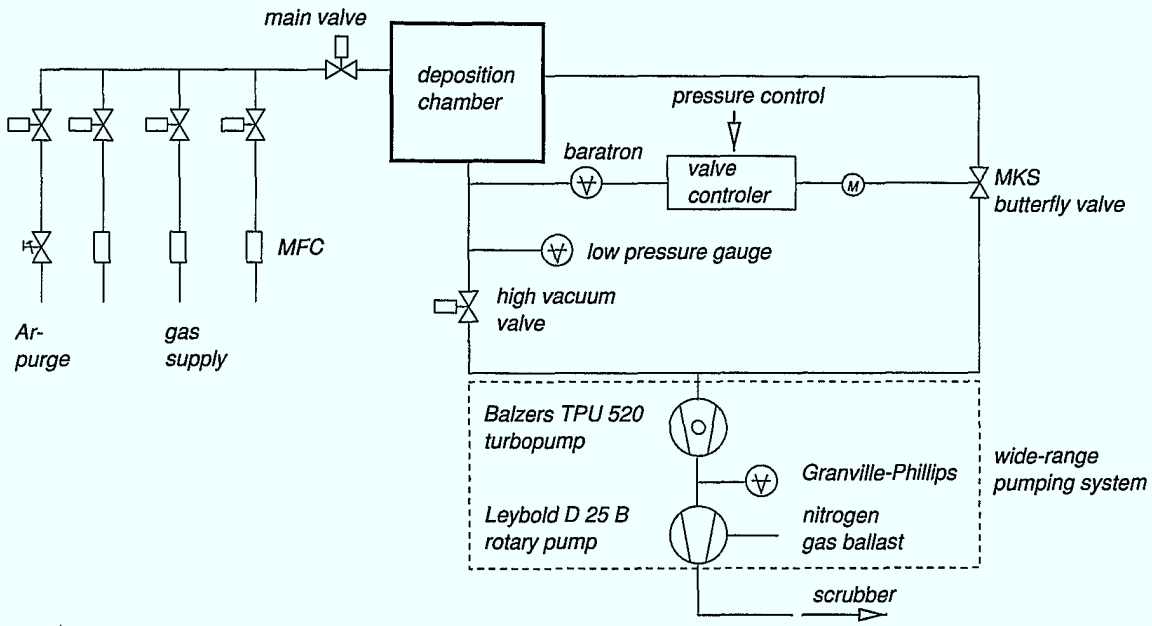

Figure 3.2: Layout of the gas supply and pumping scheme of the used 4-chamber deposition system.

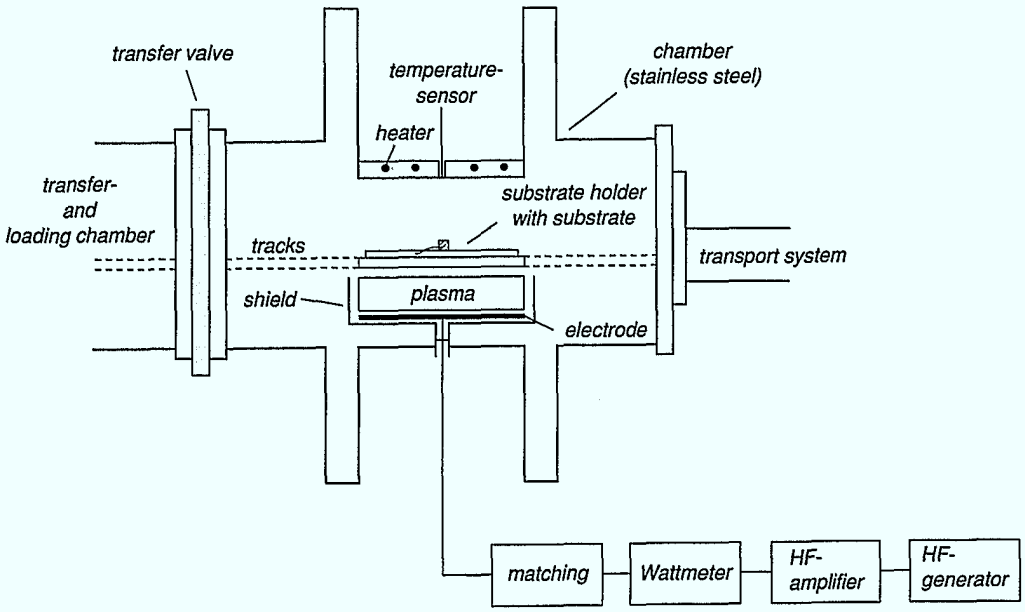

Figure 3.3: Layout of a single deposition chamber.

signal is produced in a HF generator and amplified before it is coupled into the system by means of a matchbox. The plasma power is measured with a Wattmeter between amplifier and matchbox and the matching is done by minimizing the reflected power. Important to note, the true value for the power coupled into the system is strongly dependent on wiring configuration, used frequency and matching conditions. The true value for the power fed into the system can be determined by vector-measurement of voltage and current [59]. As this is not a standard measurement in our lab all power values in this work refer to the instrument display of the Watt meter.

All chambers are designed identically except for different electrode-substrate spacings which are 1.2 cm in the p- and i-chamber and 2.0 cm in the n-chamber, respectively. Furthermore, the p-chamber contains an additional electrode radiation heater.

3.1.3 Deposition Procedure – PECVD

Corresponding to the desired temperature, the substrate was heated in one of the chambers under vacuum conditions for at least 45 – 60 minutes. To prevent residual gas influence, the chambers are pumped down to about 10^{-8} mbar[c] before each deposition process (this is the default status of the whole system). Starting with this high vacuum condition, the chamber was flushed with argon for 5 minutes at 5 Torr to achieve a temperature equalization between chamber walls, heater, and substrate before each deposition. In the next step, the desired process gases were fed in and the pressure was set. Before ignition of the plasma, the substrate was removed from the actual plasma area (ignition of the plasma is done with the heater as counter electrode). After the coupling was adjusted with the matchbox, the substrate holder was placed into the plasma region again and the deposition of the film was carried out. To stop the deposition process, the power supply was just switched off. After deposition, the chamber was flushed again with Argon at 150 mTorr to extract reactive gases out of the chamber, thereby preventing the contamination of the load lock during the transfer. After transferring the substrate holder into the load lock, the chamber was evacuated again. According to the set substrate temperature of the last deposition step, the holder remained in the load lock to cool down for a sufficient time before the load lock was vented with nitrogen and the holder was taken out.

3.2 Magnetron Sputtering

Like the PECVD method, sputtering is a well approved technique in the laboratory as well as in industry. It is commonly used for the preparation of transparent conductive coatings. More detailed information about this topic is given in the relevant literature [37, 38, 60].

In the sputter process, ions (usually Ar^+) are created by a low pressure glow discharge and accelerated towards a target by means of an electric field (DC or RF). By mechanical im-

[c] 1 bar = 10^5 Pa. See also footnote on page 16.

pact, target material is carried off and may condense on a substrate. Similar to the PECVD method, the substrate can be heated independently, thereby influencing surface reactions on the substrate. To increase the number of particles contributing to the formation of the film, a high mean free path length is desirable. This is usually achieved by application of low pressure to the glow discharge. To prevent the plasma from becoming instable in this case (the probability for the collisions maintaining the plasma is proportional to the gas density), the electron density has to be increased. This is achieved by applying magnets at the back of the cathode, forcing the electrons to follow circular trajectories because of the Lorentz-force. By choosing a suited configuration for the magnetic field, closed loops for the electron course are achieved. This increases the residence time of the electrons in the plasma region and thereby the ionization rate significantly. The disadvantage of this method is the inhomogeneous deposition due to the circular wise distribution of the ion current carrying off the target material. This is mirrored in a circular concentration of the growing film on the substrate. The homogeneity can be adjusted (within certain limits) by choosing a suited cathode-to-substrate distance. However, this particular problem does not occur in the industrial sputter process, since linear cathodes are used here.

In addition to the inert gas (e.g. Argon), reactive gases can be used as source gas. In particular for ZnO, the addition of oxygen to the sputter gas allows to control the stoichiometric composition of the growing film within certain limits. This, in turn, has strong effects on the electrical and optical properties of the prepared films (e.g. transparency, conductivity). Common process parameters are: substrate temperature, gas flow rate, applied power mode and power, applied pressure, and source gas composition.

3.2.1 Sputter Deposition System

In the following, the sputter system used throughout this work is described briefly. A more detailed description is given in [61].

All depositions were carried out with a commercial high vacuum sputter system from the Lesker company. The main chamber is equipped with 4 water-cooled 6" ring-cathodes (see figure 3.4). To prevent long pumping times when loading substrates into the chamber, a load lock separated by a transfer valve and equipped with an independent turbo pump completes the system. The deposition pressure in the main chamber can be adjusted by means of a control valve. After loading into the load lock, the substrates can be placed on one of the four lots of a rotatable roundabout. All lots are equipped with radiating heaters to adjust the substrate temperature during the sputter process. The roundabout is equipped with a shutter to cover the substrate while conducting a pre-sputter procedure before the actual deposition. The substrate temperature is about two third of the heater temperature. Two of the magnetron-cathodes are connected to a DC-generator, the other two to a RF-generator. In this work, a ceramic ZnO:Al_2O_3(2 %)-target was used for all depositions except for some ITO-films which were used for comparison. The power is fed into the system via a matchbox, the matching is done by minimizing the reflected power.

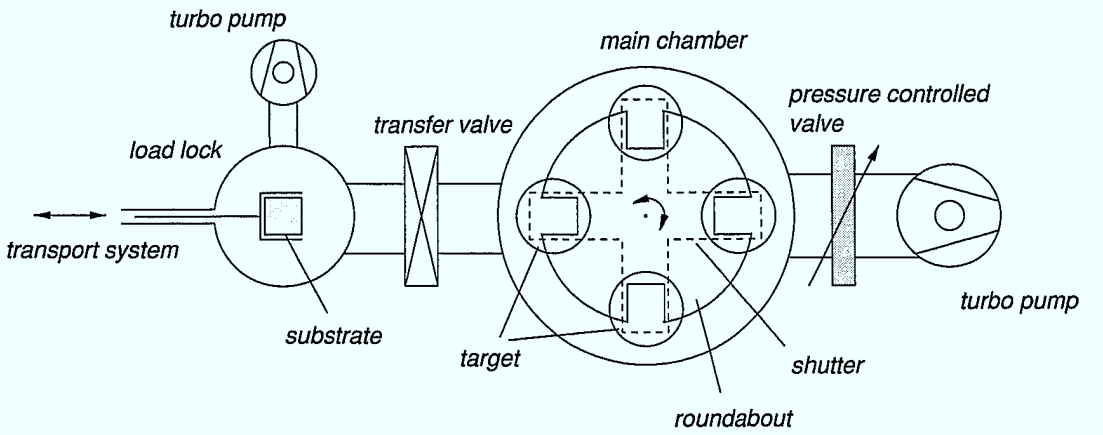

Figure 3.4: *Sketch of the magnetron sputter system used throughout this work.*

As source gases, argon and an argon-oxygen-mixture (1 % oxygen in argon) were used. The flow rate was controlled by mass-flow controllers. During the deposition procedure, the main chamber is pumped via a pressure-controlled valve.

3.2.2 Deposition Procedure – Sputtering

By default, the load lock and the main chamber are both pumped down to a pressure in the low 10^{-7} Torr-range before deposition. The loaded substrate was transfered into the main chamber and placed above the desired target. Then the substrate was heated for about 20 minutes to achieve the desired temperature. The process gases were fed into the system and with closed shutter, a pre-sputtering step of about 10 minutes was carried out to put the target into a defined oxidation status. After this, the deposition was conducted. To stop deposition, the shutter was closed again and the power was set to zero. After transfer into the load lock, the substrate cooled down before unloading.

3.3 Substrates

As substrate for the p-i-n solar cell process, we used sputtered ZnO prepared in our sputter system. For these films, 10 × 10 cm^2 or 10 × 5 cm^2 glass substrates (Corning type 7059) were used standardly. The glass substrates were cleaned before deposition as described below. The initially smooth ZnO films exhibit distinct surface roughness after a post deposition wet chemical etching step in diluted HCl. This procedure was invented in a diploma thesis [21] accompanying this work.

On the cleaned p-i-n substrates, 800 nm thick Ag grids were applied by thermal evaporation through a mask. These support the current transport of the front TCO to prevent ohmic

losses. Next, the deposition of the semiconductor layers was carried out as described in section 3.1.3. The last step was the thermal evaporation of the Ag back contact.

For the n-i-p cell development, there were several reasons leading us to the decision to use commercially available SnO_2 coated glass substrates from the Asahi company (type U) without back reflector for this study:

- Our prior experience with p-i-n development on this substrate showed that it allows a highly reproducible cell process.
- The developed n-i-p solar cell was meant to be used in stacked cells with a microcrystalline bottom cell. Optimization of the n-i-p device with respect to high current output was not necessary at this point of time.
- According to our evaluation of the substrate difficulty, a "module-like" behaviour of a working n-i-p cell was assumed. This means that a working n-i-p device can be adapted to different substrates without new development of the complete cell design.
- The i-p-TCO region is assumed to be not affected by the chosen substrate, which is an important point especially for this work.

Various stainless steel based sustrates or glass/Ag/ZnO substrates were used from time to time to screen the achieved progress.

After depositing the individual layers of the n-i-p solar cell, the front contact in this structure was applied by RF-sputtering of a highly transparent ZnO film through a mask. Since most of these contacts were carried out as an anti-reflection coating (by adjusting the thickness), the lateral conductivity of the thin top contact had to be supported by an additional grid structure (see figure 3.5b), which again was applied by thermal evaporation of silver.

For the deposition of microcrystalline p-layers, Corning glass (7059) or 100 nm a-Si:H i-layers deposited on Corning glass (to examine microcrystalline growth on a-Si:H) were used as substrates. For the examination of intrinsic a-Si:H films, Corning glass was used as well. The Corning glass and the Asahi type U substrates were cleaned with the following procedure:

1. Ca. 45 minutes ultrasonic bath in 9 % Decontam solution (Hoechst Company) at 70 °C.
2. Repeated scavenging in deionized water.
3. Ca. 30 minutes ultrasonic bath in deionized water at 70 °C.
4. Rinsing in a closed deionized water bath, until the resistance of the waste water increased to above 15 MΩ.
5. Centrifuging of the remaining water while rinsing with a warm nitrogen gas flow.

All substrates and finished solar cells were stored in plastic boxes until further usage.

Cell configuration

In the p-i-n as well as in the n-i-p case, the cell geometry was identical and defined by the silver back contact or the TCO top contact, respectively. The geometry used for both cell types is shown in figure 3.5.

While the silver was thermally evaporated through a mask, the top contact in the n-i-p case was sputtered through an identical mask. When carried out as thick top contact ($\sim 700\,\text{nm}$), shadowing effects during the sputter process occured due to the relative thick mask (1 mm), which led to very broad, smooth steps at the edge of the TCO contacts. In practice, this led to reduced fill factors of the solar cell, which is caused by the enhanced series resistance of the carriers collected from the edge area of the cell. To prevent this, a mask was used during measurement (see also section 4.2.1), which left blank smaller areas than the actual cell area defined by the top TCO. The figure also shows the grid system used to support the current collection of the top TCO when carried out as a thin anti-reflection coating (see 5.1.1).

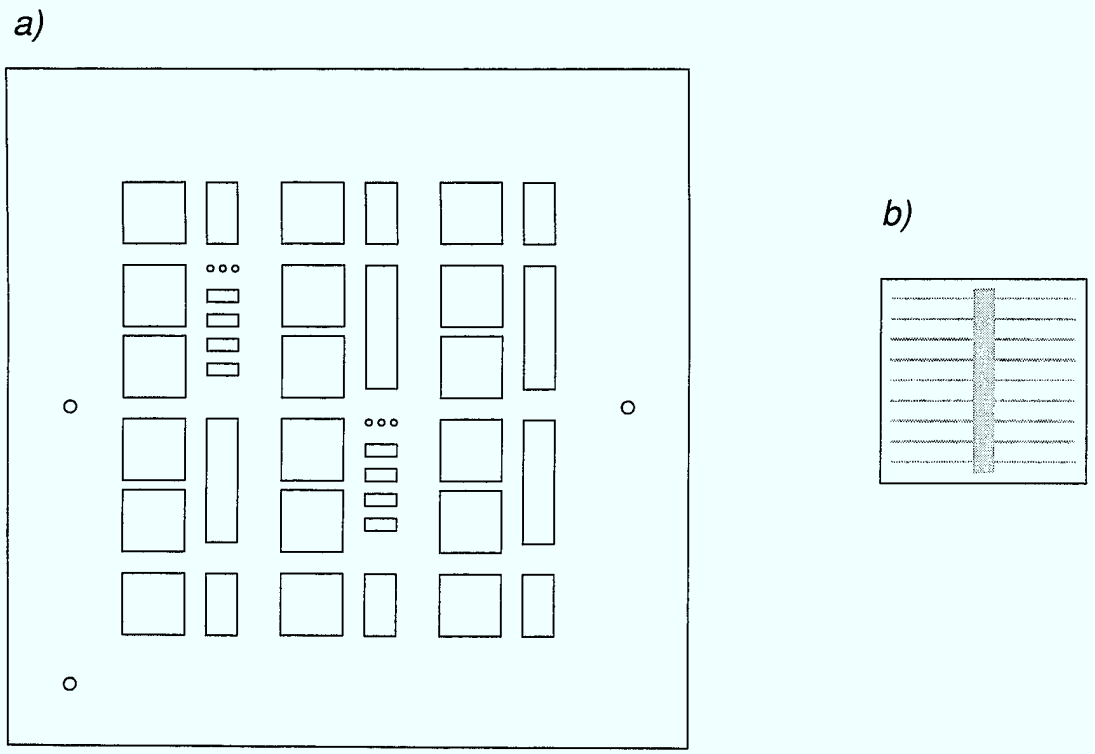

Figure 3.5: *a) Cell geometry used for p-i-n and n-i-p cells. The square cells have an area of 100 mm², the three types of rectangular cells have areas of 100, 50, and 10 mm². The small dots serve as positioning marks only. b) Grid used to support the current collection of the top TCO contact in the n-i-p case. The area of the complete grid system for the 1 cm² cells is 14.04 mm².*

Chapter 4

Characterization Methods

In this chapter, the different characterization methods and their physical background are explained. For the material development, the methods used are: determination of the optical absorption, conductivity, and the defect density. In addition, scanning electron microscopy was used for some samples. For the evaluation of the solar cell characteristics,we used current-voltage (JV) measurements before and after degradation, and spectral response measurements.

4.1 Material

The purpose of material characterization is to gain a comprehensive insight into the different material properties. However, the insertion of these materials in the solar cell device was the main point for most considerations. The following sections describe standard characterization methods which were used for all samples if possible.

Thickness determination
All thicknesses were measured using a surface profiler from Veeco Instrument Inc., type DEKTAK 3030. For the measurement, an abrupt step has to be created first. A simple method to achieve this is scratching the film with a scalpel and fitfully removing an applied tape, thereby tearing off part of the film from the substrate. With this method, very sharp steps are created, which are easy to measure with the profiler. Unfortunately, this doesn't work with all film types. In that case, the step was created by applying a drop of KOH lye to the film. The whole substrate was heated gently (max. 60°C) to accelerate the etching. In the case of ZnO, a drop of HCl acid was used instead[a]. The measurement was conducted

[a]Actually, during his diploma thesis carried out in our institute this was the way, A. Löffl [21] discovered that certain ZnO films were texturable!

at different locations to minimize the error. The accuracy is estimated to ±10 nm. Hence, for the thin microcrystalline p-layers which were used in solar cells, this method could only give an upper limit for the thickness.

4.1.1 Optical characterization

For optical characterization, a two-beam spectrometer (Perkin Elmer, type LAMBDA 19), was available. This is a high performance two-beam spectrometer for the UV, the visible, and the near infrared range which allows measurements from 185 nm to 3200 nm. Prerequisite for a correct evaluation is a careful conduction of the measurement:

- To calculate the absorption coefficient, all R and T measurements belonging together have to be carried out at the same location of the sample, since inhomogeneities in the film thickness cause errors when combining the values.
- The angle of the incident beam must be 90° for transmission measurements.

To achieve this, the samples were mounted between two plates and locked in a holder. The whole sandwich structure could be exchanged for R and T measurements without changing the relative position of the sample.

For reflection measurements, the incident light is guided onto the sample and the reflected light is measured. For transmission measurements, the sample is mounted perpendicular to the incident light. In this way, the perpendicular transmission $T_\perp$ or – after mounting an integrating sphere – the total transmission T_{tot} can be measured.

TCO

The measurements for the TCO films were conducted between 250 and 2500 nm. From reflection and transmission measurements, one can calculate the absorption $A = 1-R-T_{tot}$. The total transmission contains the diffuse amount T_{diff} of the scattered light also. A useful way to describe this amount is the haze-function $H(\lambda)$ defined as

$$H(\lambda) = \frac{T_{diff}}{T_{tot}} = \frac{T_{tot} - T_\perp}{T_{tot}}.$$

The texture of the films is of interest when the films are used as substrate in p-i-n solar cells. Unfortunately, the evaluation of the suitability of a certain substrate is very difficult since there is no known correlation between good light trapping behaviour and experimental data, e.g. the haze function. Despite this fact, the haze function is often reduced even more to its single value at – for example – 500 nm to compare different substrates in literature. The ultimate comparison of two different substrates should always be the codeposition of a solar cell device on both substrates, followed by a comparison of the solar cell characteristics.

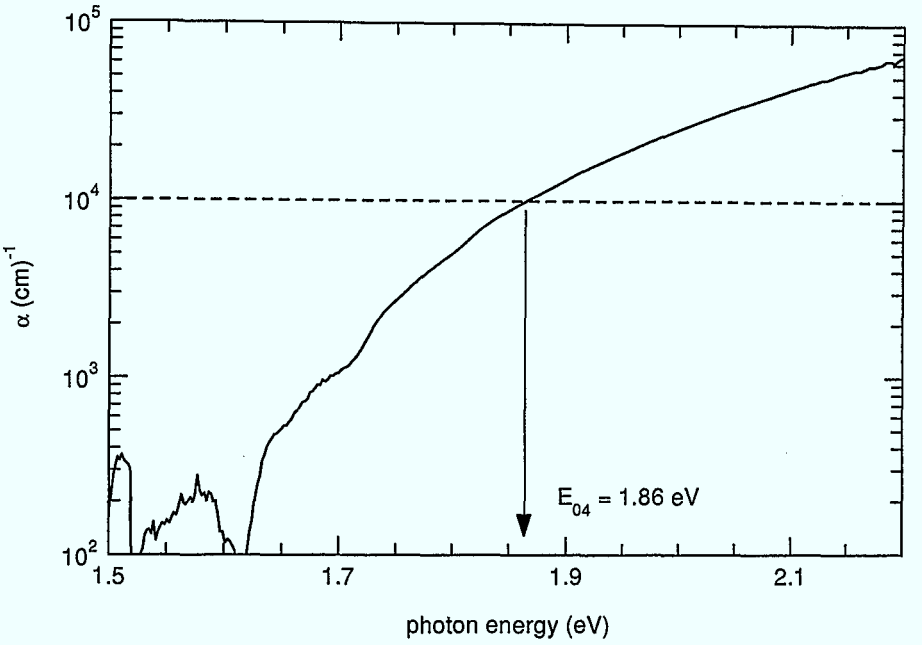

Figure 4.1: Absorption spectrum calculated by formula 4.1 and E_{04}-gap determined as described in text.

i-layers

The aim of this method applied to i-layer material is the determination of the absorption coefficient. The measurements were conducted between 400 and 800 nm which corresponds to photon energies of 3.1 and 1.6 eV. The absorption coefficient α is defined by the decrease of the light intensity in the depth d (Beers' law):

$$I(d,\lambda) = I_0 \cdot e^{-\alpha(\lambda)\cdot d}$$

Since the i-layer thicknesses (300 – 1300 nm) are in the range of the wavelength of the used measurement beam, interference effects make an evaluation difficult. Hishikawa et al. [62] proposed a way considering multiple reflections within the layer leading to nearly interference-free spectra. The absorption coefficient is then calculated by

$$\alpha(\lambda) = -\frac{1}{d} \cdot ln\left[\frac{T}{(1-R)}\right]. \tag{4.1}$$

Figure 4.1 shows a typical absorption spectrum of an i-layers as function of the photon energy gained by this method.

The difficulty in the definition of a band gap in amorphous semiconductors was already mentioned in section 2.1. In literature, mainly two ways for an evaluation of the absorption

spectra have been established: the first refers to a model – in most cases of crystalline origin – and transfers it with modifications to the amorphous case. This leads to evaluation rules to determine the optical gap, e.g. the Tauc-method [63]. The second way is a direct extraction of an energy value from the absorption spectrum at fixed α to compare different materials. Depending on the chosen value of α (e.g. $10^{3.5}, 10^4$), this leads to a more or less agreement with the values obtained by determination of the mobility edge. Since the first method did not prove sufficiently reproducible in practice, we use the specification of the so-called E_{04}-gap which refers to $\alpha = 10^4$. As a rule of thumb, this value is about 100 to 150 mV higher than values obtained with the Tauc-method.

4.1.2 Electrical characterization

Conductivity measurements give insight into the electronic properties of the material investigated. For the measurement of this parameter, two methods were used: As can be seen in figure 4.2, two coplanar contacts were applied to the film by thermal evaporation of silver. In order to be allowed to neglect current paths outside the contact geometry, the l-to-s ratio should be large. Also, a homogeneous electric field distribution is assumed between the contacts. The measured contact resistance between contact fingers and the silver contact was below 0.1Ω so it is neglected, too. All measurements were carried out at room temperature.

TCO

The sheet resistance $R_\square$ of the TCO is an important factor for the solar cell performance, since the TCO film is responsible for the loss-free transport of the generated current. The importance of $R_\square$ is mainly due to its thickness independence. By measuring the resistance R, the sheet resistance $R_\square$ can be calculated by

$$R_\square = R \times \frac{l}{s}.$$

With

$$\rho = R_\square \times d,$$

the specific resistance ρ of the material can be determined as well. This value is connected to important material parameters like charge carrier density N and mobility μ via: $\rho = (\mu N e)^{-1}$, (e is the elementary charge). Determination of N and μ was performed by Hall measurements [64].

To compare different films, the values obtained in the middle of the substrate were taken. One disadvantage of the described method is that the evaporated contacts do not allow the substrate to be used for further solar cell preparation. Hence, a second method used as a standard since it is very fast and non-destructive, is the four-point method. This method is described in detail in [65]: a probe containing four linearly arranged spring-pins is gently pressed on the substrate. A constant current I is flowing through the two outer

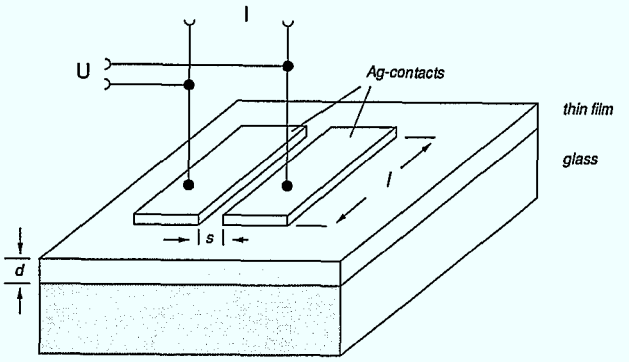

Figure 4.2: Setup for the conductivity measurement on a thin film with evaporated silver contacts. d = film thickness ($\sim 1\ \mu m$), s = contact distance (1 mm), l = contact length (10 mm).

pins, while the two inner pins are used to measure the voltage drop U. Good $R_\square$ values of TCO substrates used for p-i-n solar cells are below 10 Ω.

i-layers

To evaluate the transport behaviour, the photo- and dark-conductivity was measured with the contact scheme in figure 4.2. The photo conductivity was measured under AM1.5 illumination of the solar simulator described in paragraph 4.2.1. Voltages between 1 and 100 V were applied to the contacts and the current was measured, allowing to test the ohmic behaviour of the material. In this case, from Ohm's law

$$j = \sigma \cdot E, \qquad \text{it follows} \qquad \sigma = j \cdot \frac{1}{E} = \frac{I}{d \cdot l} \cdot \frac{s}{U} \tag{4.2}$$

U is the applied voltage, I the measured current, d the film thickness, l the contact length, and s the contact distance (see figure 4.2). The measurement was carried out with a source measure unit from Keithley Instrument Inc. , type SMU 238, with the four-probe method up to 2 cm before the contacts. Typical initial values for the photo conductivity in a-Si:H are around 10^{-5} to 10^{-4} S/cm. The dark conductivity is about 6 orders of magnitude lower than the photo conductivity and thereby below the precision of the used instrument (10^{-10}A). Therefore, the measurements were carried out with a CPM-setup (see next paragraph), which allowed the detection of these low currents. Since the sample is under vacuum conditions during this measurement, surface effects like humidity (causing leakage currents) can be neglected. Typical values for the dark conductivity a-Si:H are around 10^{-11} S/cm.

Microcrystalline p-layers

The microcrystalline p-layers were examined in the same way as described for the i-layer material. Since the conductivity of a microcrystalline p-layer is about four orders of magnitude higher than for an i-layer, the measurement sometimes was carried out on complete n-i-p devices, neglecting the influence of the relatively high-ohmic i-layer compared to the

p-layer. One advantage of this method was the possibility to characterize the p-layer material which was actually used in the device. Typical values for the conductivity in good microcrystalline p-layers are around 1 – 10 S/cm.

4.1.3 Other methods

Determination of the defect density
The constant photo current method (CPM) allows to measure the absorption coefficient for values of $\alpha \cdot d \ll 1$ down to $\alpha \sim 10^{-2}$ cm^{-1}. This range is not accessible with the *R-T*-measurement already described. The CPM method is also a photo conductivity experiment: the intensity of a monochromatic light beam is adapted to keep the generated current constant for all used wavelengths. The used wavelengths were between 565 and 1550 nm, corresponding to photon energies of 2.2 to 0.8 eV. With this method, one gets a relative devolution of the absorption coefficient. By aligning this spectrum to a spectrum obtained by the *R-T*-measurement described above, one can achieve an absolute scaling of the measured values. The principle of the method is described more detailed in [66], the experimental setup in [67]. The measurements were carried out at around 27°C.

A CPM spectrum can be divided into three parts: in the low energy range, the absorption by defects dominates the devolution of α. Towards higher energy, α increases exponentially with energy, this part is labeled Urbach tail. Here, mainly electron excitation from valence to the conduction band take place. The reciprocal slope of the absorption coefficient in the Urbach tail region is known as Urbach energy E_0. The Urbach tail region is followed by higher band-to-band transitions with corresponding energies.

As a measure of the integrated defect density N_d in a-Si:H, one can take the absorption coefficient at the photon energy of $\alpha_d = 1.2$ eV [68]: $N_d = \alpha_d \cdot C_d$. The correction factor C_d is assumed to be $2.6 \cdot 10^{16}$ cm^{-2} here [69]. Good values for the defect density and E_0 in a-Si:H are around 10^{16} cm^{-3} and below 50 meV, respectively.

Morphology
To gain some deeper insight into the correlation between the structure of the material and its optical properties, the morphology of some representative substrates was examined by means of scanning electron microscopy (SEM). This technique allows visualization of surface texture. A review of various techniques for the examination of rough surfaces is given in the work of Bennet and Mattsson [70].

4.2 Solar Cells

A good introduction in solar cell characterization is given by Heidler in [71]. An equivalent circuit and a schematic light current voltage characteristic (JV characteristic) of a solar cell is shown in figure 4.3.

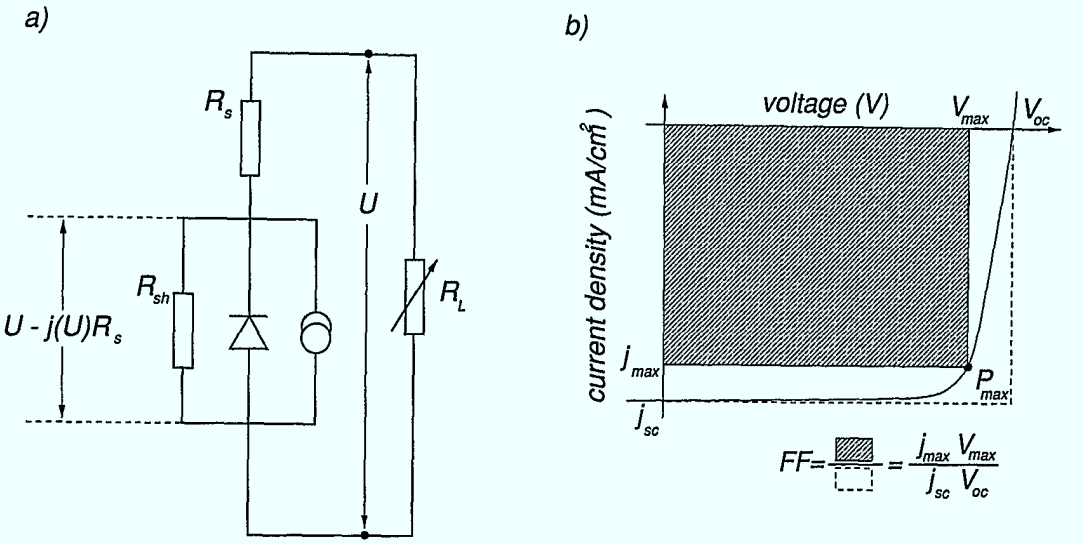

Figure 4.3: a) Equivalent circuit of a solar cell with shunt (R_{sh}), series (R_s), and load resistance (R_l) b) Scheme of a light JV characteristic with important JV parameters (see text).

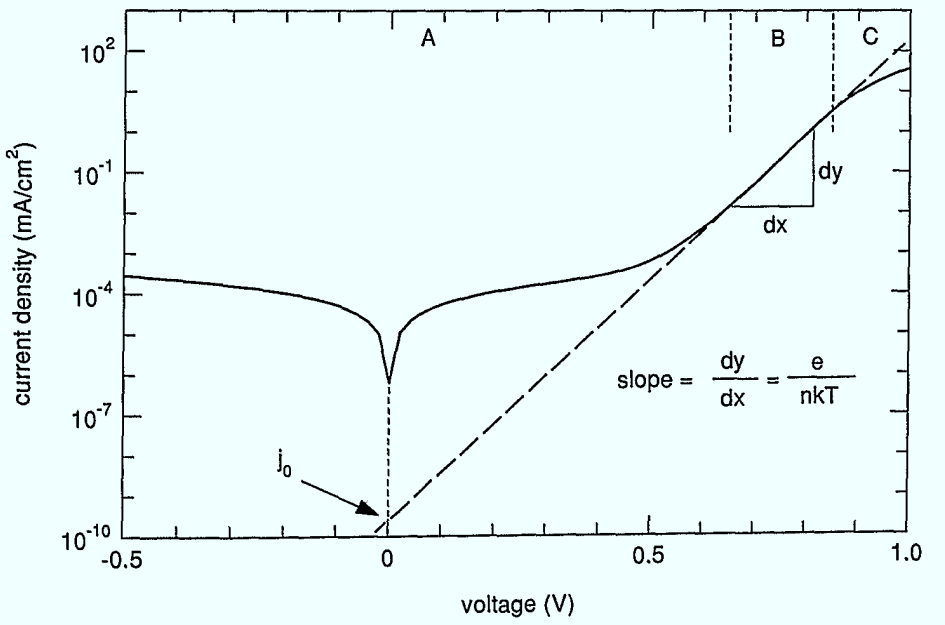

Figure 4.4: Typical dark JV characteristic of a n-i-p solar cell and corresponding dark JV parameters determined by linear fitting of the exponential part of the curve.

4.2.1 Current-voltage characteristic

The measurement of the current-voltage characteristic (JV characteristic) is the primary method to evaluate the solar cell. All light JV measurements (as well as the photo conductivity measurements described before) were performed at 25 °C with a two-source solar simulator, type WACOM-WXS-140S-Super, which is a so called "class A" simulator creating a calibrated AM1.5 spectrum with 100 mW/cm^2 light intensity. The temperature control was done with an automatic nitrogen cooling system. Before each measurement, a crystalline reference diode served as calibration for the correct light intensity and the homogeneity over the substrate area (10 by 10 cm^2). This procedure granted a very high reproducibility of the measurements. For simple spectral evaluation, a variety of band-pass and cut-off filters was available. For the dark JV characteristic, the light source was covered with a shutter; to avoid influence from scattered ambient light, the whole setup was additionally covered with a black velvet sheet.

In the p-i-n case, the 36 individual cells per substrate could be contacted simultaneously and the measurement was carried out by a software program controlling a source-measure unit from Keithly Instruments Inc., type SMU238. In the n-i-p case, the contacting was done by hand and each single JV curve had to be recorded. Only the values for the 100 mm^2 cells were considered for evaluation; the other cells were used for diagnosis means only (e.g. contact problems, current collection, etc...). To avoid undesired current collection for the n-i-p solar cells (which contain microcrystalline p-layers with high lateral conductivities), a mask was used to cover the region outside the active cell area defined by the TCO top contact. The mask was manufactured by laser scribing with edge length of 9 mm resulting in 81 mm^2 illuminated cell area. To calculate the correct current density, this was considered by means of a correction factor; the factor also took into account the area losses by the grid system[b] supporting the current collection of the top TCO if implemented as thin anti-reflection coating (see section 5.1.1).

Dark JV curve

To measure the dark JV characteristic, the applied voltage was varied between -1 and $+1$ Volt. The temperature in this case was 25 °C, too. A measured dark JV curve is shown in figure 4.4. To allow the graphical representation in a logarithmic chart, the originally negative current values for negative voltages were multiplied by -1. In zone A, the shunt resistance of the solar cell dominates the devolution of the JV curve, while in zone C, the series resistance is predominant. In zone B, the current increases exponentially with applied voltage, resulting in a linear behaviour in the logarithmic chart. Assuming that the dark JV characteristic of an a-Si:H diode can be described with

$$j_d(U) = j_0 \cdot \left(e^{\frac{e \cdot (U - j(U) \cdot R_s)}{n \cdot k \cdot T}} - 1 \right) + \frac{U - j(U) \cdot R_s}{R_{sh}}, \tag{4.3}$$

[b]The grid system shaded ~14.04 mm^2 of the cell area left blank by the mask (see figure 3.5). The factor by which the measured current density had to be multiplied therefore was $k = \frac{100}{81 - 14.04} \sim 1.49$

the parameters j_0 and n can be determined from the linear fit of the JV curve in the corresponding region if the values of R_s and R_{sh} are low and high enough, respectively.

Light JV curve

To measure the light JV characteristic, the applied voltage was standardly varied between -0.2 and $+1$ Volt in 20 mV steps. The charge carriers generated by the illumination are separated by the electric field of the solar cell and driven to the recombination junctions. The dark current and the voltage dependent photo current add up to the total current:

$$j_l(U) = j_d(U) + j_{ph}(U) \tag{4.4}$$

From the light JV characteristic, one can determine several parameters (see figure 4.3b):

- The efficiency η is defined as the ratio of the maximum power generated by the device (given by $P_{max} = j_{max} \cdot V_{max}$) and the incident radiation power. The efficiency under AM1.5 illumination is the ultimate parameter of each solar cell.

- The fill factor FF defined as

$$FF = \frac{j_{max} \cdot V_{max}}{j_{sc} \cdot V_{oc}}$$

  gives a description of the "rectangularness" of the light JV characteristic and is an integral measure of the collection efficiency at the maximum power point.

- The short-circuit current density j_{sc} is the maximum current density generated by the device.

- The open-circuit voltage V_{oc} is the maximum voltage generated by the solar cell under illumination. In first approximation, the voltage can also be calculated by equation 4.4. The assumptions used here are a constant photo current and $j_{ph} = j_{sc}$. Hence it follows (the shunt resistance is neglected)

$$V_{oc} = \frac{nkT}{e} \cdot \ln\left(\frac{j_{sc}}{j_0} + 1\right) \tag{4.5}$$

Routinely, the slope of the characteristic at V_{oc} and j_{sc} are determined in addition. The reciprocal values are labeled shunt R^*_{sh} and series R^*_s resistance, respectively. The connection between these values and the true values for the shunt and series resistance (see figure 4.3a) is not straight forward and was for example investigated in [72]. Here, the values extracted from the light JV curve are for example used for evaluation of additionally introduced contact resistances. This evaluation is based on the experience gained in our group during the development of solar cells. Since the main contributions to the resistances scale with the cell area, it is reasonable to give the values referring to the cell area; the unit is therefore $\Omega{\cdot}\mathrm{cm}^2$. Whenever the term shunt or series resistance is used in this work, the reciprocal slope at the corresponding point of the JV characteristic is meant unless otherwise stated. In order to achieve a high fill factor and V_{oc}, the series resistance should be as small and the shunt resistance as high as possible.

4.2.2 Spectral response

The spectral response (SR) of a solar cell gives more detailed insight into the functioning of the device than the integrating light JV characteristic. From SR data, conclusions about the optical losses and the field distribution in the solar cell can be drawn. The absolute $SR(\lambda)$ of a solar cell is defined by

$$SR(\lambda) = \frac{j_{ph}(\lambda)}{B} \tag{4.6}$$

with $j_{ph}(\lambda)$ as generated photo current density per wavelength interval and B the power per area of the incident light. From absolute SR data one can calculate the quantum efficiency $QE(\lambda)$ of the device by

$$QE(\lambda) = \frac{j_{ph}(\lambda)}{e \cdot \Phi} = SR(\lambda) \cdot \frac{hc}{\lambda e} \tag{4.7}$$

with Φ as the number of photons per time unit, area, and wavelength interval (e is the elementary charge, h is Planck's constant and c the speed of light). For the measurement of the quantum efficiency, the differential spectral response method was used: a monochromatic sample beam is used to generate a small photo current, and the wavelength can be varied in the desired wavelength region. All measurements were carried out at 25 °C. Setup and method are described in [73] and [74], respectively. The quantum efficiency can be interpreted as probability for the contribution of an incoming photon to the photo current (by generation *and* collection of this carrier). Figure 4.5 shows the quantum efficiency of a solar cell as function of the wavelength. The total photo current can be calculated by

$$j_{ph}(U) = e \cdot \int QE(U,\lambda)\,\Phi(\lambda)\,d\lambda \tag{4.8}$$

For multijunction cells, component cells can be measured individually (see section 2.1.3) by means of different bias illumination. E.g. to measure the top cell in a tandem cell, the bottom cell is "saturated" with red bias light. In the thin top cell, much less charge carriers than in the bottom cell are generated by the bias light. Hence the top cell limits the total current, because the current flowing through both cells must be equal (series interconnection). The superposition of this bias signal with the actual measurement signal generated by the monochromatic sample beam allows to distinguish the individual response of the top cell. In first order, the increase of the photo current of the stacked cell depends on the generation of charge carriers in the top cell. Since the signal produced by the monochromatic sample beam is very small (due to the low intensity), linearity is provided. By saturating the top cell with blue bias light, the bottom cell can be measured in the same way.

Detailed discussions on the interpretation of spectral response data of amorphous silicon based solar cells can be found in the thesis of Fischer [75] or Schönecker [76], respectively.

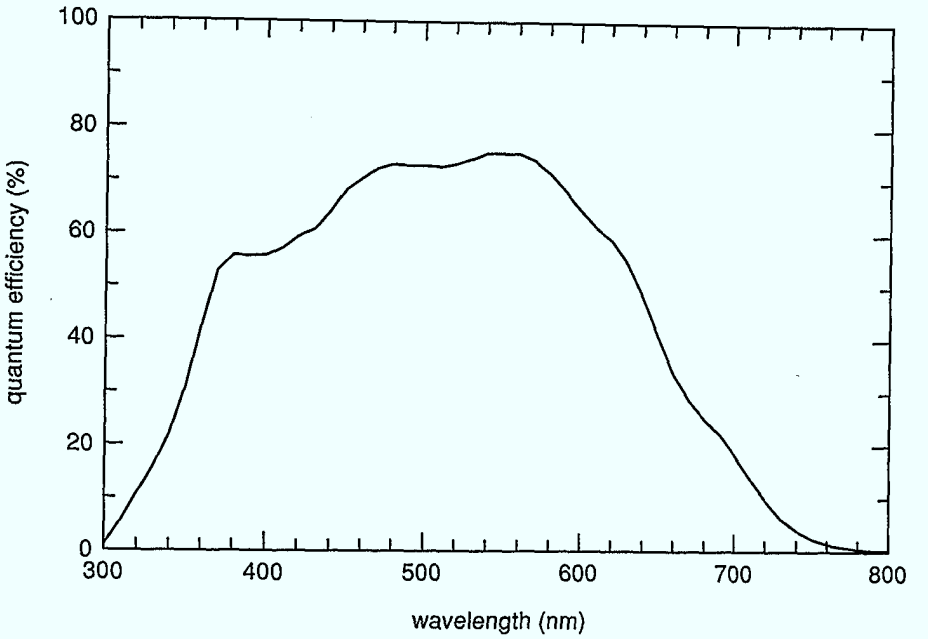

Figure 4.5: Quantum efficiency as function of the wavelength for a single junction a-Si:H p-i-n solar cell.

4.2.3 Degradation procedure

In section 2.1.2, the light induced degradation (SWE) was already mentioned. For the development of a-Si:H based solar cells, the evaluation of the long term stability is essential. To examine this effect, some typical solar cells in the p-i-n as well as in the n-i-p structure were degraded. In this work, the degradation experiments were conducted using an AM1.5 spectrum (100 mW/cm^2) at fixed solar cell temperature of 50°C and open circuit conditions, meaning that no current was flowing and that all generated carriers recombine. These conditions are defined by an international standard proposed by NREL[c]. The efficiency reached under these conditions after several hundred hours of light soaking are accepted as stabilized values [77].

The recombination rate in the described case equalizes the generation rate, which is higher than under real operation conditions, where most of the carriers are collected. By this way – the degradation of amorphous silicon is to a large extent caused by recombination processes – it should be warranted that the efficiency reached after the relatively short (600 to 1000 h) degradation procedure corresponds to values reached after years in normal outdoor operation. The chosen temperature of 50°C is approximately the value the cells exhibit when illuminated under real (full) sunlight.

[c]National Renewable Energy Laboratory, Golden, CO, USA

Chapter 5

Material Development

The results of the material development necessary for the development of p-i-n and n-i-p solar cells with zinc oxide (ZnO) front contact are presented in this chapter. First, the results of the transparent conductive oxide development are reported, including a comparison of indium-tin-oxide (ITO) and ZnO as material for the TCO top contact. The next section surveys a newly developed post deposition etching procedure which allows texturing of the initially smooth ZnO films. The microcrystalline p-layer development which is mandatory in order to obtain a low-ohmic ZnO/p contact is described in the following. Then the results obtained using RF and VHF plasma excitation frequencies are presented and compared. The last part of this chapter describes work performed to develop a low band gap absorber material for use in tandem cells.

5.1 Transparent Conductive Oxide

Zinc oxide is receiving growing attention as a TCO for amorphous and microcrystalline silicon based solar cells because of its superior transparency and hydrogen plasma resistance [78–81] compared to the commonly used fluorine doped tin oxide (SnO_2:F). Moreover, in combination with aluminum or silver, ZnO is standardly used to enhance back reflection in p-i-n and n-i-p solar cells. Especially in the latter cell type, the texture of the ZnO/metal back reflector strongly influences the device performance. In case of aluminum as back contact metal, ZnO also serves as diffusion barrier preventing contamination of the i-layer with Al [82].

Sputtered ZnO:Al films exhibiting resistivities in the range of 2×10^{-4} Ωcm and excellent transparency have already been prepared 15 years ago [83]. However, the successful application of sputtered ZnO films as front contact for a-Si:H solar cells was not reported.

For p-i-n type solar cells, textured TCO substrates with light scattering properties are essential for a high device performance. Regarding the sputtering technique, various surface textures of ZnO:Al can be achieved by reactive sputtering in Ar/H_2O atmosphere [84–86]. However, although films prepared by the addition of water vapour during deposition had a significant ability to scatter incident light, they showed a deterioration of the electrical properties.

5.1.1 Highly Conductive and Transparent ZnO Films

Minami et al. already reported a significant improvement of the electronic properties of sputtered ZnO prepared with reduced sputter gas pressure [83]. Following this approach, we were able to find the reported deposition regime as indicated in figure 5.1. On the left axis, the figure shows the resistivity ρ as function of the Ar pressure during the sputter process. We observe a clear drop in the resistivity when the pressure regime below 10 mTorr is entered. This change is attributed to structural changes in the polycrystalline material [64, 83]. In addition, there is a weak temperature dependence with slightly lower resistivities at higher substrate temperatures. A minimum resistivity of 2.2×10^{-4} Ωcm was obtained at a substrate temperature $T_s = 200°C$ and 0.3 mTorr Ar pressure for a 0.46 μm thick film which corresponds to a sheet resistance of $R_\square = 5\ \Omega$. Due to a nearly constant resistivity for films with a thickness above 100 nm prepared in the low pressure regime, sheet resistances as low as 1 Ω could be obtained with a thick film ($d = 2250$ nm). We also observe an increase in the deposition rate by lowering the gas pressure (see fig. 5.1, right axis), which is a beneficial side effect. All films showed no light scattering for visible light but an excellent transparency as desired for application in solar cells. As an example, the 0.46 μm thick film already mentioned showed an average transmission of 84.4 % between 400 and 800 nm.

Comparison of thin ITO and ZnO films

In order to test the applicability of the developed ZnO material as thin anti-reflection top contact in n-i-p solar cells, we conducted a comparison of ITO material [61] with the ZnO films described above. To avoid an annealing of the underlying solar cell, we limited the substrate temperature to values below 150 °C. All films in this series were already prepared on complete n-i-p devices and measured before applying the Ag grid system. As shown in figure 5.2, we achieved similar values for the sheet resistance $R_\square$ with both TCO materials. The increase in sheet resistance for thicknesses down to 100 nm is mainly the geometrical effect of reduced film thickness. For films below 100 nm thickness, the material properties slightly deteriorated and the sheet resistance increased more than being explained by the reduced thickness; values above 100 Ω were reached for these thin films. With both materials, it was possible to prepare films with a high transparency above 84 % (measured on glass) using substrate temperatures $\leq$150°C. For the ITO films applied later on, the resistivity showed values around 7×10^{-4} Ωcm, while the ZnO films showed resistivities around 4×10^{-4} Ωcm.

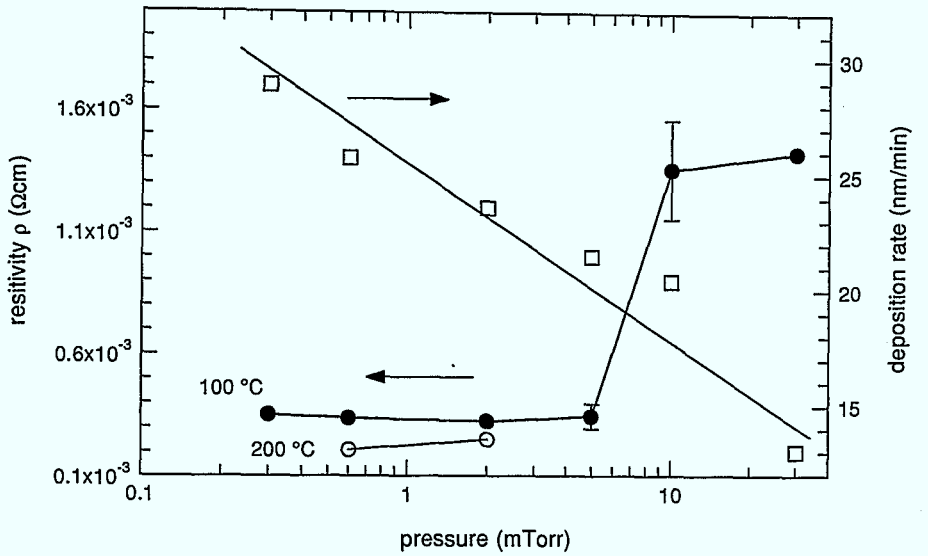

Figure 5.1: Resistivity and deposition rate as function of the Ar sputter gas pressure. The Ar flow was 10 sccm, the RF power 250 Watt and the substrate temperature 100 and 200 °C, respectively.

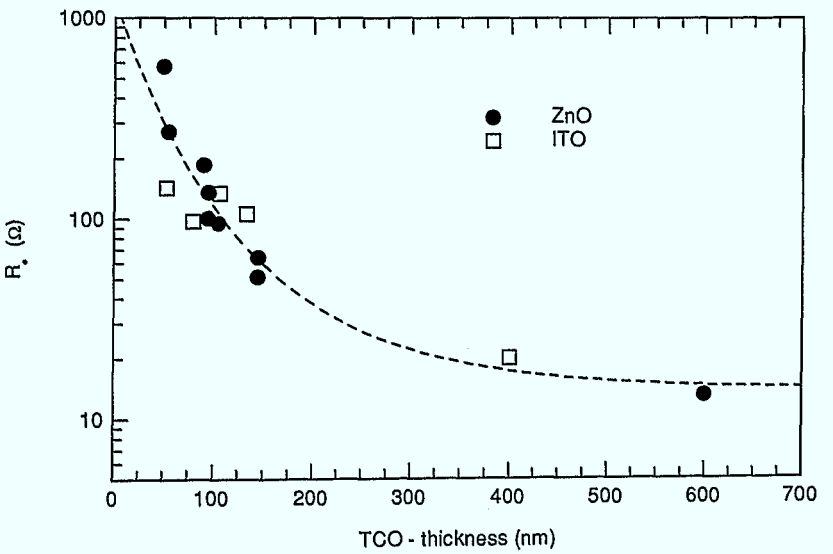

Figure 5.2: Sheet resistance as function of the film thickness for ITO and ZnO films. All films were measured in the device before applying the grid system.

5.1.2 Texture Etched ZnO

During his diploma thesis accompanying this work, A. Löffl discovered that certain ZnO films exhibited a scattering surface roughness at the edge of holes etched for later thickness evaluation of the films. This effect was used for the preparation of textured ZnO coated glass substrates [21, 22]. The material investigations related to sputtering and texture etching as well as the characterization of the light scattering properties of different ZnO films are conducted in a Ph.D. thesis by O. Kluth and are already partly published [21, 22, 64, 87].

The present work concentrates on the application of ZnO films in a-Si:H based solar cells, in particular the contact behaviour when used as front contact material in p-i-n and n-i-p type solar cells. In the following, the results of our approach for the preparation of textured ZnO films are highlighted. In this approach, the texture is achieved by a post deposition wet chemical etching step. The procedure of etching the films in diluted HCl is described more detailed in the diploma thesis of A. Löffl [21]. The films described in the following were obtained at 100°C substrate temperature and 2 mTorr in an Ar/O_2 atmosphere.

High resolution scanning electron microscope (HRSEM) micrographs illustrate the etching effect (see figure 5.3); the micrographs show the cross section of a glass/ZnO sample and the ZnO surface before and after etching. One can observe that a distinct surface roughness has been established by etching the film in 0.5 % diluted HCl acid. Further investigations of this effect showed that the ability to get a suited light scattering surface texture strongly depends on the deposition parameters applied during sputtering of the initially smooth ZnO film [64]. It is important to note that all films still show high transparencies after the etching process. Furthermore, the influence of the etching process on the electrical properties is negligible.

Figure 5.4 shows the results of optical measurements on one of these ZnO films (measured on glass). The total, specular and diffuse transmission as function of the wavelength indicate the light scattering properties of this film up to a wavelength of 700 – 800 nm. Moreover, excellent total transmission values can be observed. Figure 5.5 shows the haze function calculated from the transmission data of a film after applying different etching times. The haze-function describes the ratio of the diffuse to the total transmission (see section 4.1.1) and is a measure for the amount of scattered light per wavelength interval. It can be clearly seen, that the haze is easily controlled by varying the etching time. The light scattering properties in the long wavelength region of films with long etching times offers the potential for application in microcrystalline silicon based solar cells, since this cell type especially benefits from radiation in the higher wavelength region.

To summarize: We prepared highly conductive and transparent ZnO films on glass as well as on n-i-p devices at low substrate temperatures. A surface texture with distinct light scattering properties is obtained by a post deposition wet chemical etching step in 0.5 % diluted HCl. The light scattering properties of the p-i-n substrates can be easily controlled by the etching time in diluted HCl. With this development, a substrate for the p-i-n

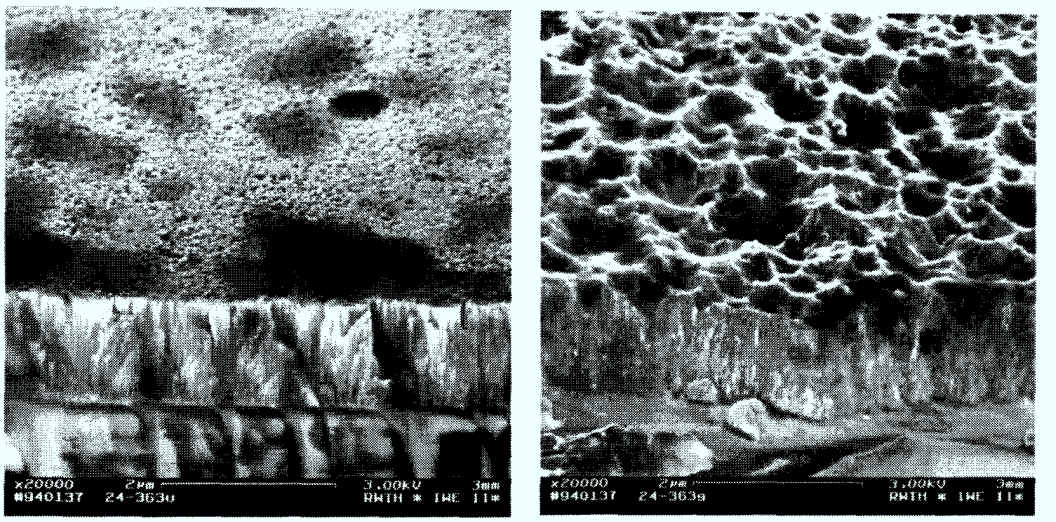

Figure 5.3: HRSEM micrographs of an as deposited (left) and texture etched (right) ZnO:Al film. Film deposition was carried out at 2 mTorr and 100 °C, the etching time was 20 s. Micrographs by S. Hoffmann, Institut für Werkstoffe der Elektrotechnik II, RWTH Aachen.

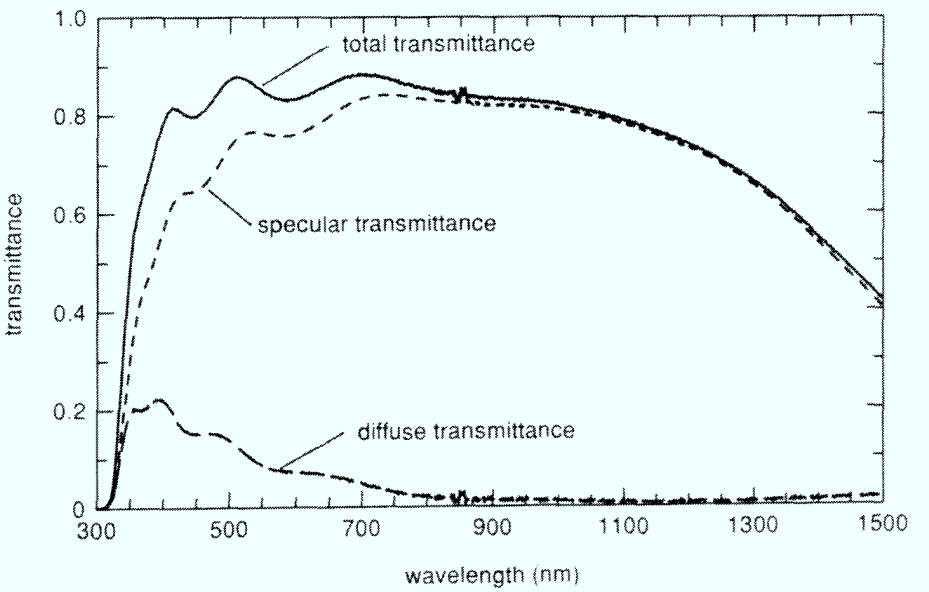

Figure 5.4: Total, specular and diffuse transmission of a texture etched ZnO:Al film. Etching was done in 0.5 % HCl-dilution.

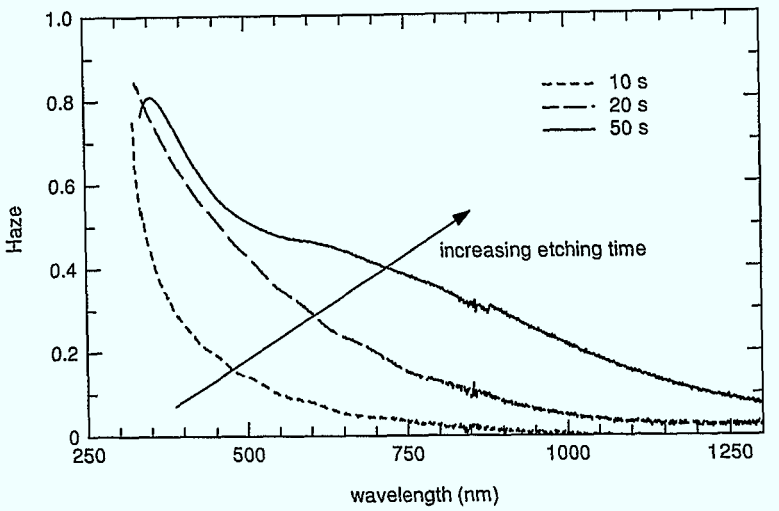

Figure 5.5: *Haze spectra of a ZnO:Al film after different etching times. Film deposition was done at 2 mTorr and 100 °C, the film thickness was 1000 nm before etching.*

investigations as well as highly conductive TCO films for application as top contact in the n-i-p cells were available.

5.2 Microcrystalline p-layers

As already explained in section 2.3, during the solar cell development it turned out that the insertion of a microcrystalline contact layer strongly improves the contact behaviour of the TCO/p contact. Thus we started the development of adapted microcrystalline p-layers for use in p-i-n and n-i-p solar cells with sputtered ZnO front contact, bearing in mind the additional requirements a p-layer has to fulfill: the p-layer should be as thin as possible to avoid optical absorption losses, but thick enough to built up a maximum V_{oc}.

Most methods commonly used for the characterization of microcrystalline films fail when employed for the investigation of very thin films [88]. Moreover, the properties of thin films may be distinctly different from those obtained in bulk material. This is one important reason which led us to the decision to use the solar cell device itself as a monitor for the evaluation of the contact layer as soon as a sufficiently high conductivity of the microcrystalline p-layers was reached. Our experience shows that this is the more promising way for evaluation of the contact behaviour of the p-layer compared to preparing p-layer samples with a following separate characterization. The latter way can only complete the

picture one gains from the working devices. Fine tuning of the deposition parameters was conducted during solar cell optimization.

Hence, to achieve quick results, with both excitation frequencies, we first optimized the deposition conditions (e.g. by changing the doping ratio, hydrogen dilution, deposition pressure, applied power[a]) with respect to maximum conductivity on glass only. However, the substrate temperature as another important parameter was varied during solar cell preparation only. Next, the roughly optimized deposition parameters were used to prepare the p-layers on a $\sim$ 100 nm thick i-layer predeposited on glass (see section 3.3). This served for the evaluation and optimization of the lateral conductivity and the growth conditions in the n-i-p structure later on (the contribution of the underlying i-layer exhibiting a conductivity lower by about $\sim$ 6 orders of magnitude can be neglected). Finally we implemented the p-layers in solar cell devices (p-i-n and n-i-p structure). Here, the FF and R_s^* , the slope of the JV curve at V_{oc} (see section 4.2.1), were used to evaluate the contact behaviour, and later on, j_{sc} was used for the optical optimization of the p-layers.

We investigated a broad deposition parameter regime for the preparation of microcrystalline p-layers, including variation of the plasma excitation frequency between 13.56 MHz and 110 MHz. The first one is a standard industrial radio frequency (labeled RF) while the latter one is in the very high frequency regime and is labeled VHF in the following. In the laboratory, the VHF technique is sometimes preferred because of its beneficial effect on microcrystalline growth [50, 89]. For large scale production there is a strong desire to use RF excitation which is alloted to industry. Moreover, it is compatible with the existing production technology and homogeneous films are more easily achieved on large areas with the RF technique.

General remark

The thickness dependency of the conductivity of a microcrystalline p-layer is shown in figure 5.6 and can be understood with the island-growth model already described in section 2.3 and taking into account that only the lateral conductivity is accessable by the measurement setup (see figure p. 29). In the beginning, only some crystallites are embedded in an amorphous matrix, and the conductivity is low. With increasing film thickness, more and more interconnections of the crystallites occur and so-called "percolation-paths" emerge, so the conductivity increases. Once the film has built up an interconnected structure, the transport is dominated by the bulk properties of the film and the conductivity saturates. Typically, this happens at a film thickness of some ten nm. This behaviour was observed for all investigated films. However, for application as contact layer in solar cell devices, the critical point here is to prepare highly conductive *thin* microcrystalline films. These films are in general to thin to be dominated by bulk properties.

[a]At this point, I would like to thank T. Roschek for conducting the RF experiments for the microcrystalline p-layer investigations at high powers within his diploma thesis.

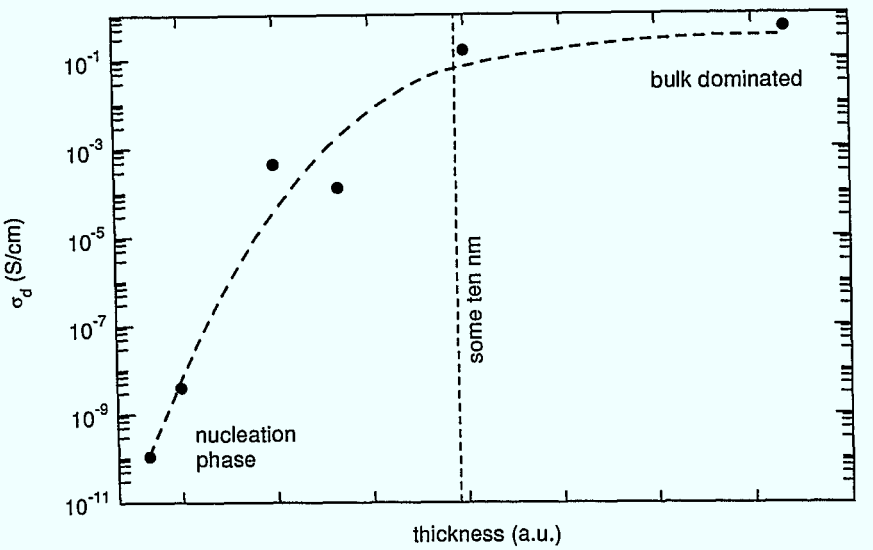

Figure 5.6: *Dark conductivity versus thickness of a microcrystalline p-layer. See text for explanation.*

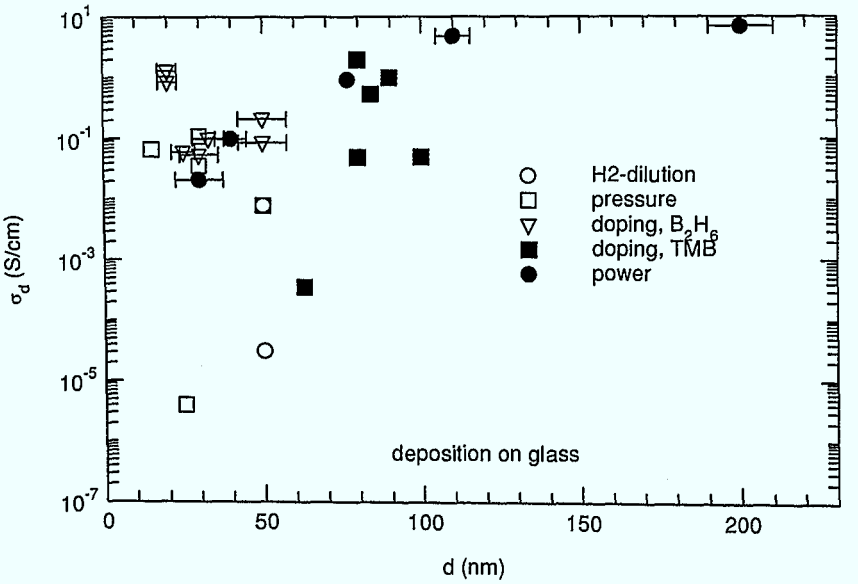

Figure 5.7: *Dark conductivity of microcrystalline p-layers prepared with the RF technique on glass. For the variation of the different parameters see text and table A.1.*

5.2.1 RF Technique

Figure 5.7 shows the dark conductivity versus film thickness of microcrystalline p-layers prepared with the RF technique on glass. Note that not all measurement points are equipped with error bars; nevertheless, the thickness error is generally around ± 10 nm absolutely and the conductivity values scatter by 1 – 2 orders of magnitude on the same substrate sometimes. This is mainly due to inhomogeneous deposition conditions which are especially critical for thin films and also depend on the conditions of the substrate surface e.g. cleanliness, initial roughness, pretreatment, etc. ...

The detailed deposition parameters of all films shown in figure 5.7 (and others, too) can be found in table A.1 in the appendix. The figure shows the dark conductivity of an optimization series as function of the film thickness. As already described in 3.1.1, a high hydrogen dilution of the process gas silane is a prerequisite for the deposition of microcrystalline silicon films. Accordingly, the first rough optimization step was the variation of the hydrogen dilution (○) at a fixed hydrogen-flow of 200 sccm by adjusting the silane-flow. After this, the pressure was varied to obtain homogeneous deposition (□). This was followed by a doping series at 3000 mTorr, 5 Watt, silane-flow of 0.75 sccm and a hydrogen-flow of 200 sccm (▽, ■). In the next step, higher power was applied (•). The most critical parameter turned out to be the pressure and the doping ratio. Here, already small variations led to drastic changes in the measured conductivity.

All films so far were doped using diborane as doping source. From previous work in our group, this gas is known to cause cross-contamination problems [90] which can be avoided by using a CO_2-plasma step between each deposition in the p-chamber. However, results were not satisfactory with respect to reproducibility. Hence, we applied trimethylboron (TMB) – $B(CH_3)_3$ – as doping source, which has a higher thermal stability than B_2H_6. Though microcrystalline growth is expected to be disturbed by the presence of carbon [91], we achieved only slightly lower conductivity values with TMB.

To widen the optical band gap of the amorphous phase within the microcrystalline film, the addition of carbon or oxygen is used [91, 92]. In our experiments, the additional use of methane – CH_4 – led to only slight deterioration of the conductivity, at least for relatively thick films (between 50 and 100 nm), see table A.1. In all cases, the optimum deposition parameters found here led to conductivities around 0.1 S/cm for thin films ($d \leq 60$ nm) with both doping gases and also when using methane; this should be sufficient for the application as contact layers in the solar cell development.

In n-i-p solar cells, the p-layer grows on an amorphous substrate (the i-layer). Hence, the growth of microcrystalline p-layers on a-Si:H was investigated in the following. Applying the optimized recipes for the microcrystalline p-layer to a-Si:H substrates, the conductivity dropped by several orders of magnitude even for relatively thick films. This indicates that the films are amorphous rather than microcrystalline – a distinct hint to the dependency of the film growth on the starting conditions determined by the substrate. Pellaton et al. [93] reported on controlled nucleation of thin microcrystalline films in the inner p/n-junction of tandem cells by means of pretreatment of the growth surface. Motivated by that work, we

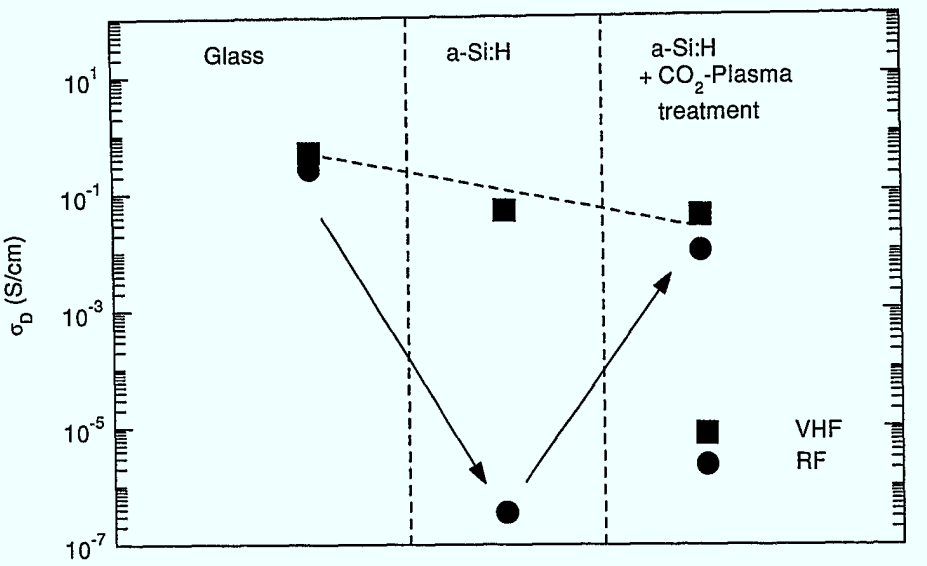

Figure 5.8: Dark conductivity of microcrystalline p-layers with various substrate conditions for the RF and VHF technique. With the RF-technique, the conductivity dropped down several orders of magnitude when deposited on intrinsic a-Si:H. By an additional CO_2-plasma treatment, it nearly recovered.

tried to promote the nucleation of our films by a pretreatment with a CO_2-plasma. Figure 5.8 shows the dark conductivity of films prepared under identical deposition conditions but different power on glass, intrinsic a-Si:H and intrinsic a-Si:H plus a CO_2-plasma treatment. After dropping by 6 orders of magnitude when prepared with low power on a-Si:H instead of glass, the conductivity recovered by 5 orders of magnitude after a CO_2-plasma treatment of the a-Si:H surface. The effect is not fully understood yet; probably the surface reaches a SiO_x-like status similar to glass (SiO_2) by oxidation. However, the pretreatment of the growth surface remains an interesting way to promote nucleation of doped films on an a-Si:H substrate. When using higher power (25 Watt), microcrystalline growth was obtained on a-Si:H without additional pretreatment and with only slight drawbacks in conductivity. As mentioned, more detailed results about our investigations using high power can be found in the diploma thesis of T. Roschek [94].

5.2.2 VHF Technique

Extensive work on the preparation of microcrystalline p-layers at very high frequencies (70 MHz) was already conducted in the Ph.D. thesis of R. Flückiger [95]. We were able

to start our study on basis of this thesis and our experience gained with the RF investigations of microcrystalline p-layers. We started our investigations at 110 MHz with adapted deposition parameters. A lower pressure was necessary in order to achieve stable plasma conditions (200 mTorr, 10 Watt). The most critical parameter for *thin* microcrystalline p-layers with respect to high conductivities in the work of Flückiger as well as in our own experiments turned out to be the doping ratio. Flückiger found an optimum ratio of 0.6 % diborane in silane at 70 MHz. In good agreement, our experiments at 110 MHz yielded a value between 0.6 and 0.7 %. Since our first experiments immediately led to thin microcrystalline films with very high conductivities, no detailed investigation of the parameter space was conducted with the VHF technique. We obtained values up to 1.5 S/cm for the dark conductivity of films prepared on glass and around 0.1 S/cm on intrinsic a-Si:H without additional steps (see figure 5.8). Also, the replacement of diborane with the thermally more stable trimethylboron caused no significant drawbacks in conductivity but led to a higher reproducibility of the results. Similar to the RF technique, fine tuning of the deposition parameters was conducted during the solar cell development.

5.2.3 RF versus VHF technique - Conclusion

In both cases, an optimization of the deposition parameters led to preparation of thin microcrystalline p-layers with satisfying homogeneity. The process window for preparation of high quality films is very narrow in both cases. However, the preparation of microcrystalline doped p-layers on a-Si:H was more difficult to achieve with the RF technique; with RF excitation, higher powers were necessary to obtain microcrystalline growth on a-Si:H without additional conditioning of the growth surface. Moreover, the conductivity of films prepared with the VHF technique was slightly higher on an a-Si:H substrate.

The goal of this optimization study – to obtain highly conductive microcrystalline p-layers on glass as well as on a-Si:H – has been achieved. Now solar cells incorporating these films as contact layer will show the suitability of the developed p-layers.

5.3 Intrinsic a-Si:H Material

As mentioned in section 2.1.3, different band gaps of the absorber layers in the individual cells of a tandem cell allow a more efficient use of the solar radiation. The successful development of wide gap material for the application in the top cell of tandem solar cells was already done in our group [10, 96, 97]. So far, we standardly use i-layer material with a band gap of $E_{04} = 1.86$ eV as absorber material in the bottom cell. The question remained, if it is possible to develop a-Si:H films with a lower band gap for the use in bottom cells. Moreover, for the a-Si:H/μc-Si (micromorph) tandem cell, the amorphous top cell has to match the high current delivered by the microcrystalline bottom cell; here, a low band gap absorber is desired, too.

5.3.1 Literature Concepts

A wide variety of concepts to prepare low gap a-Si:H material can be found in literature. All concepts have in common the desire to influence the growth mechanism in a way to prefer the growth of a-Si:H with a compact structure and low amount of hydrogen, which should preferably occur in Si–H bonding configuration. Most attempts can be categorized into of the groups described in the following.

One direct way for lowering the band gap is to increase the substrate temperature during growth of the film [98, 99]. However, attention has to be payed to impurity incorporation caused by higher outgasing rates of the reactor walls. Moreover, in the p-i-n structure, experience shows that the solar cell performance deteriorates when temperatures above 200 °C are used [100]. Another way is the attempt to promote surface reactions during growth of the intrinsic material by application of additional energy directly to the growth surface. This can for example be done by gas heating [101], vibrations generated by a piezoelectric device [102], in situ ultraviolet laser treatment [103], influencing the precursor selection and energy [104, 105], or by additional feeding of inert gases like He, Ar, Ne into the plasma. In the latter case, observations are quite contradictory: some groups report lower band gap with inert gas dilution of silane [106, 107] while others report higher or equal optical gap with this method [108, 109]. Low deposition rates are also seen as a way to support the growth of a rigid and stable a-Si:H network [62, 110–112]. Other concepts like the chemical annealing or layer-by-layer technique [113, 114] are still under discussion.

5.3.2 Followed Approaches

In this study, we followed the most promising attempts which could be conducted without major changes of the deposition system in our own laboratory.

Use of Helium dilution of the process gas
The work on helium diluted i-layer material was conducted together with R. Platz from the University of Neuchâtel (Switzerland) and was mainly motivated by results from Ray et al. [106]. These authors reported the decrease of the optical gap by more than 150 meV at higher pressures using helium dilution of the silane process gas. Our main goal in this subtopic was to reproduce these results. Since the problem in transferring results from different reactor geometries is always given, we made a broad "scan" of the parameter space. We deposited 25 He-diluted intrinsic layers comprising a dilution series (He-flow to SiH_4-flow ratio 1–30), a pressure series at dilution 15 (1.3–6 Torr) and 5 (1.5–3 Torr) and a power series (2–6 Watt) at 1.3 Torr and dilution 15. The FTIR method was used to determine the hydrogen content via the integrated absorption of the 630–mode [115] and the microstructure factor via the ratio of the 2080 to the 2080+2000–mode [116, 117].

Although we found the hydrogen content to vary between 8 % and 13 %, the E_{04} gap remained remarkably constant, which is quite surprising considering the fact that usually a strong correlation between hydrogen content and band gap is reported (e.g. [118] and

references therein). However, neither the determination of the hydrogen content via IR-spectroscopy nor the mentioned correlation is clearly seen by all groups. It was possible to prepare i-layer material with a low hydrogen content and values of the microstructure factor still below 0.1. Another interesting point was the increase in the deposition rate by a factor of 3 compared to our standard i-layer material ($\approx$ 1 Å/s). This is of particular interest for production.

During the variation of the parameters, we sometimes observed sparking during deposition and after the helium experiments the reactor had to be cleaned due to the formation of yellow dust during the deposition process. It remains an open question if this was caused by the use of helium or simply by the wide variation of deposition parameters.

Application of high substrate temperatures

The effect of higher substrate temperatures was investigated after equipping our deposition system with high-temperature capable heaters which allowed heater temperatures up to 700 °C (substrate temperature $\approx$ 450 °C). Figure 5.9 shows the absorption coefficients versus photon energy of i-layers prepared at different substrate temperatures as indicated in the figure. Table 5.1 shows the experimental results obtained at 400 °C substrate temperature compared to our so-called standard material which is deposited at 200 °C with a hydrogen dilution of 1. By raising the substrate temperature up to 400 °C, it was possible to decrease the E_{04} gap by about 180 meV. In addition, the deposition rate increased from 1.3 Å/s at 200 °C to 1.67 Å/s at 400 °C. However, the films showed a higher defect density as determined by CPM spectra compared to our standard device quality material prepared at 200 °C. By an optimization of the process parameters we could improve the material quality again, but the values were still worse compared to the standard material. A previous result obtained in a diploma thesis [96] was the observed trend of a higher defect density N_d and a higher Urbach energy E_0 with lower band gap, which is confirmed by the results obtained here. Another interesting side effect was the achievement of extremely high deposition rates ($>$ 20 Å/s) by the application of high power at high gas flow rates.

Preliminary remark: during the solar cell development at these high substrate temperatures ($\sim$ 400 °C), severe substrate related problems occurred during deposition which are not clarified yet (darkening of the substrates, peeling of the silver grids, etc ...). The solar cells deposited in this high temperature regime could not be characterized. However, since the main interest of this work was to demonstrate and compare the potential of the two different solar cell structures and not to optimize the final device performance to the very best, no further investigations were made related to this topic.

Effect of gas heating

The motivation to preheat the gas before introducing it into the plasma came from promising reports in literature, e.g. [101]. For the gas heating study, the last part of the main gas line into the reactor was equipped with a heating device to heat the pipe up to 600 °C. The setup is sketched in figure 5.10. The gas heater temperature was set with a proper temperature controller.

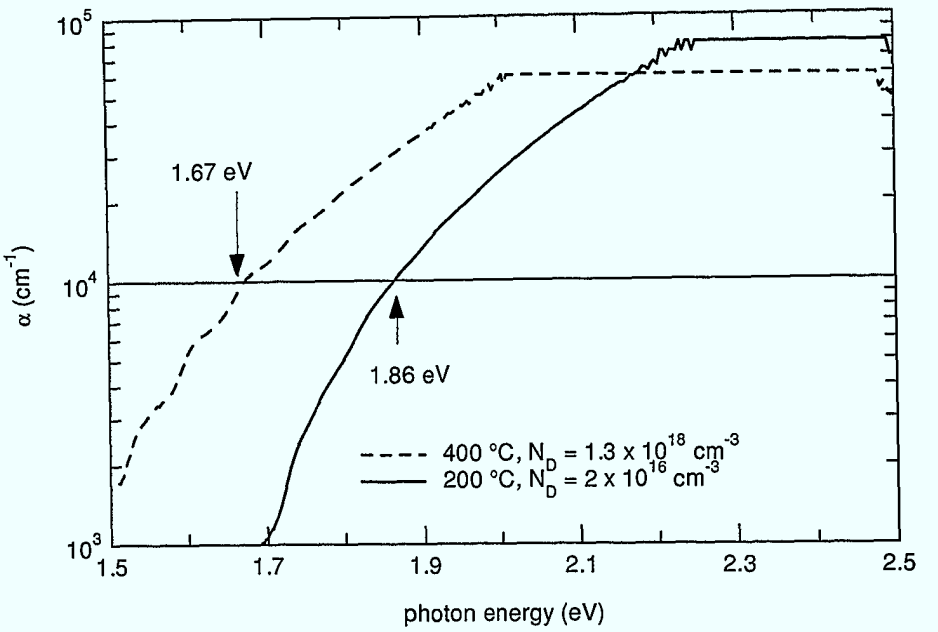

Figure 5.9: *Absorption coefficient versus photon energy for an i-layer prepared at 400 °C substrate temperature compared with standard i-layer material prepared at 200 °C. The defect density N_d was determined by CPM.*

T_s (°C)	T_{gas} (°C)	d (μm)	E_{04} (eV)	σ_d (S/cm)	E_f (eV)	E_0 (meV)	N_d (cm^{-3})	remark dep. par.
400	0	1.58	1.68	2.58e-10	-0.7	56	1.3e18	pure silane
400	0	0.96	1.75	3.33e-10	-0.69	52	2.0e17	H_2-dil. 10
400	0	1.17	1.76	2.36e-10	-0.7	52	1.1e17	1500 mTorr
400	0	2.2	1.79	1.87e-10	-0.71	56	1.4e17	high power
200	0	0.7	1.86	6.43e-11	-0.74	51	2.5e16	"standard"
200	600	0.65	1.85	2.28e-12	-0.82	46	4.2e15	"standard"

Table 5.1: *Material parameters obtained at high substrate temperatures (substrate temperature T_s, gas heating temperature T_{gas}, thickness d, E_{04} gap, dark conductivity σ_d, Fermi level position E_f, Urbach energy E_0, and defect density N_d). The last column gives a rough description of the deposition parameter altered. The photo conductivity of all films shown here is in the 10^{-5} S/cm range. The last row shows one sample prepared at standard temperature but with additional gas heating.*

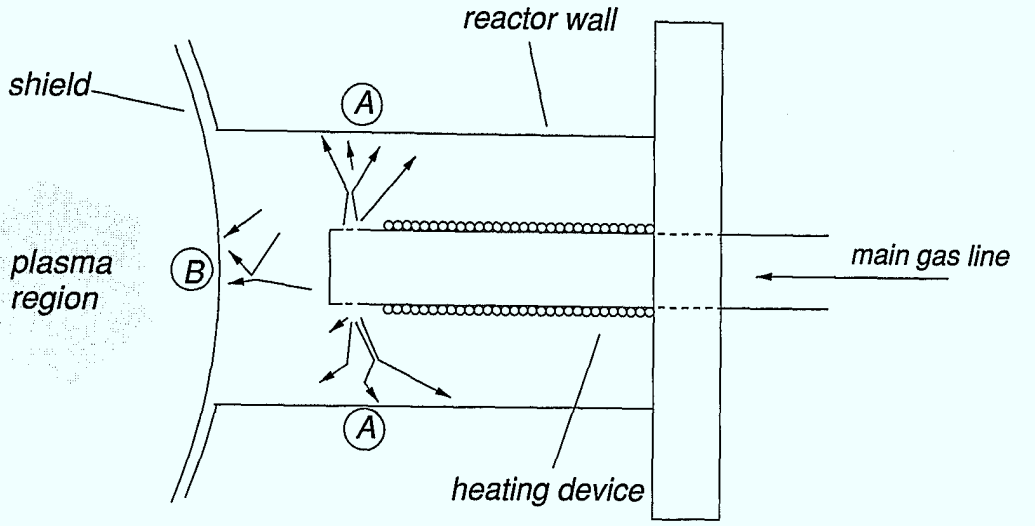

Figure 5.10: Schematic sketch of the gas heating setup. The heating device was connected to a controller to set the temperature in the range between room temperature and 600 °C.

At first glance surprisingly, the band gap of the i-layers did show no effect at all, even when using temperatures of 600 °C. The only reasonable explanation in our opinion is an ineffective gas heating: As indicated in figure 5.10, the heated gas first hits the relatively cold reactor wall (spot A). After this, the shield which confines the plasma (and has no elevated temperature, too) has to be passed (spot B). In the pressure regime of $p \approx 1$ Torr, a single gas molecule has a mean free path length l in the sub-mm-range ($l \approx (\frac{p}{kT} \cdot 4\pi r^2)^{-1}$), with r $\approx 1 \times 10^{-10}$ m as the molecule radius), resulting in more than 20 collisions before reaching the beginning of the plasma region. To equalize its temperature with the surrounding gas atmosphere, only 2 – 3 collisions are necessary. Thus, it stands to reason, that the gas most probably is cooled down again when reaching the plasma region.

Interestingly enough, the film prepared with these high preheating temperatures showed a defect density which was lower than anything observed before in our lab as determined by CPM measurements, namely 4.2×10^{15} cm^{-3}. Also the Urbach Energy E_0 showed an extremely low value of only 46 meV (see table 5.1). A standard i-layer prepared at 200 °C contains around 2.5×10^{16} cm^{-3} defects and shows an E_0 value of about 51 meV. The improvement could be due to a different precursor composition of the gas molecules when contributing to the growth of the film, since by the preheating step a significant amount of the gas was already dissociated thermally before reaching the plasma. Due to a lack of time, this interesting effect was not investigated further. Solely a single p-i-n solar cell containing this low defect material as absorber material was prepared and degraded together with a standard p-i-n solar cell containing a standard i-layer (both cells were prepared on Asahi type U substrates). No beneficial effect of the gas heating was observed after 1000 h of light soaking.

In summary, neither the use of helium dilution nor the gas heating affected the band gap of the prepared i-layers significantly. Interesting side effects were an enhanced growth rate by using helium dilution and the decrease of the defect density by almost one order of magnitude due to the gas preheating step. Raising the substrate temperature resulted in the decrease of the E_{04} gap of about 180 meV at 400 °C, which is well known from literature reports. However, the film quality deteriorated compared to our standard i-layer material prepared at 200 °C.

Chapter 6

Solar Cell Development

In this chapter, first the p-i-n development on textured ZnO substrates is presented, followed by the results on n-i-p solar cells with ZnO front contact. Both parts begin with the implementation of the microcrystalline p-layers described in the previous chapter. The crucial requirements necessary to achieve a high FF and a high V_{oc} are pointed out. This is followed by the results of the blue response optimization in order to obtain a high short circuit current density necessary for maximum efficiencies. The status achieved by combination of all optimized materials is presented together with the achieved results for highly efficient tandem solar cells. The application of low band gap i-layers in p-i-n and n-i-p cells is discussed briefly.

6.1 p-i-n Solar Cells on ZnO

The successful development of ZnO coated substrates with excellent light scattering properties motivated the development of p-i-n cells on these ZnO substrates. The films developed combine a high transparency with the high conductivity needed for the front contact. The substrates used throughout this study consisted of post deposition texture etched ZnO films on glass with varying initial thicknesses between 0.5 and 1 μm. All solar cells contain a standard amorphous i- and n-layer prepared at 200 °C.

In all cases, FF and R_s^* served as a monitor for the quality of the p/TCO contact barrier. Amongst the 36 solar cells on each substrate, various sizes of cells were present (see figure 3.5). By comparing the FF and R_s^* values of differently sized cells, one can distinguish between a p/TCO contact barrier and a high sheet resistance of the top TCO, both causing a low FF: A contact barrier does not scale with the cell area, while a high sheet resistance

of the top TCO takes more effect in the case of higher absolute currents[a], since ohmic losses increase with the square of the current ($P_{loss} = I^2 \cdot R$)

Before presenting the amorphous-p/ZnO contact problem and its solution by means of adapted microcrystalline p-layers, the good light trapping properties obtained with the newly developed ZnO material are demonstrated. Note that parts of this work have already been published [22, 120]. Figure 6.1 compares the quantum efficiency of two single p-i-n solar cells with the same i-layer thickness (360 nm) and an amorphous p-layer prepared on smooth and textured etched ZnO/glass substrates. The back contact of both cells is highly reflective ZnO/Ag. Comparing the two cells, we observe an increase of j_{sc} by about 3 mA/cm^2 for the cell on the texture etched substrate to an overall value of 16 mA/cm^2. The main improvement is due to an enhanced absorption by multiple internal reflection of light in the long wavelength region ("light trapping"). The achievement of the high short-circuit current-density demonstrates the good optical properties of the texture etched ZnO substrates for p-i-n solar cells. However, both cells exhibit relatively low FF below 63 % due to the poor electronic quality of the amorphous-p/ZnO contact. In the following, the p-i-n solar cell development was conducted on these texture etched ZnO substrates.

Why do we need a microcrystalline p-layer at all when using ZnO as TCO material? Figure 6.2 clearly illustrates the problem of the amorphous p/ZnO contact; the figure shows the JV curve of a p-i-n solar cell containing an amorphous p-layer on a ZnO substrate and for comparison the JV curve of a codeposited cell prepared on a SnO_2 substrate. A contact barrier at the ZnO/amorphous-p interface [40] leads to the "S"-shaped curve of the cell on ZnO. This contact barrier deteriorates the fill factor of the device. In contrast, the solar cell on the SnO_2 coated substrate does not show this anomaly.

6.1.1 Development of a Microcrystalline p-layer on ZnO

From previous work on p-i-n type solar cells [40–42] we already know that the insertion of a microcrystalline contact layer between the amorphous p-layer and the ZnO film provides a low-ohmic TCO/p contact, however, the additional film introduces optical losses. Following these results, we started our work with the insertion of a microcrystalline p-layer between the ZnO and the amorphous p-layer. Since it is reported that high excitation frequencies are beneficial for the growth of microcrystalline silicon [50], we started our investigations with the microcrystalline p-layers developed with VHF excitation at 110 MHz. Most series were repeated later on using RF frequencies with high power (25 Watt). Also, in the beginning, diborane was chosen as doping source. However, later on we switched to the thermally more stable trimethylboron ($B(CH_3)_3$), which caused no drawbacks in device performance after some fine tuning steps.

[a] Another way to examine the resistances is to vary the light intensity; a contact barrier is present at all intensities, while a high sheet resistance only dominates the JV curve at high intensity. M. Götz of the Neuchâtel group has conducted detailed investigations using this method within his thesis [119].

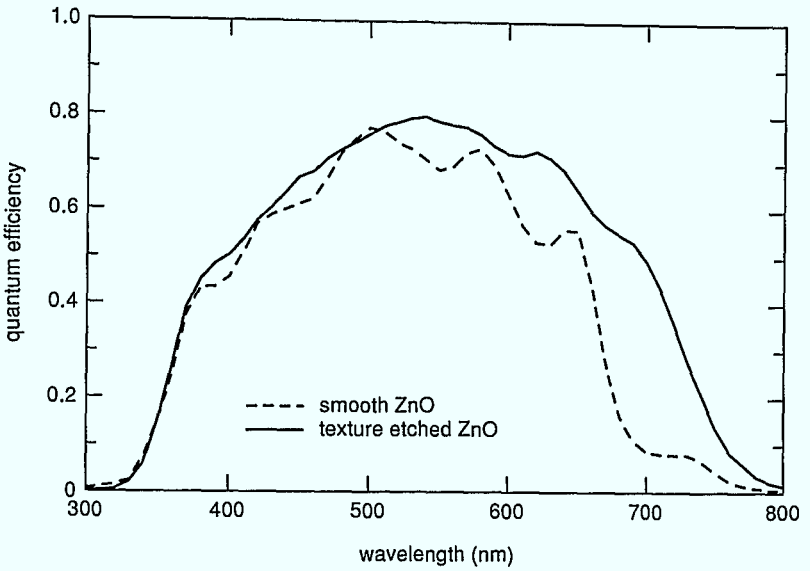

Figure 6.1: Quantum efficiency of two p-i-n solar cells with amorphous p-layer on ZnO substrates. The solid line represents a cell on an as-deposited (smooth) substrate, while the other corresponds to a cell prepared on a texture etched substrate. Both cells contain a highly reflective ZnO/Ag back contact.

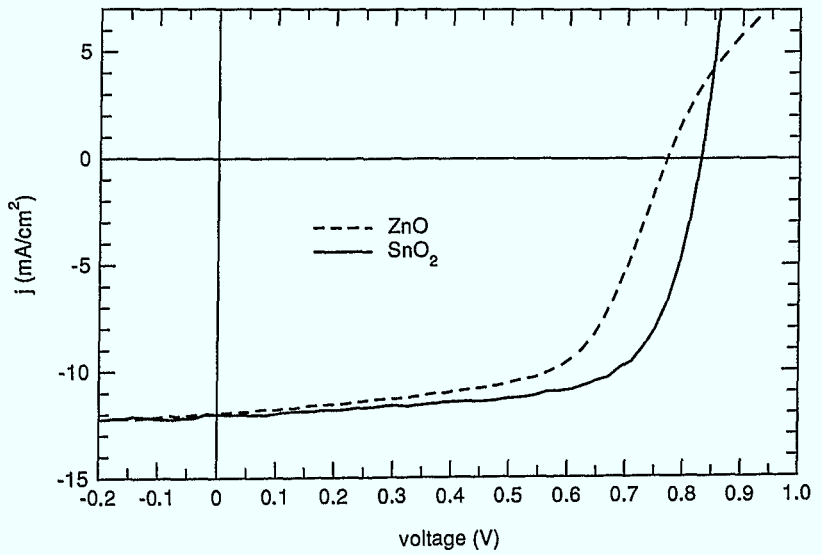

Figure 6.2: JV curve of a solar cell with an amorphous p-layer and a ZnO front contact (dashed). For comparison, the same cell on a SnO_2 substrate is shown (solid). One can clearly observe the "S"-shape behaviour at $j = 0$.

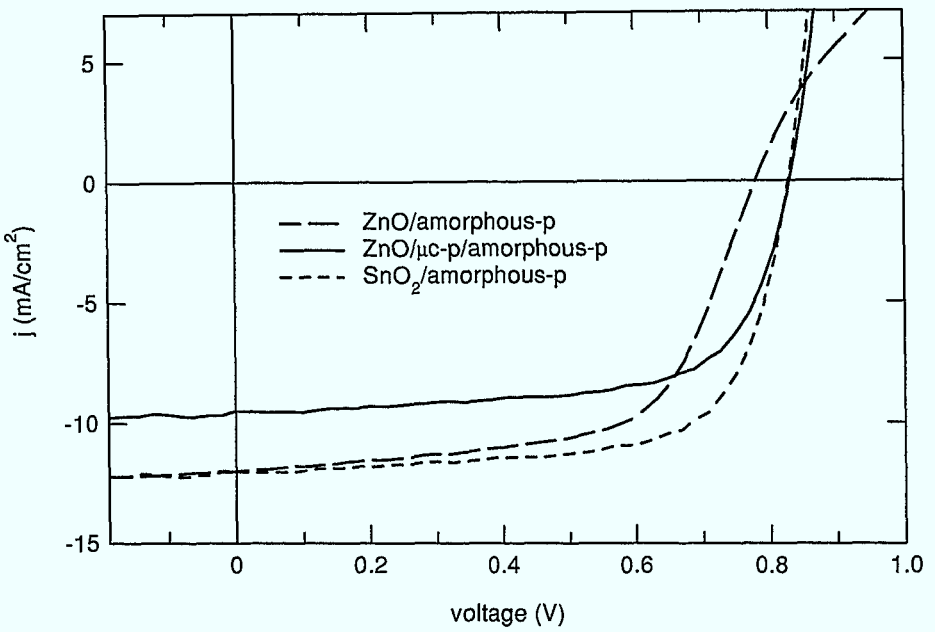

Figure 6.3: *JV characteristics of amorphous silicon solar cells with various p-layer structures.*

The p/ZnO contact

Compared to the purely amorphous p-layer, the insertion of a relatively thick microcrystalline p-layer improved the FF by about 4–6 % absolutely to values above 71 %. The corresponding JV curve is shown in figure 6.3 together with the two curves of figure 6.2. The improved contact behaviour indicated by a high FF can be clearly observed. However, the additional layer introduces optical absorption losses which consequently reduce the current delivered by the solar cell. After this demonstration, which showed that microcrystalline contact layers in principle solve the amorphous-p/ZnO contact problem, further optimization series followed: Figure 6.4 shows the FF of amorphous p-i-n solar cells with an inserted microcrystalline p-layer between the ZnO and the amorphous p-layer on the left axis. The circles and squares correspond to microcrystalline p-layers prepared with the RF and VHF technique, respectively, while the triangles correspond to the right axis and show the R_s^* values obtained from the JV characteristics (VHF cells only). The x-axis shows the deposition time, since a thickness measurement of these thin films between the ZnO and amorphous p-layer is extremely difficult. Moreover, the deposition rates obtained for bulk films on glass with the RF and VHF technique (both $\sim$ 2 Å/s) can be distinctly different from the ones obtained on the texture etched ZnO substrate. Also the uncer-

tainty about the incubation time for the film growth complicates the correct evaluation of the thickness. One observes, that high FF's above 70 % are obtained after exceeding a certain minimum thickness of the microcrystalline p-layer. This correlates with a decrease of the series resistance (shown for VHF microcrystalline p-layers only). Considering the scattering of the values, no significant difference can be observed between microcrystalline p-layers prepared with the RF and the VHF technique. For both techniques, a time of 90 s seems to produce a sufficient thickness for a low-ohmic p/ZnO contact. Thicker p-layers only result in lower j_{sc} simply explained by enhanced absorption losses. All cells shown in the figure have a V_{oc} value around 850 mV; the V_{oc} behaviour will be treated later on.

Remark: Since the time of 90 seconds is very close to the time when the film nucleation starts, it is not clear whether the ZnO surface is already homogeneously covered or not fully interconnected microcrystalline Si islands already provide a good contact. The thickness of these islands or of the homogeneous microcrystalline p-layer is probably below 20 nm, whereas the feature size of the texture etched ZnO surface is in the range of 200 – 600 nm (see also figure 5.3).

Figure 6.5 compares two cell series where all microcrystalline p-layers were prepared with the VHF technique and the same deposition parameters while the deposition time of the microcrystalline p-layer was varied. One series (squares) contained an additional amorphous p-layer. As can be seen, the application of a microcrystalline p-layer alone leads to a delayed built-up of the FF. Furthermore, we note that the maximum FF obtained in this case is lower than the one obtained with the double p-layer structure. In addition, only low V_{oc} values were obtained: the V_{oc} increased from 540 to 760 mV with increasing p-layer thickness. This important fact will be treated further in the next part of this chapter.

In summary: In combination with an amorphous p-layer, a thin microcrystalline p-layer with a certain minimum thickness is sufficient to obtain p-i-n solar cells on ZnO with high FF's above 70 % and low R_s^* values around 5.5 Ω. This result was obtained with the RF as well as the VHF technique. The replacement of diborane by TMB as doping source for the microcrystalline p-layer led to similar cell performance but better reproducibility in case of TMB. Without an amorphous p-layer, thick microcrystalline p-layers are necessary to build up a high FF, however, the maximum value in the latter case stays below the values obtained with the microcrystalline/amorphous double structure.

V_{oc} considerations

So far, it has remained an open question whether the microcrystalline p-layer is only necessary to obtain a low-ohmic contact or if it is also capable to build up a sufficiently high V_{oc}. In this context, it may be referred to various reports where high V_{oc} values are claimed to be caused by the application of microcrystalline p-layers [43, 44]. The following investigations were performed with solar cells solely containing a microcrystalline p-layer.

Figure 6.6 shows the V_{oc} with varying hydrogen dilution of the process gas silane[b] during deposition of the p-layer. The microcrystalline p-layer was prepared with a TMB flow of 0.22 sccm and a silane flow of 1.68 sccm, while the hydrogen flow was adapted. The

[b] For definition of the hydrogen dilution see section 3.1.1.

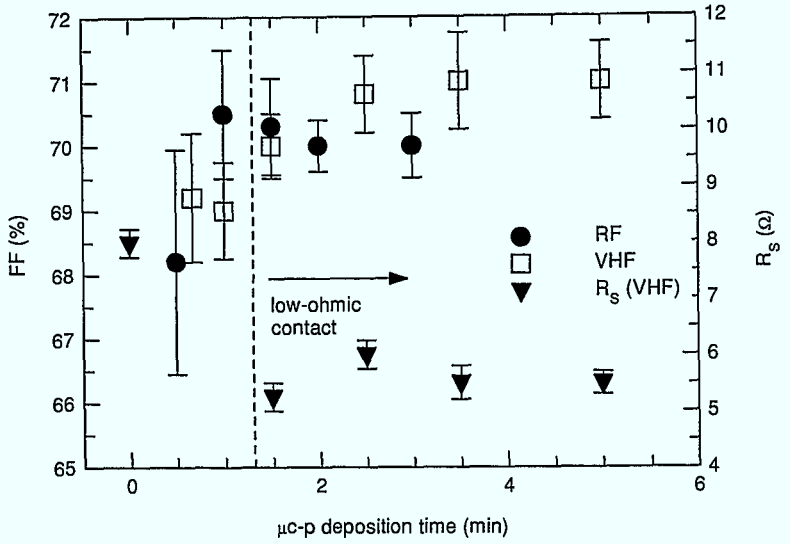

Figure 6.4: FF (left axis) and series resistance R_s^* obtained from the JV characteristic (right axis) versus deposition time of the microcrystalline p-layer. All cells contain an additional amorphous p-layer.

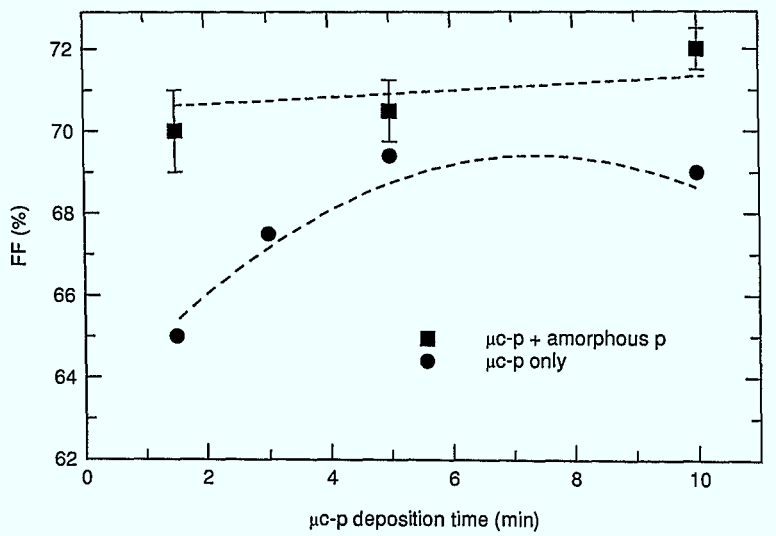

Figure 6.5: FF versus microcrystalline p-layer deposition time. The squares correspond to cells with an additional amorphous p-layer, the circles to cells with a microcrystalline p-layer only. The microcrystalline p-layers were prepared with the VHF technique.

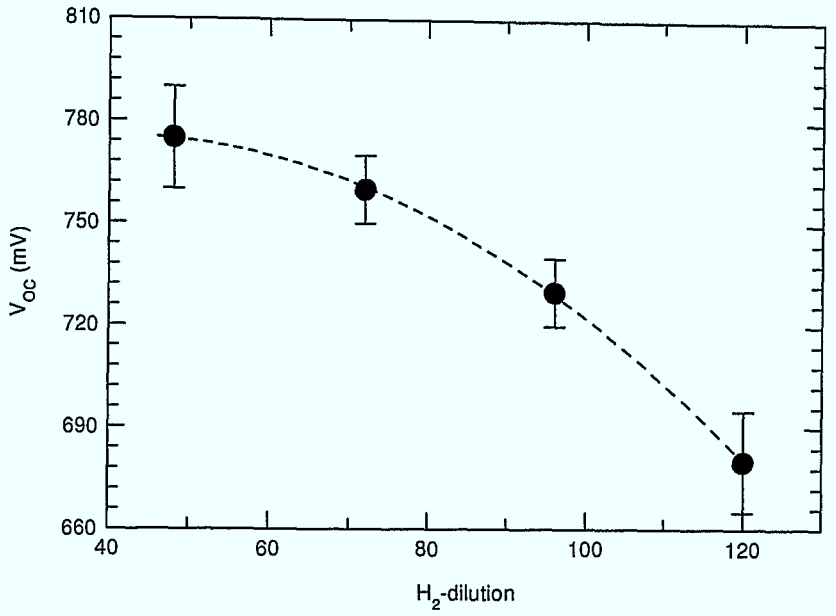

Figure 6.6: V_{oc} versus hydrogen dilution of the process gas silane. Excitation frequency during deposition of the p-layer was 110 MHz (VHF).

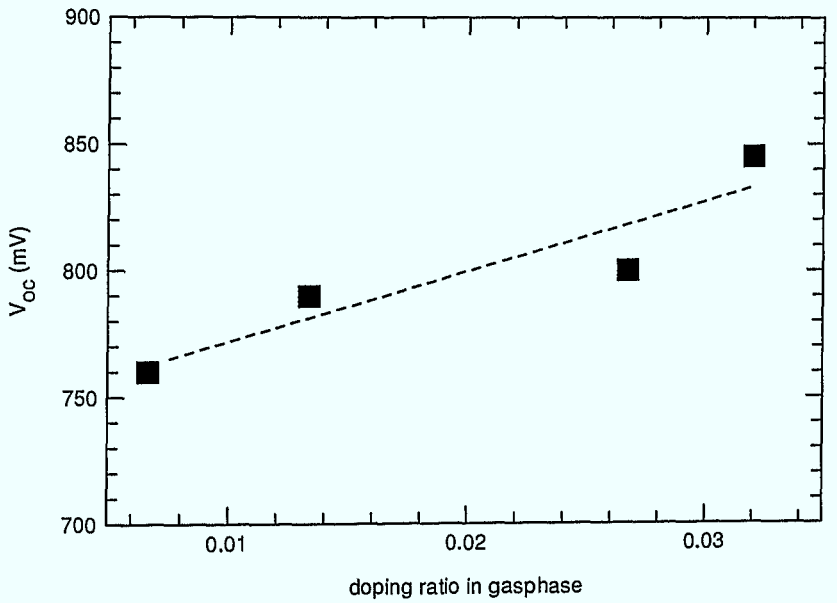

Figure 6.7: V_{oc} versus doping ratio during deposition of the microcrystalline p-layer. For further deposition parameters see text.

deposition time was 5 minutes in all cases, and the excitation frequency 110 MHz. With higher hydrogen dilution, a significant decrease in V_{oc} is observed. The FF of all cells in the figure is high (69 - 71 %). Due to a higher deposition rate in the more amorphous deposition regime, the thickness of the p-layers prepared with lower hydrogen dilution is probably slightly bigger than with higher dilution, so a superposition of the observed effect with the thickness dependency of the V_{oc} is observed. However, the observed increase can not be solely explained by a thickness effect.

In the next figure, the variation of the doping ratio and its effect on V_{oc} is presented. All cells were prepared using a silane flow of 2.1 sccm and a hydrogen flow of 200 sccm. Again, 110 MHz was used as excitation frequency. We observe a nearly linear increase of the V_{oc} with increasing doping ratio. The FF of all cells is around 69 %. At a very low doping ratio of 0.3 % (not shown here), a distinct drop of V_{oc} down to 500 mV was observed, together with a low FF value of only 64 %. The cell containing the microcrystalline p-layer with the highest doping ratio shows a high V_{oc} of 845 mV but already a decrease in FF to 68 % and - more severe - a drop in the short circuit current density below 13 mA/cm^2 (compared to 15 mA/cm^2 in the "standard" cell).

As a matter of fact, both variations of the deposition parameters have in common, that a shift in the deposition regime is achieved: With lower hydrogen dilution and higher doping ratio, the microcrystalline growth is disturbed and a shift to more amorphous growth is obtained (this can be seen in the conductivity measurements during microcrystalline p-layer development). Note that the high FF's of the cells considered indicate that still microcrystalline growth is obtained. For cells containing p-layers with similar thickness (estimated!), the shift to the more amorphous regime is also seen in a decrease of j_{sc} with increasing doping ratio (not shown here). This can be attributed to optical absorption losses in the amorphous phase which has an absorption coefficient of about a factor of 100 higher than the microcrystalline phase in the short wavelength region. Hence, the optical losses are particularly observed in the blue wavelength region of the corresponding spectral response curves.

As a last series, we conducted a thickness variation of the microcrystalline p-layer with and without amorphous p-layer while holding all deposition parameters constant. In particular, we used a silane flow of 2.1 (0.75), a TMB flow of 0.7 (0.2) and a hydrogen flow of 200 (200) sccm for the microcrystalline p-layer deposition with VHF (RF) frequency. The results can be seen in figure 6.8, showing the obtained V_{oc} versus deposition time of the microcrystalline p-layer. Without an amorphous p-layer and with increasing deposition time, the p-layer builds up the V_{oc} to a saturation value which is $\sim$ 750 mV here (VHF). This value can surely be optimized to slightly higher values by shifting the deposition conditions to the more amorphous regime. Most probably, this will be achieved at the expense of the FF (and j_{sc}) which is around 69 % for all cells shown here. On the other hand, when using an amorphous p-layer in addition, a high V_{oc} value around 845 mV is obtained from the beginning of growth of the microcrystalline p-layer (RF and VHF). This value corresponds to values obtained with optimized p-i-n solar cells on SnO_2 substrates containing a purely amorphous p-layer.

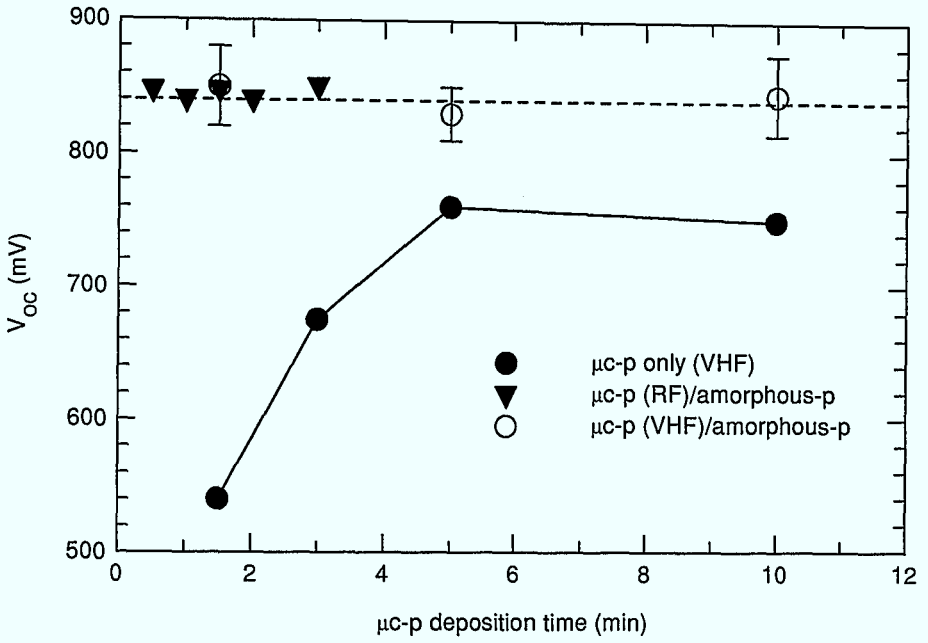

Figure 6.8: *V_{oc} versus deposition time of the microcrystalline p-layer for cells with and without an additional amorphous p-layer.*

To conclude: The common observation of the previous paragraphs is that the more amorphous the deposition regime during growth of the microcrystalline p-layer the higher is the observed V_{oc}. With an amorphous/microcrystalline double p-layer structure, the V_{oc} always exhibits the same high value as observed for a purely amorphous p-layer on SnO_2. Hence, we conclude that for a high V_{oc} the amorphous p-layer is necessary.

The blue response

So far, only the electrical parameters FF and V_{oc} were taken into account for the optimization of the solar cells. In order to maximize the efficiency of the device, a high j_{sc} is necessary, too. According to Beers' law, a p-layer does only absorb a negligible amount of light in the wavelength region above 550 nm (estimated with $d \sim 50$ nm and α of intrinsic a-Si:H). Therefore a BG7 band filter was used during the JV measurement to evaluate the optical absorption losses in the short wavelength region. This filter restricts the spectrum to the range between 400 and 540 nm. In addition, the light intensity is only about 50 %. Hence, differences in the short-circuit current-density observed with the BG7 filter have to be roughly doubled in order to estimate the effect under AM1.5 illumination. From the p-i-n development on SnO_2 coated substrates conducted in our group before, we know that 3.5 – 3.6 mA/cm^2 is a "normal" value while 3.8 – 4.0 mA/cm^2 is an excellent value for j_{sc} under AM1.5*BG7 illumination. The amorphous p-layer used for all p-i-n solar cells on

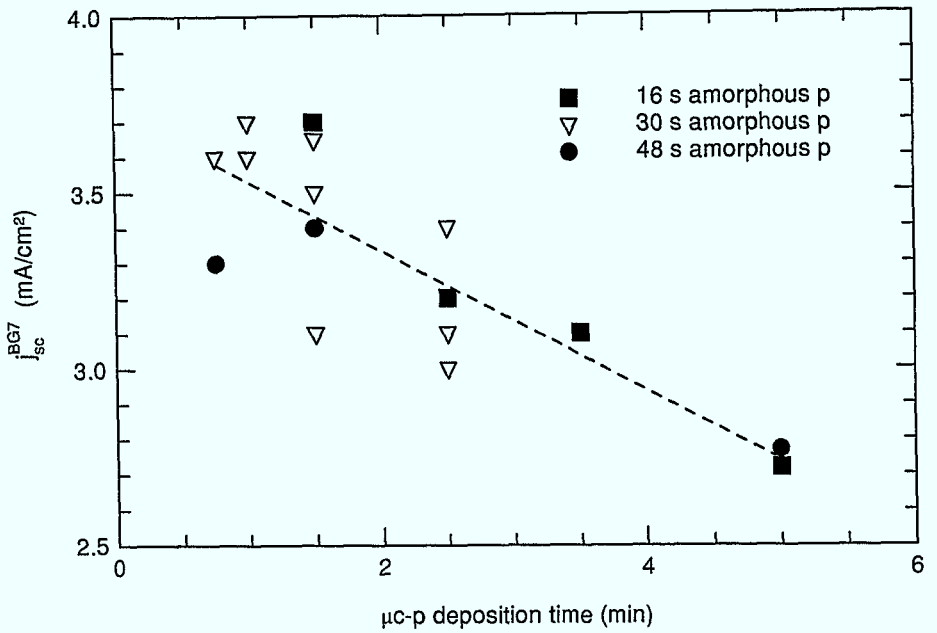

Figure 6.9: *Short-circuit current-density obtained under AM1.5*BG7 illumination as function of the microcrystalline p-layer thickness for different thicknesses of the amorphous p-layer. The microcrystalline p-layers were deposited with the VHF technique.*

ZnO was developed and optimized for p-i-n cells on SnO_2 in previous years already. In this study, we restricted the optimization of the double p-layer structure to a thickness optimization of each layer. In addition, we added small amounts of methane (CH_4) to widen the band gap of the amorphous phase within the microcrystalline p-layer by means of carbon alloying, but no significant effects were observed.

Figure 6.9 shows the short-circuit current-density obtained under AM1.5*BG7 illumination for various p-layers. The microcrystalline p-layers were prepared using the VHF technique. The series also comprised ZnO substrates with different etching times, explaining the scattering of the values for identical deposition times. The x-axis shows the deposition time for the microcrystalline p-layer. As expected, the current yield increases both with a thinner amorphous and a thinner microcrystalline p-layer. The V_{oc} values obtained were $\sim$ 830 mV, $\sim$ 850 mV, and $\sim$ 855 mV for the 16 s, 30 s and 48 s amorphous p-layer. The FF for cells with very thin microcrystalline p-layer slightly decreased. The best compromise between electrical (FF and V_{oc}) and optical (j_{sc}) optimization was found to be 90 s and 30 s for the deposition time of the microcrystalline and the amorphous p-layer, respectively. Similar to the results obtained for the low-ohmic p/ZnO contact, the optimum deposition time for the microcrystalline p-layer turned out to be the same for RF and VHF excitation frequency.

The addition of methane performed exemplary showed no beneficial effect nor did it affect the solar cell performance adversely. Since the microcrystalline p-layer was only very thin, the presumed amount of amorphous phase is probably too low to benefit from a widening of the optical gap by carbon to an extent noticeable in the short-circuit current-density.

6.1.2 Highly Efficient p-i-n Type Solar Cells

To demonstrate the suitability of the followed approaches, a series of three single p-i-n cells on different substrates was prepared. We performed a degradation study with identical cells on the laboratory standard substrate Asahi U, a commercially available SnO_2 floatline TCO and on our newly developed texture etched ZnO substrate. All cells were deposited with the same deposition parameters except for the adapted p-layer. The i-layer thickness was 360 nm. To enhance the current yield, all cells contained a highly reflective ZnO/Ag back reflector. Figure 6.10 summarizes the key result: Both the Asahi U and the ZnO substrate show a similar and significant higher efficiency than the floatline substrate in the initial as well as the stabilized state. This is mainly due to an enhanced current yield by the superior light coupling as outlined in more detail in the JV data given in table 6.1. Stabilized efficiencies of 7.6 %, 7.5 % and 6.5 % were achieved on Asahi U, ZnO and the floatline substrate, respectively. This again demonstrates the excellent suitability of the texture etched ZnO substrate for the application in solar cells.

Next, a series of tandem cells was prepared. Table 6.2 summarizes the results of the tandem cells. The implementation of the best cell as the top cell in an a-Si:H/a-Si:H tandem cell on texture etched ZnO together with i-layer material prepared with high hydrogen dilution of the process gas [16] led to further improvement of the efficiency: we prepared a 10.2 % initial tandem cell which showed a low degradation and stabilized at 9.2 % stable efficiency after 900 h of light soaking. The same cell (without microcrystalline p-layer) on an Asahi type U SnO_2 substrate also showed 9.2 % stable efficiency after 1000 h of light soaking and was our record efficiency so far [16]. The implementation of an optimized amorphous top cell into an a-Si:H/μc-Si:H "micromorph" tandem cell led to an initial efficiency of 11.1 %. This cell is expected to degrade less compared to its completely amorphous counterpart; the degradation study of this cell is under way.

6.2 n-i-p Solar Cells with ZnO Front Contact

It is not self-evident that the p/ZnO contact in the case of n-i-p cells shows the same behaviour as in p-i-n type solar cells, since the growth of the microcrystalline layer is extremly dependant on the choice of the substrate. Moreover, it is not clear how the subsequent sputtering of the ZnO front contact affects the contact behaviour. Consequently, we had to perform an investigation of the p/TCO region in n-i-p type solar cells. For the solar cell development in general, the choice of the substrate is crucial for the deposition yield and the final device performance. For reasons already explained in section 3.3, we used

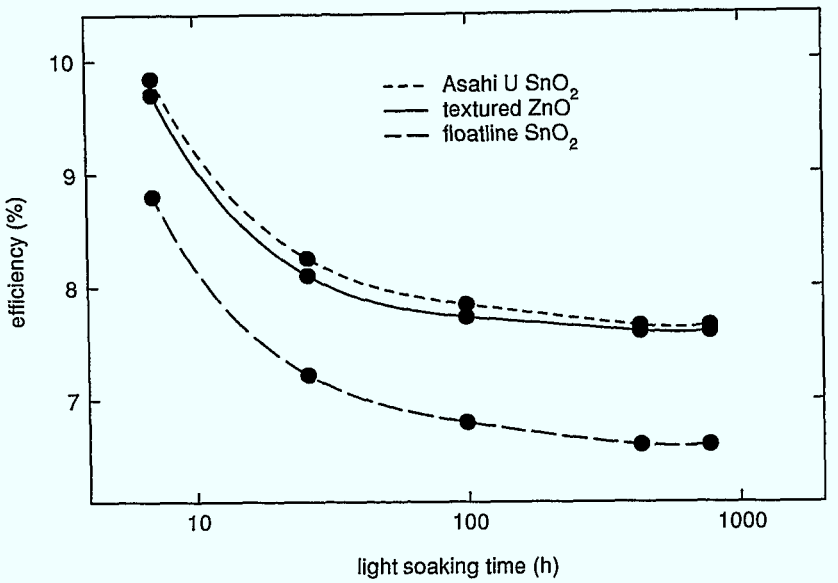

Figure 6.10: *Efficiency of p-i-n cells prepared on Asahi U, floatline TCO and texture etched ZnO as function of the light soaking time.*

substrate	FF (%)	V_{oc} (mV)	j_{sc} (mA/cm^2)	$\eta_{initial}$ (%)	η_{stable} (%)
textured ZnO	72	850	16	9.9	7.5
Asahi U SnO_2	73	830	16	10.1	7.6
floatline SnO_2	72	810	14	8.8	6.5

Table 6.1: *JV data of three p-i-n cells prepared on Asahi U, floatline TCO and texture etched ZnO. The JV data refer to initial values, the η_{stable} values refer to 900 or 1000 h of light soaking time, respectively.*

substrate	cell type	FF (%)	V_{oc} (mV)	j_{sc} (mA/cm^2)	$\eta_{initial}$ (%)	η_{stable} (%)
textured ZnO	a-Si:H/a-Si:H	72.2	1714	8.3	10.2	9.2
Asahi U SnO_2	a-Si:H/a-Si:H [16]	72.1	1750	7.9	10	9.2
textured ZnO	a-Si:H/μc-Si	69.1	1353	11.9	11.1	–

Table 6.2: *p-i-n solar cell results achieved on textured ZnO substrates compared with previous results on Asahi U substrates. The JV data refer to the initial values. The η_{stable} values refer to 900 or 1000 h of light soaking time, respectively. All cells have an area of 1 cm^2.*

SnO_2 coated glass substrates (Asahi type U) without back reflector for the study of the i-p-TCO-region in the n-i-p configuration. As in the p-i-n case, the FF and the R_s^* values served as a monitor for the evaluation of the p/ZnO contact barrier. Note that parts of the following section have already been published in [121].

Most experiments comprised a codeposition of n-i-p cells on Asahi type U and Corning glass substrates. While the part on the TCO substrate was completed with ZnO top contacts before further characterization, we evaporated Ag contacts on the glass samples to evaluate the conductivity of the p-layer. Since the $\sim$ 400 nm thick i-layer has a conductivity much lower than the p-layer, its contribution can be neglected in this case. By the codeposition, we were able to characterize the p-layer actually used in the solar cell. On both substrates, the i-layer covers the substrate before deposition of the microcrystalline p-layer. Slight differences in the growth of the microcrystalline p-layer are at most due to the different conductivity of the substrate and to differences of the surface roughness.

6.2.1 The TCO top Contact

Usually, highly conductive and transparent ITO top contacts are used for n-i-p type solar cells. The typical film thickness is around 80 nm to fulfill the anti-reflection condition. First, we compared highly conductive and transparent ITO material with the ZnO films obtained in the low pressure regime (see 5.1.1). We performed a thickness series to evaluate the suitability as anti-reflection coating for both materials. The ITO films applied showed resistivities around 7×10^{-4} Ωcm, while the used ZnO films showed values around 4×10^{-4} Ωcm. All cells in this subsection contain an electrically optimized microcrystalline p-layer described in section 6.2.2.

ZnO versus ITO

For both TCO materials, as it is expected from the similar refraction index (n $\approx$ 2), the anti-reflection condition is fulfilled for nearly the same film thickness between 60 and 80 nm. As can be seen in figure 6.11, the corresponding solar cells show a sharp maximum in the efficiency, which is due to an increase in the short-circuit current density j_{sc} of about 2.5 mA/cm^2. The maximum j_{sc} achieved with ZnO is as high as with ITO. In addition, we observed no difference in FF or V_{oc} due to the two different TCO materials. The FF of all cells in this series was typically 70 % and the V_{oc} around 850 mV. Since the cells were developed for the use as top cell in tandem devices, transparent substrates (Asahi type U) have been used, explaining the relatively low absolute values of the efficiency in this series. In the following, ZnO was chosen as the favorite material for the top TCO contact.

Influence of the sputter conditions on the solar cell performance

In a further series of experiments, the ZnO sputter conditions were optimized with respect to the solar cell performance. A significant effect was observed during variation of the sputter pressure: Figure 6.12 shows the FF of n-i-p solar cells as function of the sputter gas pressure during deposition of the first 20 nm of the top contact. With increasing pressure, the FF increases from 70 % up to about 72 % at 80 mTorr. At even higher

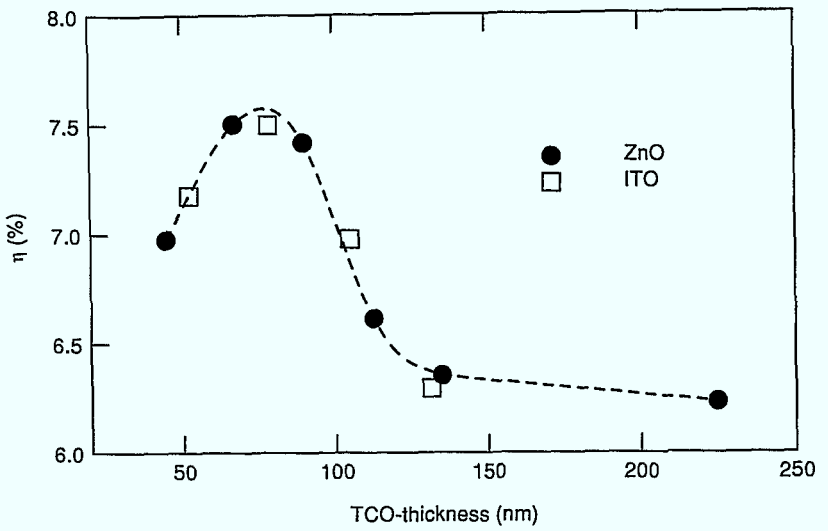

Figure 6.11: Efficiency η as function of the TCO film thickness of the top contact for ITO and ZnO material.

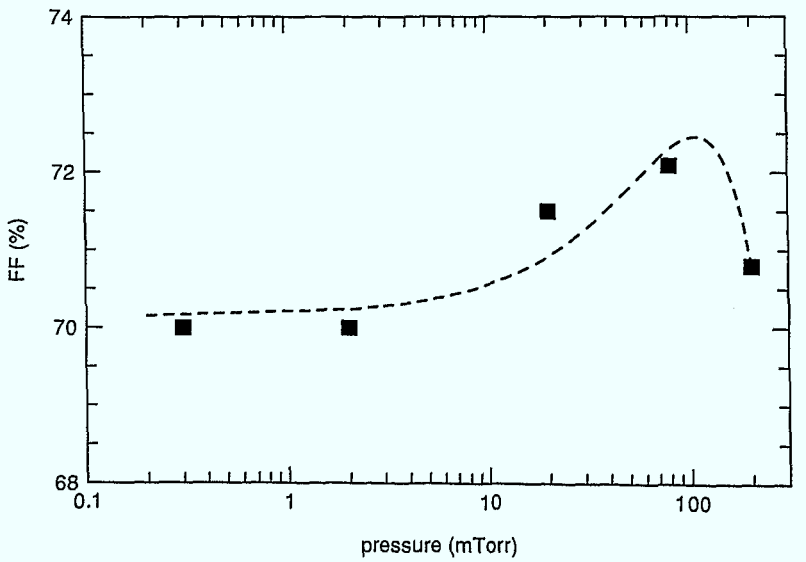

Figure 6.12: Fill factor of n-i-p solar cells as function of the sputter gas pressure during deposition of the first 20 nm of the ZnO top contact.

pressures, arcing and spark over in the plasma could be observed, and the FF dropped down again. An explanation of the beneficial effect of raising the sputter gas pressure could be the lowering of the mean free energy of the impinging molecules on the growth surface due to the decreasing mean free path length with higher pressure. This could lead to less deteriorating effects at the sensitive p/TCO-interface. However, it is important to note that ZnO-films prepared at higher pressures ($p > 10$ mTorr) exhibit distinctly higher resistivities compared to films deposited in the low pressure regime [22, 83]. Therefore, only the very first part of the ZnO top contact was prepared at higher pressure, while the rest of the deposition was carried out at 2 mTorr to maintain a low sheet resistance.

The variation of the substrate temperature between room temperature and 250 °C showed no influence (two samples only) on the solar cell performance. The variation in power between 150 and 750 W seemed to lower the yield of the solar cells only (without influence on the cell performance!), e.g. more shunted solar cells were observed.

In summary, we successfully applied sputtered ZnO as material for the front contact of n-i-p type solar cells without any drawback in device performance.

6.2.2 The ZnO/p Contact

Interestingly enough, when applying a purely amorphous p-layer for the first n-i-p solar cells, the JV characteristic turned out to be very similar to the p-i-n type cells prepared on glass/ZnO with an amorphous p-layer (see figure 6.2). Similar to the p-i-n cell development, we performed a thickness series with a highly conductive microcrystalline p-layer to investigate the contact behaviour and to improve the FF of the n-i-p cells. Figure 6.13 shows the FF on the left axis and the conductivity of the corresponding microcrystalline p-layer on the right axis, both as function of the p-layer thickness[c]. Note that the thickness measurement contains an error of about ± 10 nm because it is difficult to determine the incubation time of the microcrystalline p-layer growth on an a-Si:H film. As expected (see also figure 5.6), the conductivity increases with increasing thickness of the microcrystalline p-layer [24, 46] and saturates at a value around 0.1 S/cm. In contrast to the relatively slow rise of the conductivity, the FF is already high from the beginning of growth of the microcrystalline p-layer. The small decrease in FF with increasing p-layer thickness can be explained by current collection from areas not defined by the TCO top contact.

Hence it follows that – similar to the p-i-n configuration – already a very thin microcrystalline p-layer is sufficient to provide a low-ohmic p/TCO-contact, which is reflected in a high FF. It is not necessary to maximize the *lateral* conductivity by a thicker p-layer.

V_{oc} considerations

Figure 6.14 shows the V_{oc} development with respect to the p-layer thickness for solar cells containing different p-layers. Again, errors in the thickness determination have to be

[c] In contrast to the p-i-n cells, the thickness of the p-layers codeposited on the glass/a-Si:H substrate could be calculated from the thickness of the complete layer structure, where the i-layer thickness is known.

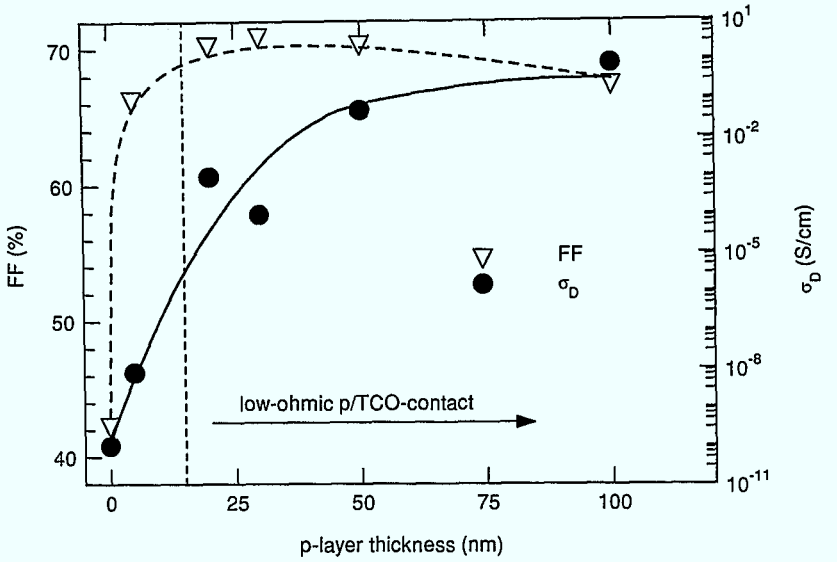

Figure 6.13: *FF (triangles, left axis) and dark conductivity σ_d (circles, right axis) versus thickness of the microcrystalline p-layer.*

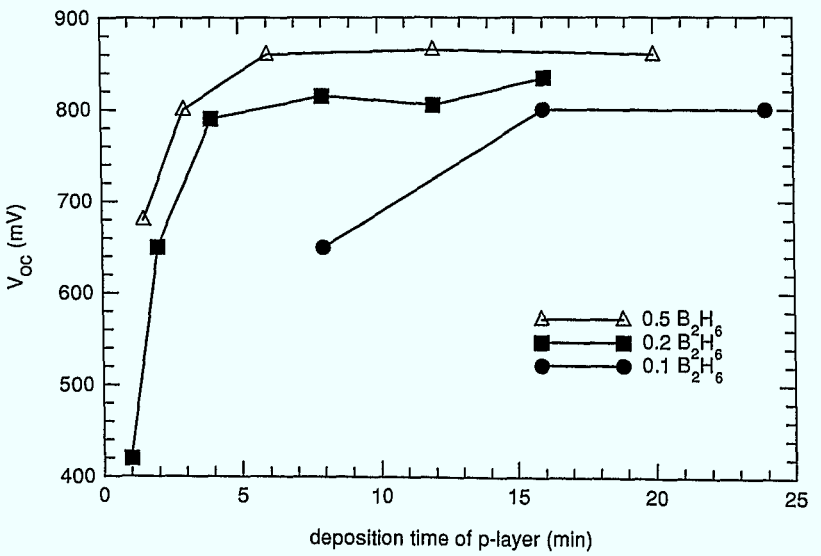

Figure 6.14: *V_{oc} of different p-layers as function of the p-layer deposition time for different doping ratios.*

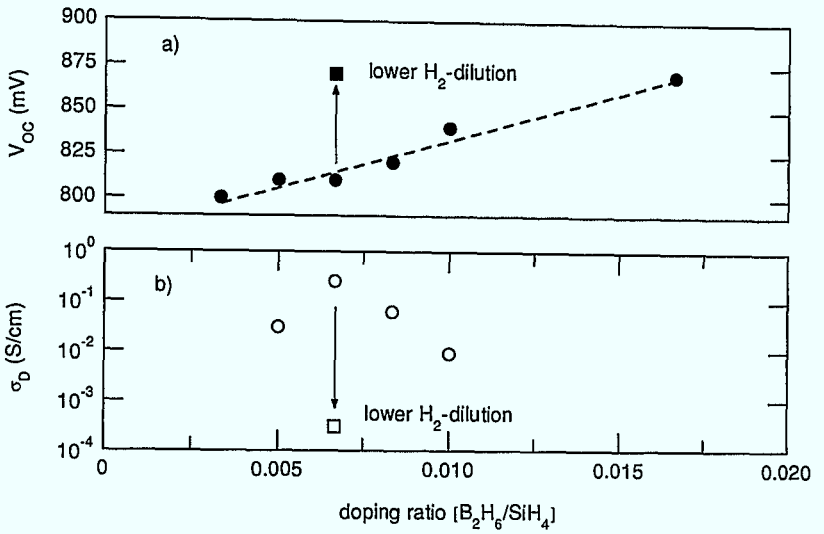

Figure 6.15: *a) V_{oc} of n-i-p solar cells and b) dark conductivity of the corresponding p-layers, both as function of the doping ratio in the gas phase. Excitation frequency was 110 MHz.*

considered, since the thickness evaluation of these thin films on the amorphous substrate is extremely difficult. The nominal deposition rate is around 0.8 Å/s, the deposition time varied between 1 and 24 minutes. We can observe an increase of the V_{oc} value with increasing p-layer thickness up to a saturation value where no further improvement is to be seen. This behaviour can be observed for all p-layers in general. The saturation value depends critically on the deposition conditions, e.g. doping ratio and hydrogen dilution. For a higher doping ratio, the deposition conditions lead to more amorphous growth of the microcrystalline p-layer as indicated by the conductivity measurements. From the figure it becomes clear, that the V_{oc} is higher when the doping ratio is high or the deposition is shifted to the more amorphous regime, respectively. Figure 6.15a shows the saturation values for the V_{oc} as function of the doping ratio (flow ratio of diborane to silane). The conductivity of the corresponding p-layers is shown in figure 6.15b. In good agreement with Flückiger et al. [122], we found the maximum conductivity at a doping ratio of about 0.7 % (VHF excitation). The high conductivity of > 0.1 S/cm implies that the Fermi level position is close to the valence band providing a high built-in voltage possible with this p-layer. However, despite this fact, the V_{oc} obtained with this p-layer exhibits only an intermediate value of about 810 mV. Ellipsometric studies carried out on these p-layers by S. Hamma [123] confirmed that the p-layers with the highest crystalline fraction (and thereby the highest conductivity) do *not* result in the highest V_{oc}. Instead, a steady increase of the V_{oc} up to 870 mV is observed with increasing doping ratio of the gas phase using a standard i-layer process while Graph 6.15b, showing the dark conductivity, indicates a

shift to the more amorphous deposition regime with increasing doping ratio. However, the high FF of the solar cells as well as the absolute values of the conductivity indicate, that these p-layers still contain a significant amount of crystalline phase.

From our experience with the solar cells on ZnO in the p-i-n configuration, we already know that a low-ohmic p/TCO contact together with a high V_{oc} is only achieved by use of a double p-layer with an amorphous p-layer inserted between the microcrystalline p- and the i-layer. Hence, from the results obtained here we assumed that for a high V_{oc} in the n-i-p configuration, the amorphous phase within the microcrystalline p-layer is needed. To further confirm this assumption, we went back to the highly microcrystalline p-layer with an intermediate V_{oc} and shifted to a more amorphous deposition regime by intentionally lowering the hydrogen dilution (square in 6.15): the conductivity drops down again, indicating more amorphous deposition conditions, while the V_{oc} strongly increases, both results supporting our understanding of the relation between the V_{oc} and the p-layer structure.

From the presented results, we draw the conclusion that the V_{oc} strongly depends on the structural properties of the microcrystalline p-layer and that for a high V_{oc} the amorphous phase within the microcrystalline p-layer is essential.

The blue response

All n-i-p cells so far showed a relatively low blue response. Figure 6.16 compares the quantum efficiency of an electrically optimized n-i-p cell with an already optimized p-i-n cell on ZnO described in the last section. The obvious lower red response is due to the fact that the nip cells are deposited on transparent SnO_2 substrates and is not of interest here (the development of highly reflective back reflector substrates is still under way). Much more important are the observed optical losses in the blue wavelength region. Despite the fact that the top contact was conducted as an anti-reflection coating – which leads to higher maximum response around 550 nm – massive losses below 550 nm can be observed. However, the same microcrystalline p-layer recipe together with an identical ZnO top contact applied to a fully microcrystalline n-i-p cell leads to a high quantum efficiency in the considered wavelength region[d] (dotted line). In the fully microcrystalline device, the p-layer can directly nucleate on the microcrystalline i-layer, so no significant amount of amorphous phase is present. Hence, we explain the lower blue response of the amorphous n-i-p cell by absorption losses in the amorphous phase of the microcrystalline p-layer. Consequently, the goal of the blue response optimization is to reduce the absorption losses in the amorphous phase of the microcrystalline p-layer. Since the importance of the amorphous phase for a high V_{oc} sets close limits to the reduction of the amorphous phase, a widening of the band gap of the amorphous phase has to be achieved.

Like in the case of p-i-n cells, the available attempts to widen the gap of the amorphous phase of the p-layer are alloying with carbon (or oxygen) or a lower deposition temperature. Of course, a thickness optimization with respect to high V_{oc} and j_{sc} has to be conducted, too. In the n-i-p configuration, this optimization process is rather interactive, since the separation between the microcrystalline and the amorphous p-layer is not really possible;

[d]The data support by O. Vetterl is gratefully acknowledged.

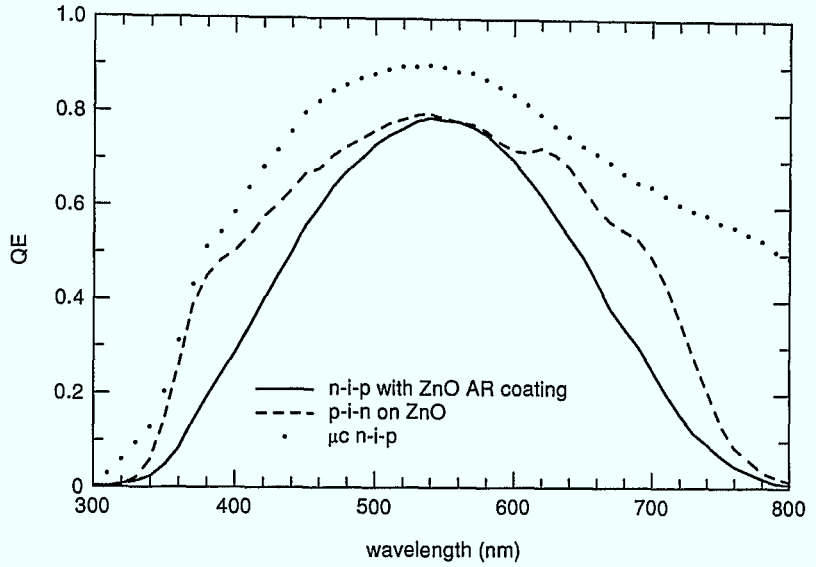

Figure 6.16: Quantum efficiency of an amorphous and a fully microcrystalline n-i-p cell, both with anti-reflection ZnO top contact, compared to a p-i-n cell on ZnO.

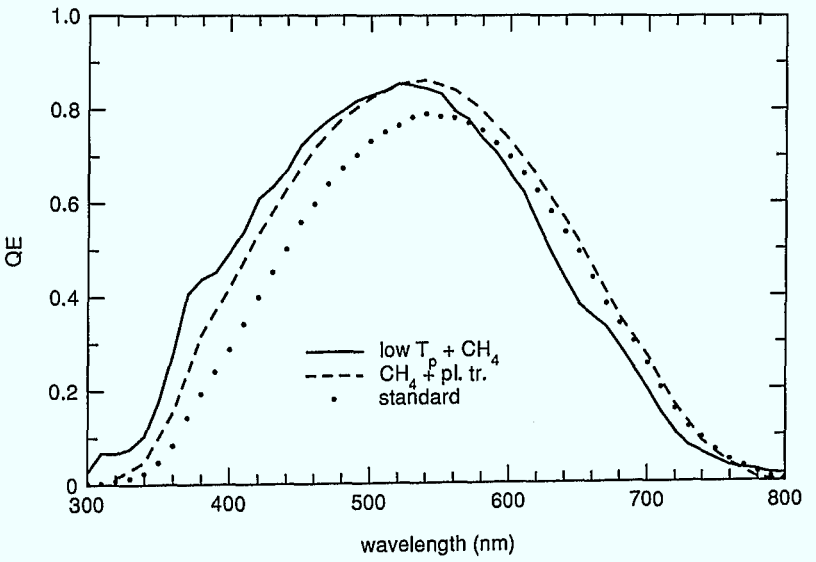

Figure 6.17: Quantum efficiency of n-i-p solar cells containing various microcrystalline p-layers (pl. tr. = plasma treatment).

even when promoting microcrystalline growth (e.g. by an intermediate CO_2-plasma), the growth conditions at the beginning are always dominated by the amorphous substrate. Since it was not possible to nucleate a microcrystalline p-layer on an amorphous p-layer, we could not prepare amorphous/microcrystalline double p-layers like in the p-i-n case. The complex cross-dependencies make the correct evaluation of the experiments more difficult than in the p-i-n configuration, where a clear distinction of the two p-layers in terms of their function is possible.

Figure 6.17 shows the quantum efficiency as function of the wavelength for various n-i-p solar cells with differently prepared p-layers, representing the key results of the blue response optimization. To achieve the desired higher transparency, small amounts of methane were added to the gas phase during deposition of the microcrystalline p-layer. Additionally, a beneficial effect of a pure H_2-plasma after the first part of the microcrystalline p-layer to promote microcrystalline growth on the underlying, more amorphous part of the p-layer was observed. The dashed line in the figure shows that compared to the p-layer prepared without carbon, an improvement in the wavelength region below 550 nm can be observed due to the use of the extra plasma treatment and methane in the gasphase (differences in the red wavelength region are due to slight variations of the i-layer thickness). No deterioration in V_{oc} or FF was detected for these cells. Thus, carbon alloying and promotion of microcrystalline growth by means of an extra plasma treatment seem to improve the blue response. However, some losses compared to an optimized p-i-n cell still remained.

As a second approach, the substrate temperature during deposition of the microcrystalline p-layer was lowered to widen the band gap of the amorphous phase within the microcrystalline p-layer. Since the initial growth changes with decreasing temperature, a fine tuning of the deposition parameters was necessary first. Figure 6.17 also shows the quantum efficiency of a cell containing a microcrystalline p-layer prepared at 140 °C and with addition of methane to the gas phase (solid line), together with the quantum efficiency of the cell at standard temperature (200 °C) and without methane (dotted line). The combination of alloying and low substrate temperature led to a strongly improved blue response. Moreover, the achieved results support the hypothesis of absorption losses in the amorphous phase as cause of the poor blue response. The achieved quantum efficiency in the blue wavelength region is similar to the one achieved for the optimized p-i-n cell on ZnO. To illustrate this, the quantum efficiency of the optimized p-i-n and n-i-p cells with ZnO front contact are compared in figure 6.18. Beyond the similar blue response of the two cells, a significant current gain for the n-i-p cell was obtained due to the anti-reflection effect; this can be seen in the difference of the achieved maximum QE which is 80 % for the p-i-n cell and above 85 % for the n-i-p cell. The observable "losses" in the red part of the spectrum are only due to the missing back reflector of the n-i-p cell.

In summary: carbon alloying and preparation at low substrate temperature were suited to reduce optical absorption losses of the microcrystalline p-layer which we attributed to absorption within the amorphous phase. Also the promotion of microcrystalline growth by means of an additional plasma treatment is a promising way to reduce the fraction of the amorphous phase within the microcrystalline p-layer.

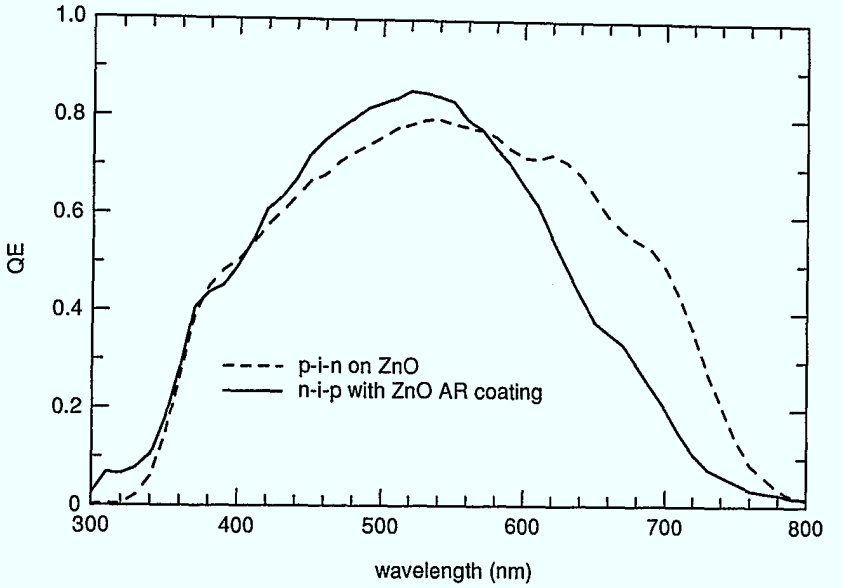

Figure 6.18: *Quantum efficiency as function of wavelength for optimized p-i-n and n-i-p solar cells with ZnO front contact. For explanations see text.*

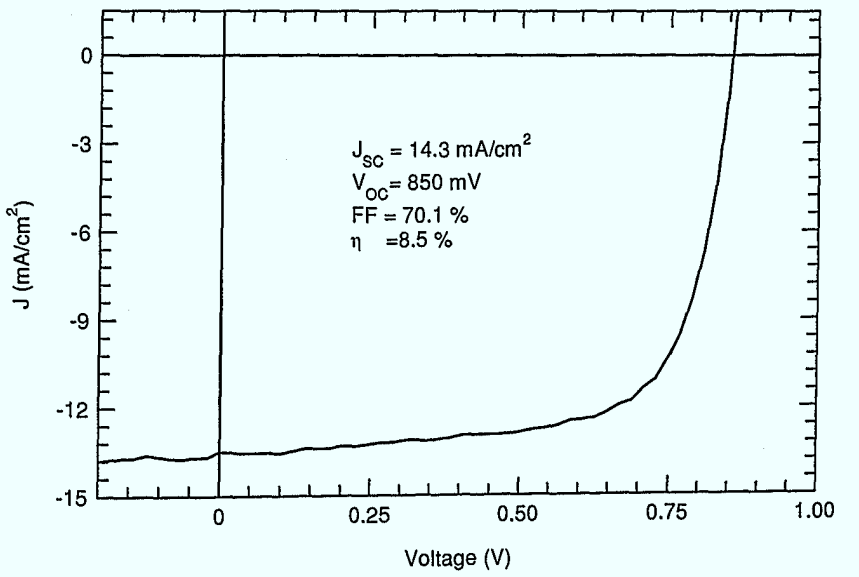

Figure 6.19: *JV characteristic of the best n-i-p single cell. The cell contains an optimized microcrystalline p-layer in the anti-reflection design. Due to the transparent substrate the current is relatively low.*

After implementing the electrically and optically optimized microcrystalline p-layer, the best n-i-p single cell exhibited an efficiency of 8.5 % on a transparent substrate. Figure 6.19 shows the JV curve of this cell. The cell contains a ZnO top contact in the anti-reflection design and an adapted microcrystalline p-layer prepared at 160 °C with carbon alloying. The high FF of 70.1 % indicates the low-ohmic ZnO/p contact, the V_{oc} is 850 mV. Due to the transparent substrate, the j_{sc} exhibits only 14.3 mA/cm^2.

6.2.3 Highly Efficient n-i-p Solar Cells

First of all, it has to be stressed that the n-i-p development was not aiming at the development of maximum efficiencies for a-Si:H solar cells because the development of an efficient light trapping relying on a textured back reflector would have lead beyond the scope of this thesis. The understanding of the (for our group) new n-i-p technology was the main goal of this study. Moreover, since the technological goal aimed at the development of a top cell for a microcrystalline/amorphous tandem cell within the NEST project, the development of a highly reflective ZnO/Ag substrate concentrated on the application in the microcrystalline bottom cell. In the thesis of O. Kluth, highly reflective light scattering back reflectors for microcrystalline n-i-p solar cells have been developed [124]. The optimized amorphous n-i-p cell described in the previous section was applied to microcrystalline bottom cells prepared on this back reflector by our group as well as by the IMT group (Institute de Microtechnique, University of Neuchâtel, Switzerland). The implementation of the n-i-p top cell process in the micromorph tandem cell led to a high initial efficiency of 10.6 % (69.3 % FF, 1.33 V, 11.5 mA/cm^2). This demonstrates the potential of the top cell development as well as the suitability of our approach to separate the optimization of the top cell from the complete device. The adaptation of the top cell to the microcrystalline bottom cell was achieved by application of a low-ohmic inner n/p junction which was performed with microcrystalline films. The degradation study of this cell is still under way.

Remark: An exemplary degraded amorphous n-i-p single cell showed strong degradation, which we attribute to the missing encapsulation of the sensitive front region of the device. The corresponding cell in the p-i-n configuration is protected by the glass substrate and showed no unusual degradation, indicating that no additional degradation is introduced by applying ZnO as TCO material. Moreover, ZnO is already in use for CIS modules with effective encapsulations. However, long term stability of ZnO films for application in thin film solar cells is still a current issue of research [125, 126].

Chapter 7

Comparison of p-i-n and n-i-p Cells

In this chapter, a comparative discussion of the key findings for p-i-n and n-i-p solar cells will be given. The similarities of the TCO/p/i interface in both structures are pointed out. Differences for the application of high temperature i-layer material are described and some considerations related to the different light coupling are presented. After this, some evaluations dealing with technological aspects of the two different cell structures will finish this chapter.

7.1 Discussion

The key findings of the comparative study of the two cell structures – p-i-n and n-i-p solar cells with ZnO front contact – are:

- In both structures, the effect of the contact barrier at the ZnO/amorphous-p interface is reduced by the insertion of a thin, microcrystalline p-layer.
- In both structures, an amorphous phase between the microcrystalline p-layer and the i-layer is essential to build up a high V_{oc}.
- The implementation of low gap i-layer material prepared at high temperatures leads to a deterioration of the p/i interface in the p-i-n structure causing a drop in the V_{oc}, while the V_{oc} of the corresponding n-i-p cells is simply related to the decrease in band gap of the i-layer.
- For laboratory cells, the n-i-p cell offers the advantageous possibility of an anti-reflection design for the TCO front contact.

In the following, these findings will be discussed in detail.

The ZnO/p contact barrier

The first remarkable fact when comparing amorphous silicon solar cells with ZnO front contact is that the high-ohmic amorphous-p/ZnO behaviour manifests itself in the p-i-n and in the n-i-p structure in the same way: the JV characteristic of solar cells with amorphous p/ZnO contact show a high series resistance which deteriorates the FF of the device. The "S"-shape of the JV curve and the independence of this additional series resistance from the p-layer thickness indicates a contact barrier at the TCO/p interface.

In former reports [40–42] considering p-i-n cells only, the origin of the problem was explained by an interaction of the hydrogen-rich plasma with the ZnO surface during the PECVD process. This is expected to lead to a wider depletion region in the p-layer thereby deteriorating the tunnel characteristic of this contact. In case of the n-i-p structure, the device is already deposited before applying the ZnO contact by means of a sputter process in an Ar/O_2 atmosphere, so no hydrogen plasma interaction can be involved. The only hydrogen present is the one bound within the amorphous p-layer. Diffusion of hydrogen from the p-layer towards the ZnO interface could be a possible explanation for the contact barrier. Also a more unfavorable band offset related to the ZnO/amorphous-p material combination – compared to SnO_2/amorphous-p – could be possible. A pinning of the Fermi-level by interface defects would cause a contact barrier, too. More work has to be dedicated to this topic to clarify the appearance of the contact barrier in both cell structures.

Electrical and optical optimization of the p-layer

The presented results show that in both structures, the insertion of a microcrystalline contact layer leads to a low-ohmic contact behaviour. The qualitative behaviour of the FF and the V_{oc} with respect to the p-layer structure also turned out to be very similar in both cell structures: a thin microcrystalline p-layer provides the low-ohmic ZnO/p contact, while an amorphous phase is required in order to build up a high V_{oc}.

In the p-i-n type solar cells, a clear separation of the microcrystalline and the amorphous p-layer is possible, which enables us to draw this conclusion: On ZnO, it is possible to obtain immediate growth of microcrystalline p-doped films. Hence, it is possible to adapt the thickness of the optimized microcrystalline p-layer and the subsequent deposition of an amorphous p-layer separately. The corresponding series of experiments showed that in the wide parameter regime investigated, a microcrystalline p-layer alone never resulted in a V_{oc} comparable to solar cells with an amorphous p-layer. With a double p-layer structure (ZnO/μc-p/amorphous-p/i-layer), we always achieved a high V_{oc} equal to the one obtained with an amorphous p-layer alone. Only an extremely thin microcrystalline p-layer is necessary to obtain a loss free ZnO/p contact in this case. This is mirrored in JV characteristics of p-i-n cells on ZnO showing high FF's above 72 %.

In the case of n-i-p cells with ZnO front contact, this separation is not possible due to different nucleation on the underlying amorphous i-layer: microcrystalline growth of the p-layer is difficult to achieve on an amorphous substrate and there is always a more or less fast transition between amorphous and microcrystalline growth. However – according to

our understanding of the growth of microcrystalline silicon on intrinsic a-Si:H (see section 2.3) – the growth of the microcrystalline p-layer accommodates the "proper" p-layer structure: in the starting phase, the nucleation starts with its high amount of amorphous phase necessary to built up a high V_{oc}, while later on the micro-crystallites are formed towards the ZnO top contact, thereby providing a low-ohmic ZnO/p contact. Our experiments confirmed that shifting of the deposition conditions to the more amorphous regime – while still a high conductivity is maintained – leads to a higher V_{oc}. With highly microcrystalline films indicated by high conductivity values and high amount of crystalline phase as measured by ellipsometry, only an intermediate value for V_{oc} could be obtained, even if thick microcrystalline p-layers were applied.

Hence we conclude that the optimum structure for the TCO/p/i region for both cell structures is: ZnO/microcrystalline-p/amorphous-p/i.

To reduce the absorption losses in the p-layer, a thickness optimization for both individual p-layers was sufficient in the p-i-n structure. Of course, a lot of work has already been dedicated to the optimization of the amorphous p-layer during the solar cell development in the previous years. Additional carbon alloying to widen the band gap of the amorphous phase within the microcrystalline p-layer showed no observable effect in this study. A possible explanation could be that microcrystalline growth immediately starts without a high amount of amorphous phase on the underlying ZnO substrate; no significant benefits from the widening of the gap can be expected in this case.

The deposition order in the n-i-p structure offers more possibilities for optimization. However, the optimization is complex and interactive since many cross dependencies have to be taken into account which are related to nucleation of microcrystalline films on the amorphous i-layer. The observed current losses in the blue part of the spectrum can mainly be attributed to absorption losses within the amorphous phase present in the microcrystalline p-layer. Alloying with carbon and lowering of the substrate temperature during deposition of the p-layer turned out to be suited means to achieve highly transparent p-layers without drawback in FF or V_{oc}. The lowering of the deposition temperature can also strongly increase the V_{oc} of the corresponding cells, as reported in [127].

The results described are still valid when using TMB as doping source during preparation of the microcrystalline p-layer instead of diborane. With TMB, a higher reproducibility was observed due to its higher thermal stability. Thermal dissociation of diborane at the reactor walls and the heater cause fluctuations which can be strongly reduced by a CO_2 plasma between the deposition runs as confirmed by SIMS measurements [90, 128]. Also the plasma excitation frequency does not affect the validity of the main statements. With both the RF and the VHF excitation, it was possible to achieve microcrystalline growth in a small process window. However, in the case of n-i-p cells (when growing on an amorphous substrate) even with high RF powers the maximum FF achieved remained below the values obtained with the VHF technique. This may be due to the fact, that more VHF depositions were performed, so further optimization of the RF process could still lead to improvements. In p-i-n cells, we obtained equivalent results with the RF and the VHF technique.

Low gap i-material at high substrate temperatures

Band gap tuning for application in stacked cells is an important way to increase the stabilized efficiency of the device. For a-Si:H/a-Si:H tandem cells, the top cell can be designed with a wide band gap i-layer prepared with high hydrogen dilution [10, 16] to produce a high open circuit voltage, while the band gap of the bottom cell should be reduced to maintain a high red response. For application in micromorph tandem cells, however, the high current of the microcrystalline bottom cell has to be matched. Here, low band gap absorbers are necessary to reduce the thickness of the degrading amorphous top cell.

Our efforts in the preparation of low gap a-Si:H i-layer material below 200 °C were not successful. Deposition at high substrate temperatures is the only way so far (in our group) to lower the band gap of the absorbing i-layer, however, with small drawbacks in material quality. A small cell series was deposited with this material to investigate the effects in both cell structures. Our investigations in the high temperature deposition regime followed reports by Takahama et al. [100].

Figure 7.1 shows our results on this topic: for substrate temperatures below 200 °C, the V_{oc} decrease of cells with both cell structures follows the decrease of the band gap of the i-layer. For substrate temperatures above 200 °C, a drop in V_{oc} for cells in the p-i-n structure can be observed which cannot be explained by the lower band gap of the i-layer. In addition, a significant increase in the absorption coefficient of the wide band gap p-layer is observed after annealing [98]. In contrast, the V_{oc} decrease of cells in the n-i-p structure still corresponds to the lowering of the band gap of the i-layer with higher substrate temperature, as indicated by the dotted line showing the E_{04} gap of the implemented i-layers. In a series of annealing experiments, we exactly reproduced the results reported by Takahama and confirmed the conclusion that the nature of the excessive drop in V_{oc} for p-i-n solar cells can be attributed to the deterioration of the p/i-interface due to the subsequent high temperature deposition of the i-layer.

From these considerations, it becomes clear that the n-i-p structure is more flexible for the choice of the deposition temperature also in tandem cells. The physical demands for the band gap tuning (low band gap = high substrate temperature) perfectly match the prerequisites given by the the n-i-p solar cell design (the bottom cell with the low band gap has to be deposited first). Since in the n-i-p structure, the p/i-interface is formed *after* the high temperature step of i-layer, no deteriorating effects have to be feared.

Light coupling

To obtain high efficiency solar cells, optimization of the light coupling is necessary to achieve maximum current output. The p-i-n and the n-i-p structure offer different possibilities to maximize the amount of light entering the absorbing i-layer. Figure 7.2 shows three possible applications of adapted light coupling for the p-i-n structure (7.2a) as well as the n-i-p structure (7.2b,c). All applications were realized with sputtered ZnO films. Texturing was achieved by post deposition etching in diluted HCl.

Figure 7.2a shows the p-i-n structure, which is usually deposited on a light scattering TCO/glass substrate. Optimization of the light coupling in this cell design can be per-

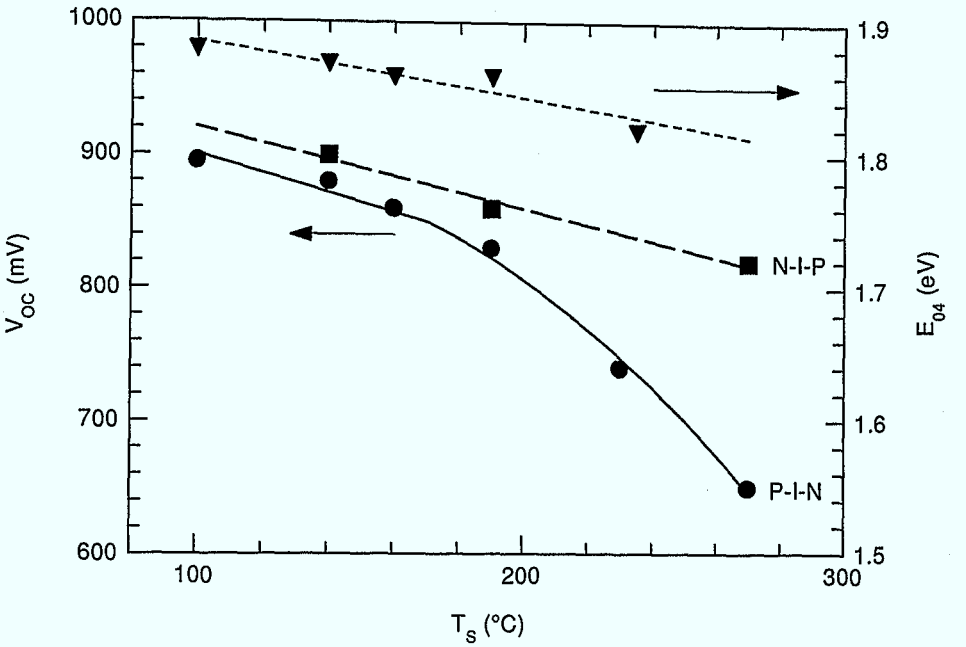

Figure 7.1: *V_{oc} (left axis) of solar cells and E_{04}-gap (right axis) of the corresponding i-layer as function of the substrate temperature T_s during deposition of the i-layer.*

formed by an optimization of the transparency and the surface texture of the ZnO film. Together with a highly reflective back reflector, the TCO substrate also controls the light trapping properties of the cell. However, the TCO also has to fulfill requirements regarding high conductivity – our experience showed that it is very difficult to fulfill all three demands (i.e. transparency, conductivity, and light scattering) with a single film. To reduce reflection losses, single or double layered anti reflection coatings can be applied. However, the reflection of glass itself is only 4 %, and the maximum gain in current expected is rather low, so this additional step is usually not considered for production because of the expected higher costs. Optical optimization to reduce absorption losses of the amorphous or microcrystalline p-layer by widening the band gap of the amorphous phase can be performed by carbon or oxygen alloying. The maximum quantum efficiency obtained for p-i-n cells (without anti reflection coating) is $\sim$ 80 % at 550 nm.

In Figure 7.2b, a textured ZnO/Ag substrate in combination with a ZnO front contact in anti-reflection design is shown. The anti-reflection coating maximizes the amount of light coupled into the cell. Optical optimization of the p-layer can be performed similarly to the p-i-n case. The n-i-p design in addition allows the low temperature deposition of the microcrystalline p-layer to widen the band gap (and enhance the V_{oc}), since the p-layer is

deposited as the last layer and hence deterioration of the p/i-interface by thermal annealing will not occur. The light trapping is controlled by the textured back reflector with no special requirements regarding conductivity or transparency in the short wavelength region. Hence, a separate optimization of light coupling and light trapping is possible here.

Because the anti-reflection coating is very thin ($\sim$ 80 nm), the attainable sheet resistance is to high if a series connection in modules is desired. Sketch c) shows a possible solution when conducting the ZnO top TCO as a thick contact: like for the p-i-n substrates, the wet chemical etching of the ZnO surface is used to obtain a suited surface texture to enhance the current output. Figure 7.3 shows the quantum efficiency of two codeposited n-i-p solar cells, one of them containing a texture etched front contact (for both cells, the top contact thickness is around 700 nm). In addition, both cells contain a texture etched back reflector as indicated in figure 7.2c). The overall quantum efficiency observed for these two cells is relatively low due to the high amount of reflected light (the ZnO/air interface reflects around 11 % of the incoming light!) and the optically non optimized p-layer used here. An improvement in j_{sc} of 5 % relative, without any loss in FF and V_{oc} can be observed for the cell with the texture etched front contact. For production, the textured ZnO front contact can be optically adjusted to the encapsulation material to reduce the amount of reflected light. The maximum quantum efficiency obtained for cells in the n-i-p design is $\sim$ 90 % at 550 nm, if the top contact is designed as anti-reflection coating.

In summary: when using the same material system for the p-i-n and n-i-p structure (namely ZnO/microcrystalline-p/amorphous-p/i/n/ZnO/Ag), one can proceed with the assumption that the n-i-p structure has an advantage over the p-i-n structure since the top TCO contact can be performed as a thin anti-reflection coating which enhances the quantum efficiency of the device without additional process steps (see also figure 6.18). However, due to a high sheet resistance of the thin TCO film, an additional grid system is necessary, causing a smaller active area of the cell. Moreover, a separate optimization of the light trapping ability is possible by optimization of the back reflector within certain limits.

Strictly speaking, the statements above are only valid for laboratory cells for the following reasons: to fully exploit the advantages of thin film technology, one wants to make use of the monolithic series connection. The p-i-n structure is fully compatible with the used laser scribing technique to achieve this.

7.2 Additional Aspects

Despite the advantages of the n-i-p technology mentioned in the previous section – the cell process is more adapted to the material requirements for different band gaps in tandem cells and the top contact can be conducted as anti-reflection coating providing a higher current yield – there are other basic aspects related to the differences in technology for the p-i-n and the n-i-p structure, which can influence the decision towards a preference of one technology. These aspects were not treated in this work. A summary of aspects is given in table 7.1, which will be briefly discussed in the following:

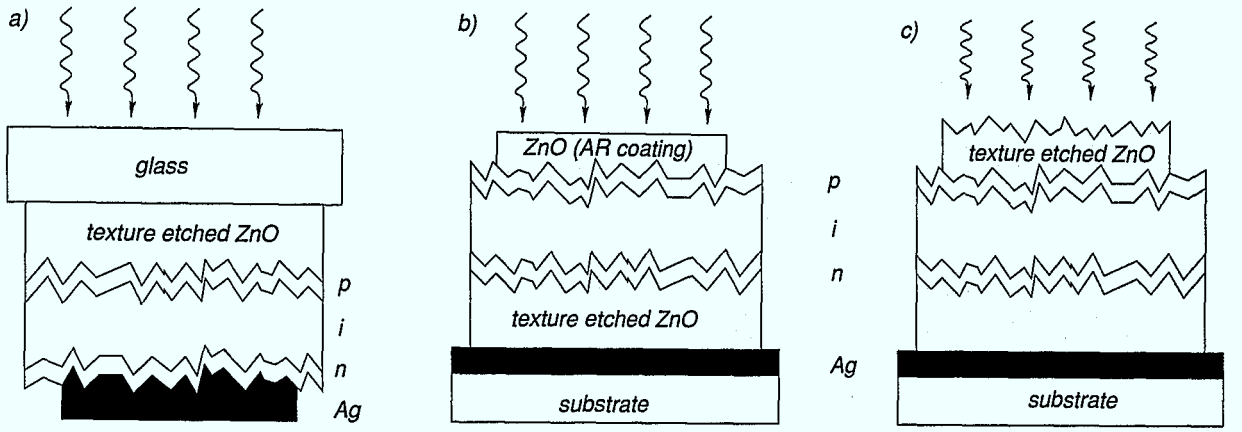

Figure 7.2: Schematic diagram of three investigated applications for ZnO films: a) textured front TCO for p-i-n cells, b) textured ZnO/Ag back reflector and front contact in the anti-reflection design, and c) textured back reflector and textured front TCO.

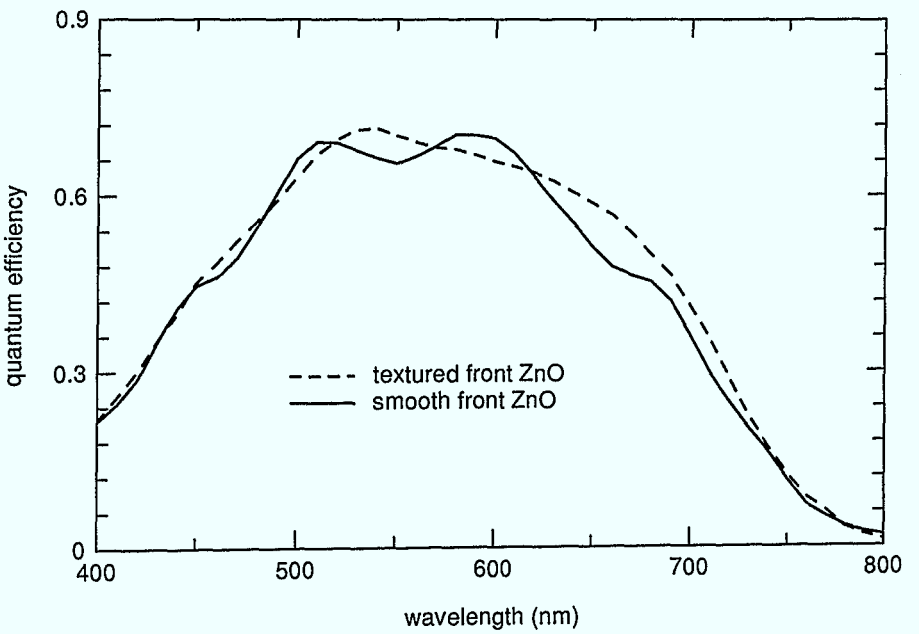

Figure 7.3: Comparison of the quantum efficiency of two n-i-p cells, one of them containing a texture etched ZnO front contact. Both cells are prepared on a texture etched back reflector.

	superstrate (p-i-n)	substrate (n-i-p)
substrate material	glass	glass, metal, plastic, foils...
series conncection	fully compatible with the laser scribing technology	complicated on conductive substrates
encapsulation	only from back side	requirements regarding transparency and long term stability
η_{max}(Lab.)	10.6 % (1 cm^2)	13.0 % (0.25 cm^2)
η_{max}(Mod.)	9.5 % (1200 cm^2)	10.5 % (909 cm^2)

Table 7.1: *Comparison of various technical aspects regarding the superstrate and substrate technology. Stabilized record efficiencies for laboratory cells (Lab.) and prototype modules (Mod.) cited from [130].*

The p-i-n technology itself is based on the availability of a cheap transparent substrate with suited light scattering properties. In most cases, this will be a TCO coated glass substrate. The handling of these rigid substrates is done by an easy and well established automated process. The n-i-p technology offers a wide variety of cheap substrates (metal or plastic foils, glass, etc.) amongst which the flexible ones have the potential for cheap, continuous roll-to-roll processing [129].

For application in solar power generators, a series conncetion of the solar cells is necessary to obtain the desired voltage output of the module. Here, the p-i-n cell technology is fully compatible with the laser scribing technique used for the monolithic series connection. In the n-i-p structure, the series interconnection requires a larger expense when using a conducting substrate since it has to be insulated first. In addition, the laser scribing technique can only be used when the top contact exceeds a certain thickness due to the high sheet resistance when using a thin top contact. Hence, either no internal series interconnection can be performed or the anti reflection advantage gets lost.

Concerning an effective protection against environmental impacts, the glass substrate in the p-i-n structure already provides efficient encapsulation from the front side and there are no special requirements for the encapsulation at the back side so that this last step can be achieved at rather low costs. In contrast, the front encapsulation in case of n-i-p solar cells has to fulfill requirements with respect to transparency and long term stability. Even when renouncing the series connection, the module has to be protected by an encapsulation disturbing the anti-reflection effect. However, the required encapsulation can be optimized optically together with the TCO top contact to maximize the amount of light coupled in (e.g. by matching of the refraction index).

To our point of view, there is no clear preference for either cell design considering module production. Some precise numbers can supply evidence to the balanced situation: the last row in table 7.1 shows the record efficiencies for laboratory results and (proto-

type) module production of two companies, of which the United Solar System Corporation (USSC) produces amorphous silicon solar cells in the n-i-p (substrate) structure, while SANYO prefers the p-i-n (superstrate) structure. The structure of the n-i-p cell is stainless steel/Ag/ZnO/a-SiGe:H/a-SiGe:H/a-Si:H/ITO, the Ag/ZnO reflector on stainless steel being highly reflective with adapted light scattering properties. Note that USSC does *not* perform the monolithic series connection. The p-i-n cell is deposited on a SnO_2 coated glass substrate (Asahi U) in an a-Si:H/a-SiGe:H structure. One can observe a drastic difference in laboratory record efficiency. However, the difference in stabilized record efficiency for a prototype module is much smaller. It remains an open question how the high efficiencies reached for both cell types can be transfered to production – all commercially available modules show efficiencies below 8 %. Detailed discussion of the gap between laboratory record efficiencies and the ones achieved in module production can be found in [130, 131].

TCO material

Another technical aspect is the choice of the TCO material and its deposition technique for the application as front contact and as material for the highly reflective TCO/metal back reflector. In this work, we decided to use sputtered ZnO as material for the front contact as well as for the highly reflective back reflector.

Sputtering in general is a well established industrial technique which allows large area production at low cost. It is a low temperature capable technique (< 250 °C) providing low energy consumption during the manufacturing process. It is fully compatible with a variety of cheap subtrate materials (e.g. Float glass) and allows coatings on almost any desired large area. Compared to Indium-tin-oxide (ITO) containing the rare element Indium, ZnO offers cheaper target costs. In combination with aluminum for a highly reflective back contact, ZnO also serves as a diffusion barrier to prevent contamination of the i-layer [82].

For the p-i-n technology, the development of the texture etched ZnO substrates offers the (future) potential to solve the supply problem of high quality TCO substrates in industry. ZnO also reduces the number of deposition techniques needed for the p-i-n solar cell manufacturing process, since sputtered ZnO is also used in combination with metal to prepare highly reflective back contacts to increase the current yield. The additional use of the APCVD or MOCVD technique for the preparation of the SnO_2 substrates currently used can be avoided. In the n-i-p case, ZnO offers the option to create an highly reflective, light scattering back reflector substrate needed for an effective light trapping. Moreover, this study showed that it is possible to replace the commonly used ITO with the more abundant and cheaper ZnO as material for the top contact.

To summarize, the choice of ZnO prepared with the sputter technique as TCO material has a number of specific technologically relevant advantages and offers a big cost reduction potential.

Chapter 8

Summary and Outlook

The objective of this thesis was the comparison of amorphous silicon solar cells in the p-i-n and the n-i-p structure. For both cell structures, sputtered ZnO films were established as front contact. The emphasis in this thesis was laid on the understanding of the restrictions and requirements which are introduced by the ZnO/p contact of amorphous silicon solar cells in the p-i-n and the n-i-p structure.

So far, in literature, comparisons of the two cell types were either based on experiments of different groups or on experiments of the same group but for different material systems, both lacking an important requirement for a comparative evaluation. Here, for the first time a comparison of the two structures was performed using the same deposition systems for both cell types, thereby guaranteeing the same material quality of the single p-, i-, and n-layers as well as the front TCO material. All components used consisted of device quality material in terms of electrical, optical, and microstructural properties. This allowed us to examine and evaluate the two cell structures using identical high quality material systems for the complete device. Of course, there are other aspects influencing the preference of one structure or the other, which were not treated in this thesis. A brief discussion of these aspects were given in section 7.2.

The experiments on solar cells showed that the problem at the amorphous-p/ZnO interface manifests itself in the p-i-n as well as in the n-i-p cell structure in the same way by an emerging contact barrier. In both cases, the independence on the p-layer thickness indicate the interface nature of this effect. As already known from earlier studies on p-i-n cells with ZnO front contact conducted in our group, the insertion of a microcrystalline contact layer solves this problem. During this work, it was found that also in the n-i-p structure with ZnO front contact, a microcrystalline p-layer is sufficient to reduce the influence of the contact barrier.

In a comprehensive study on microcrystalline p-layers we demonstrated that highly conductive films can be obtained with the industrially relevant RF technique at a plasma excitation frequency of 13.56 MHz as well as with the VHF technique at 110 MHz. Highly microcrystalline p-layers showing conductivities in the 0.1 S/cm range were realized on glass as

well as on intrinsic a-Si:H. The conductivities achieved with diborane and trimethylboron as doping source, respectively, were comparable high.

In the case of p-i-n solar cells, the deposition order is ideally suited to examine the influences of the TCO/p/i-region on the solar cell performance. From the corresponding experiments, the major perception gained during this work is that for p-i-n solar cells an amorphous/microcrystalline double p-layer led to optimum results. In n-i-p type solar cells, the investigation is more difficult due to complex cross dependencies related to the growth of a microcrystalline silicon film on an amorphous substrate. In this cell structure we found that the V_{oc} strongly depends on the structural properties of the p-layer and an amorphous phase between the low-ohmic microcrystalline-p/ZnO contact and the i-layer is essential to build up a high V_{oc}. This stands in contrast to earlier work, which claimed that the high V_{oc}'s obtained were the consequence of using highly microcrystalline p-layers.

To avoid optical absorption losses in the p-layer, a widening of the band gap by means of carbon or oxygen alloying or a lowering of the substrate temperature, respectively, is a common way. In the p-i-n case, a thickness optimization of both the amorphous and the microcrystalline p-layer already led to highly transparent wide gap p-layers which did not further benefit from carbon alloying. In the n-i-p solar cells, we successfully demonstrated that carbon alloying is a suited approach to reduce absorption losses of the microcrystalline p-layer. By lowering the substrate temperature during deposition of the p-layer, a further improvement was possible; this is a specific advantage of the n-i-p technology since the low temperature deposited p-layer is prepared as the last layer. After the optical optimization, we reached the same quantum efficiency in the blue wavelength region for both cell types. Due to the top contact, which was conducted as anti-reflection coating, the maximum quantum efficiency obtained for the n-i-p solar cells was higher than for p-i-n type cells. This is another advantage of the n-i-p technology.

The study on low band gap i-layer deposition showed that the decrease of the band gap by additional use of helium dilution during preparation of the i-layer reported by Ray et al. [106] could not be confirmed in the investigated deposition regime. A gas heating study resulted in material with extremely low defect density accompanied by a decrease in the Urbach energy E_0, but no lowering of the band gap was achieved. The increase of the deposition temperature to 400 °C led to a decrease in the E_{04}-gap by 180 meV compared to our standard i-layer material prepared at 200 °C. However, the defect density was increased even after optimization of the deposition conditions.

By using elevated substrate temperatures during deposition of the i-layer, we implemented low gap i-layer material in p-i-n and n-i-p solar cells and were able to confirm earlier results reported by Takahama et al. : in the p-i-n case, substrate temperatures above 200 °C lead to a deterioration of the p/i-interface resulting in a drastic drop in V_{oc}. In contrast, the V_{oc} of the corresponding n-i-p devices only decreases according to the lower band gap of the i-layer. However, within this thesis, the specific advantage of the more adapted deposition order in tandem cells with the n-i-p structure could not be exploited to an extent where higher solar cell efficiency was achieved.

Implementation of wide gap i-layers prepared at low substrate temperatures and high hydrogen dilution during deposition of the i-layer, which were developed previously, already demonstrated that higher V_{oc} values and higher stabilized efficiencies are obtained in the case of p-i-n solar cells. Our efforts in preparing high efficient p-i-n and n-i-p solar cells with ZnO front contact showed that this concept is still valid for the n-i-p development. This means that future improvements made in the material quality and device design can be applied to p-i-n and n-i-p solar cells equivalently.

To prepare highly efficient solar cells, we developed highly conductive and transparent ZnO films on glass substrates as well as on complete n-i-p devices in a sputter deposition regime below 10 mTorr and at low substrate temperatures (100°C). A post deposition wet chemical etching procedure in diluted HCl was introduced to texturize the initially smooth ZnO films. The light scattering properties can be simply tuned by variation of the etching time. The developed films served as coating for p-i-n substrates as well as top contact for n-i-p cells.

For the p-i-n cell type, our solution of the amorphous-p/ZnO problem by means of an adapted microcrystalline/amorphous double p-layer structure and the good optical and electrical properties of the developed ZnO substrates are mirrored in high FF's and high short circuit current densities obtained on these substrates. A maximum initial efficiency of 10.2 % was obtained for an a-Si:H/a-Si:H tandem cell prepared on texture etched ZnO. The stable efficiency after 800 h of light soaking was 9.2 %. This is an excellent value, also with respect to the technology status of tandem cells on SnO_2 substrates (Ashai U) in our and other groups. By implementation of an optimized amorphous top cell into a micromorph tandem cell, an initial efficiency of 11.1 % was achieved.

The objective of establishing the n-i-p technology and preparing functioning n-i-p devices with satisfying properties has been achieved. This comprises a reliable, reproducible n-i-p cell process. The achieved status based on the mentioned developments is a n-i-p solar cell containing a microcrystalline p-layer prepared with the VHF technique showing an initial efficiency of 8.5 % (V_{oc} =850 mV, FF=70.1 %, j_{sc} =14.3 mA/cm^2) on a transparent substrate. This cell also served as a top cell in an inverted micromorph tandem cell with 10.6 % initial efficiency which was prepared in our group.

Outlook

Beyond the scientific study and comparison of p-i-n and n-i-p cells, the technological development of the studied cell structures yielded a number of results highly relevant for industrial application and implementation: The optical and electrical properties of the TCO substrate is essential for the development of highly efficient p-i-n modules. Currently, only SnO_2-based TCO substrates with non-optimal quality are available for large area production. To overcome this limiting element for module production, the application for a joint venture between research and industry is already under way.

The successful development of a p-i-n solar cell on our newly developed texture etched ZnO substrate, which showed a stabilized efficiency of 9.2 % after more than 900 h of light soaking, clearly demonstrated that

- an adapted microcrystalline p-layer design solves the amorphous-p/ZnO problem and
- ZnO is a promising alternative substrate material to the commercially available SnO_2 substrates.

Our group will be responsible for the process up-scaling, which will be performed in a newly installed 30 × 30 cm^2 PECVD deposition system. This will close the gap between our experimental 10 × 10 cm^2 deposition system and large scale industrial production systems.

Major effort is currently dedicated to the development of RF deposited microcrystalline p-layers, since major problems are expected for the up-scaling of a VHF process. These problems are related to matching problems of high frequency power into large area reactors in connection with the high uniformity desired for the manufacturing process. The homogeneity of the thin layers has to be granted in order to obtain a high yield across the whole substrate area, which is especially important for later production issues. For the same reason, the developed cell process has to be highly reproducible to facilitate the transfer from the laboratory process to the production line. Fine tuning for the optical optimization of an adapted microcrystalline/amorphous double p-layer structure will be regarded. Alloying with carbon or oxygen and more experiments on low temperature deposition will be investigated in this context. Also a preconditioning of the ZnO substrate surface may be necessary to achieve homogeneous growth of the microcrystalline p-layer.

Future work will be dedicated to high rate sputter deposition of ZnO. This could be a decisive cost relevant element when planning a production of ZnO substrates for the p-i-n development as well as for a thick top contact in cells with the n-i-p design which would allow the monolithic series connection. Recent investigations of our group showed, that DC sputtered ZnO films can also be textured in diluted HCl [87]. DC sputtering from metallic targets allows very high deposition rates and offers a further cost reduction potential. However, up-scaling of this technique has still to be demonstrated.

For the development of p-i-n substrates on ZnO basis, material related problems have to be solved, too: Since ZnO shows a lower absorption in the near IR region of the spectrum compared to SnO_2, investigations and adaption of the laser scribing process have to be conducted in order to obtain a high ohmic disruption of the ZnO film for the series connection. Another problem to be solved is the homogeneous etching and cleaning procedure for large area substrates since ZnO is a highly soluble material in acid and lye (exactly this effect is used for the texturing of these substrates!).

For the n-i-p technology, future effort should be dedicated to the development of highly reflective substrates on basis of glass/Ag/ZnO and stainless steel. The successful replacement of the commonly used ITO with sputtered ZnO as front contact material without

drawback in device performance offers the possibility to produce n-i-p solar cells at substantially lower production costs. The development of an inverted micromorph cell with 10.6 % initial efficiency showed the potential of this promising material combination. There is a strong desire for high rate deposition of intrinsic microcrystalline silicon films to provide a short deposition time for the device. This necessitates further collaboration with other European research groups. A problem to be solved when extending the n-i-p activity will be the stability of ZnO when used as front contact, which is critical for the long term reliability of the modules. This will be closely related to a suited encapsulation procedure as protection against environmental impacts.

In conclusion, the investigations described in this thesis can contribute to improvements of the efficiency of thin film solar cells in the p-i-n as well as the n-i-p technology. In addition, this study pointed out promising ways for cost reduction which can lead to further development of the photovoltaic technology.

Appendix A

Deposition Parameters for Microcrystalline p-layer Development

RF-technique
The substrate temperature throughout this study was $\sim$ 200 °C, the hydrogen flow was 200 sccm and the silane flow 0.75 sccm. The used frequency was 13.56 MHz. Note: B_2H_6 is delivered as a 5 %-mixture in helium, and TMB is a 2 %-mixture in helium. The gas correction factors for the different mass flow controllers (MFC) are *not* taken into account in the table[a] (all MFC's are calibrated with nitrogen).

[a]The factors are as follows: 1.3 for the diborane controller, 1.36 for the TMB-controller and 0.72 for the methane controller.

Nr.	gas flow (sccm)			pressure	power	time	thickness	rate	σ_d
	B_2H_6	TMB	CH_4	(mTorr)	(Watt)	(min.)	(nm)	Å/s	(S/cm)
96217	0.072	0	0	3500	5	33	50	0.25	0.008
96219	0.072	0	0	2000	5	16	25	0.27	4e-6
96220	0.072	0	0	2500	5	21	30	0.23	0.036
96221	0.072	0	0	3000	5	20	30	0.25	0.11
96223	0.072	0	0	3000	5	10	15	0.25	0.067
96225	0.072	0	0	3000	5	40	100	0.42	0.039
96226	0.072	0	0	3000	5	92	200	0.37	0.015
96227	0.072	0	0	3000	5	15	30	0.32	0.06
96228	0.08	0	0	3000	5	20	33	0.28	0.1
96229	0.09	0	0	3000	5	20	50	0.42	0.17
96230	0.06	0	0	3000	5	20	50	0.42	0.4
96231	0.1	0	0	3000	5	20	25	0.22	0.1
96232	0.05	0	0	3000	5	20	20	0.17	2.1
96233	0.04	0	0	3000	5	20	20	0.17	1.3
98394	0.06	0	0	3000	5	20	30	0.25	0.26
98396	0.06	0	0	3000	10	20	40	0.33	0.12
98402	0.06	0	0	3000	25	20	110	0.92	4
98406	0.06	0	0	3000	25	10	80	1.33	1
98407	0.06	0	0	3000	25	40	200	0.83	10
98434	0	0.06	0	3000	25	20	60	0.5	4e-4
98435	0	0.12	0	3000	25	20	80	0.67	0.16
98451	0	0.144	0	3000	25	20	90	0.75	0.45
98462	0	0.108	0	3000	25	20	75	0.63	1.5
98464	0	0.18	0	3000	25	20	80	0.67	1
98465	0	0.24	0	3000	25	20	100	0.83	0.05
98466	0	0.3	0	3000	25	20	90	0.75	6.5e-3
98467	0	0.36	0	3000	25	20	95	0.79	1e-5
99023	0	0.144	0.2	3000	25	20	70	0.58	0.5
99028	0	0.144	0.1	3000	25	20	80	0.67	1.8
99029	0	0.144	0.3	3000	25	20	75	0.63	0.17
99030	0	0.1	0.2	3000	25	20	70	0.58	0.2
99031	0	0.1	0.1	3000	25	20	60	0.5	0.2
99032	0	0.1	0.3	3000	25	20	200	1.67	0.04

Table A.1: *The table contains the deposition parameters during the optimization study of the microcrystalline p-layers on glass. The first column shows an internal identification number of each sample. The next 3 columns show the doping and alloying gas flow (without correction factors of the MFC's). This is followed by the deposition pressure, the applied RF-power and the deposition time as well as the thickness measured with a step profiler. From the latter two, the deposition rate is calculated. The dark conductivity value is averaged from at least 3 spots on each sample if possible (sometimes only one or two values were accessible due to inhomogeneous deposition.)*

Bibliography

[1] *Proceedings of the* 26^{th} *IEEE Photovoltaic Specialist Conference*, Anaheim (1997).

[2] *Material Research Society Symposium Proceedings*, San Francisco (1998).

[3] J. Schmidt, H.A. Ossenbrink, P. Helm, H. Ehmann and E.D. Dunlop (ed.). *Proceedings of the* 2^{nd} *World Conference on Photovoltaic Solar Energy Conversion*, Vienna (1998).

[4] A. CATALANO. *Solar Cells Made of Amorphous and Microcrystalline Semiconductors.* In *Amorphous and Microcrystalline Semiconductor Devices: Optoelectronic Devices*, J. Kanicki (ed.), Vol. 2, p. 9 – 75. Artech House, Inc., Boston, London (1991).

[5] D.E. CARLSON and C.R. WRONSKI. *Amorphous Silicon Solar Cell.* Applied Physics Letters **28**(11) 671 – 673 (1976).

[6] D.L. STAEBLER and C.R. WRONSKI. *Reversible Conductivity Changes in Discharge Amorphous Si.* Applied Physics Letters **31**(4) L292 – L294 (1977).

[7] Y. HISHIKAWA, S. TSUGE, N. NAKAMURA, S. TSUDA, S. NAKANO and Y. KUWANO. *Device-Quality Wide-Gap Hydrogenated Amorphous Silicon Films Deposited by Plasma Chemical Vapor Deposition at Low Substrate Temperatures.* Journal of Applied Physics **69**(1) 508 – 510 (1991).

[8] J. YANG, X. XU and S. GUHA. *Stability Studies of Hydrogenated Amorphous Silicon Alloy Solar Cells Prepared with Hydrogen Dilution.* Material Research Society Symposium Proceedings **336** 687 – 692 (1994).

[9] P. SIAMCHAI, A. YAMADA, M. KONAGAI, J.H. JANG and K.S. LIM. *Improvement of a-Si Solar Cells Fabricated by Mercury-Sensitized Photo-CVD Using* H_2 *Dilution Method.* In *Proceedings of the* 1^{st} *WCPEC*, p. 492 – 495, Hawaii (1994).

[10] S. WIEDER, B. RECH, C. BENEKING, F. SIEBKE, W. REETZ and H. WAGNER. *Influences of Hydrogen Dilution and Substrate Temperature on the Initial and Stabilized Performance of a-Si:H Solar Cells.* In *Proceedings of the* 13^{th} *EC PVSEC*, p. 613 – 616, Nice (1995).

[11] Y. TAWADA, M. KONDO, H. OKAMOTO and Y. HAMAKAWA. *Hydrogenated Amorphous Silicon Carbide as a Window Material for High Efficiency Solar Cells.* Solar Energy Materials **6** 299 – 315 (1982).

[12] S. GUHA, J. YANG, P. NATH and M. HACK. *Enhancement of Open Circuit Voltage in High Efficiency Amorphous Silicon Alloy Solar Cells.* Applied Physics Letters **49**(4) 218 – 219 (1986).

[13] Y. UCHIDA. *Light-Induced Degradation in Amorphous Silicon Solar Cells.* In *Proceedings of the* 7^{th} *EC PVSEC*, p. 395 – 401, Sevilla (1986).

[14] M.S. BENNETT and K. RAJAN. *The Stability of Multi-Junction a-Si Solar Cells.* In *Proceedings of the* 20^{th} *IEEE PVSC*, p. 67 – 72, Las Vegas (1988).

[15] H. SAKAI and Y. ICHIKAWA. *Process Technology for a-Si/a-Si Doble Stacked Tandem Solar Cells with Stabilized 10 % Efficiency.* Journal of Non-Crystalline Solids **137 & 138** 1155 – 1160 (1991).

[16] B. RECH, C. BENEKING, S. WIEDER, T. EICKHOFF and H. WAGNER. *Development of a–Si:H/a–Si:H Stacked Solar Cells with High Efficiency and High Light Stability.* In *Proceedings of the* 13^{th} *EC PVSEC*, Nice (1995). 613 – 616.

[17] G. NAKAMURA, K. SATO and Y. YUKIMOTO. *High Performance Tandem Amorphous Solar Cells.* In *Proceedings of the* 16^{th} *IEEE PVSC*, p. 1331 – 1337, San Diego (1982).

[18] J. YANG, A. BANERJEE and S. GUHA. *Triple–Junction Amorphous Silicon Alloy Solar Cell with 14.6 % Initial and 13.0 % Stable Conversion Efficiency.* Applied Physics Letters p. 2975 – 2977 (1997).

[19] K. YAMAMOTO, M. YOSHIMI, T. SUZUKI, Y. TAWADA, Y. OKAMOTO and A. NAKAJIMA. *Below 5 μm Thin film Poly-Si Solar Cell on Glass Substrate Fabricated at Low Substrate Temperature.* In *Proceedings of the* 2^{nd} *WCPEC*, p. 1284 – 1289, Vienna (1998).

[20] K. SATO, Y. GOTOH, Y. WAKAYAMA, Y. HAYASHI, K. ADACHI and H. NISHIMURA. *Highly Textured SnO_2:F TCO Films for a-Si Solar Cells.* Technical Report 42, Asahi Glass Co. (1992). Reports of the Research Laboraory.

[21] A. LÖFFL. *Präparation hochleitfähiger transparenter Zinkoxidschichten mit kontrollierter Texturierung für Dünnschichtsolarzellen.* Diploma thesis, Fachhochschule München (1997).

[22] A. LÖFFL, S. WIEDER, B. RECH, O. KLUTH, C. BENEKING and H. WAGNER. *Al-doped ZnO Films for Thin-Film Solar Cells with Very Low Sheet Resistance and Controlled Texture.* In *Proceedings of the* 14^{th} *EC PVSEC*, p. 2089 – 2092, Barcelona (1997).

[23] R.A. STREET. *Hydrogenated Amorphous Silicon.* Cambridge Solid State Science Series. Cambridge University Press, Cambridge (1991).

[24] W. LUFT and Y.S. TSUO. *Hydrogenated Amorphous Silicon Alloy Deposition Processes.* Applied physics series. Marcel Dekker, Inc., New York (1993).

[25] A. MADAN and M.P. SHAW. *The Physics and Application of Amorphous Semiconductors.* Academic Press, Boston (1988).

[26] J.I. Pankove (ed.). *Semiconductors and Semimetals*, Vol. 21 A–D. Academic Press, New York (1984).

[27] H. WAGNER. *Anwendungen von amorphen Siliziumschichten.* In *17. IFF Fereinkurs: Dünne Schichten und Schichtsysteme*, p. 689 – 696. Forschungszentrum Jülich (1986).

[28] W.E. SPEAR and P.G. LE COMBER. *Substitutional Doping of Amorphous Silicon.* Solid State Communications **17** 1193 – 1196 (1975).

[29] M. STUTZMANN, D.K. BIEGELSEN and R.A. STREET. *Detailed Investigation of Doping in Hydrogenated Amorphous Silicon.* Physical Review B **35**(11) 5666 (1987).

[30] N. SCHULTZ. *Präparation und Charakterisierung transparenter Metalloxid–Schichten für Solarzellen aus amorphem Silizium.* Diploma thesis, RWTH Aachen (1994).

[31] C. BENEKING, B. RECH, T. EICKHOFF, Y.G. MICHAEL, N. SCHULTZ and H. WAGNER. *Preparation and Light Stability of a-Si/a-Si Stacked Solar Cells.* In *Proceedings of the* 12^{th} *EC PVSEC, Amsterdam*, p. 683 (1994).

[32] M. STUTZMANN. *Weak Bond – Dangling Bond Conversion in Amorphous Silicon.* Philosophical Magazine B **56** 63 – 70 (1987).

[33] J. MEIER, S. DUBAIL, R. FLÜCKIGER, D. FISCHER, H. KEPPNER and A. SHAH. *Intrinsic Mycrocrystalline (μc-Si:H) – a Promising New Thin Film Solar Cell Material.* In *Proceedings of the* 24^{th} *IEEE PVSC*, p. 409 – 412, Hawaii (1994).

[34] B. RECH. *Solarzellen aus amorphem Silizium mit hohem stabilen Wirkungsgrad.* Dissertation, RWTH Aachen (1997). Bericht des Forschungszentrums Jülich, ISSN 0944–2952.

[35] A. BANERJEE and S. GUHA. *Study of Back Reflectors for Aorphous Silicon Alloy Solar Cell Application.* Journal of Applied Physics **69** 1030 – 1035 (1991).

[36] K. YAMAMOTO, M. YOSHIMI, T. SUZUKI, Y. OKAMOTO, Y. TAWADA and A. NAKAJIMA. *Thin Film Poly-Si Solar Cell With "STAR Structure" on Glass Substrate Fabricated at Low Temperature.* In *Proceedings of the* 26^{th} *IEEE PVSC*, p. 575 – 580, Anaheim (1997).

[37] K.L. CHOPRA, S. MAJOR and D.K. PANDYA. *Transparent Conductors - a Status Review.* Thin Solid Films **102** 1 – 46 (1983).

[38] J.C. VOSSEN. *Transparent Conducting Films.* Physics of Thin films **9** 1 – 71 (1977).

[39] B. RECH, C. BENEKING, S. WIEDER, U. ZASTROW, F. BIRMANS, W. APPENZELLER, O. KLUTH, H. STIEBIG, J. FÖLSCH, H. WAGNER, W. FRAMMELSBERGER, R. GEYER, P. LECHNER, H. RÜBEL, H. SCHADE and H. MAURUS. *Challenges in a-Si PV Technology Transfer: From Research Lab to Production Line.* In *Proceedings of the* 2^{nd} *WCPEC*, p. 391 – 396, Vienna (1998).

[40] M. KUBON, E. BÖHMER, F. SIEBKE, B. RECH, C. BENEKING and H. WAGNER. *Solution of the ZnO/p Contact Problem in a-Si:H based Solar Cells.* Solar Energy Materials **41/42** 485 – 492 (1996).

[41] E. BÖHMER, B. SIEBKE, F. RECH, C. BENEKING and H. WAGNER. *More Insights into the ZnO/a-SiC:H(B) Interface — an Improved TCO/p Contact.* Material Research Society Symposium Proceedings **426** 519 – 524 (1996).

[42] K. WINZ, B. RECH, T. EICKHOFF, C. BENEKING, C.M. FORTMANN, P. HAPKE and H. WAGNER. *Optoelectronic Properties of Thin Amorphous and Microcrystalline p-Type Silicon Based Films Developed for Amorphous Silicon-Based Solar Cells.* Material Research Society Symposium Proceedings **420** 819 – 824 (1996).

[43] Y. HATTORI, D. KRUANGAM, K. KATOH, Y. NITTA, H. OKAMOTO and Y. HAMAKAWA. *High-Conductive Wide Band Gap p-Type a-SiC:H Prepared by ECR CVD and its Application to High Efficiency a-Si Based Solar Cells.* In *Proceedings of the* 19^{th} *IEEE PVSC*, p. 689 – 694, New Orleans (1987).

[44] W. MA, T. SAIDA, C.C. LIM, S. AOYMA, H. OKAMOTO and Y. HAMAKAWA. *The Utilization of Microcrystalline Si and SiC for the Efficiency Improvement in a-Si Solar Cells.* In *Proceedings of the* 1^{st} *WCPEC*, p. 417 – 420, Hawaii (1994).

[45] M. KOLTER. *Herstellung und Charakterisierung von Kontaktschichten in Solarzellen aus amorphem Silizium.* Diploma thesis, RWTH Aachen (1993). Bericht des Forschungszentrums Jülich 2751, ISSN 0366–0885.

[46] L. YANG, L. CHEN, S. WIEDEMANN and A. CATALANO. *Microcrystalline Silicon in a-Si:H Based Multijunction Solar Cells.* Material Research Society Symposium Proceedings **283** 463 – 470 (1993).

[47] A. BANERJEE, Y. YANG, T. GLATFELTER, K. HOFFMANN and S. GUHA. *Experimental Study of p-Layers in "Tunnel" Junctions for High Efficiency Amorphous Silicon Alloy Multijuntion Solar Cells Modules.* Applied Physics Letters **64** 1517 – 1519 (1994).

[48] R. COLLINS and Y. YANG. *In Situ Ellipsometry of Thin-Film Deposition: Implications for Amorphous and Microcrystalline Si Growth.* Journal of Vacuum Science and Technology B **7** 1155 – 1161 (1989).

[49] F. FINGER, R. CARIUS, P. HAPKE, L. HOUBEN, M. LUYSBERG and M. TZOLOV. *Growth and Structure of Microcrystalline Silicon Prepared with Glow Discharge at Various Plasma Excitation Frequencies.* Material Research Society Symposium Proceedings **452** 725 – 736 (1997).

[50] M. TZOLOV, F. FINGER, R. CARIUS and P. HAPKE. *Optical and Transport Studies on Thin Microcrystalline Silicon Films Prepared by Very High Frequency Glow Discharge for Solar Cell Applications.* Journal of Applied Physics **81** 7376 – 7385 (1997).

[51] L. HOUBEN. *Plasmaabscheidung von mikrokristallinem Silizium: Merkmale der Mikrostruktur und deren Deutung im Sinne von Wachstumsvorgängen.* Dissertation, Heinrich-Heine-Universität Düsseldorf (1998).

[52] B. CHAPMAN. *Glow Discharge Processes.* John Wiley & Sons, New York, Chichester, Brisbane, Toronto, Singapore (1980).

[53] R.A. HAEFER. *Oberflächen– und Dünnschicht–Technologie Teil I, Beschichtungen von Oberflächen.* Springer–Verlag, Berlin, Heidelberg, New York, London, Paris, Tokyo (1987).

[54] H. FREY and G. KIENEL. *Dünnschichttechnologie.* VDI Verlag, Düsseldorf (1987).

[55] C.C. TSAI. *Plasma Deposition of Amorphous and Crystalline Silicon: The Effect of Hydrogen on the Growth, Structure and Electronic Properties.* In *Amorphous Silicon and Related Materials*, H. Fritzsche (ed.), p. 123 – 147. Academic Press (1988).

[56] N. SHIBATA, K. FUKADA, H. OHTOSHI, J. HANNA, S. ODA and I. SHIMIZU. *Growth of Amorphous and Crystalline Silicon by HR–CVD (Hydrogen Radical Enhanced CVD).* Material Research Society Symposium Proceedings **26** 225 – 243 (1987).

[57] A. MATSUDA. *Formation Kinetics and Control of Microcrystallte in μc-Si:H from Glow Discharge Plasma.* Journal of Non-Crystalline Solids **59&60** 767 – 774 (1983).

[58] B. RECH. *Funktionsschichten mit großem Bandabstand für Solarzellen aus amorphem Silizium.* Diploma thesis, RWTH Aachen (1993).

[59] C. BENEKING, F. FINGER and H. WAGNER. *Silane Deposition Plasma and Reactor Characterization in the VHF Range.* In *Proceedings of the* 11^{th} *EC PVSEC*, p. 586 – 589, Montreux (1992).

[60] H.K. PULKER. *Coatings on Glass.* Elsevier, Amsterdam, Oxford, New York, Tokyo (1984).

[61] O. KLUTH. *Präparation und Charakterisierung von texturierten Metalloxid-Schichten für Dünschichtsolarzellen.* Diploma thesis, RWTH Aachen (1996).

[62] Y. HISHIKAWA, N. NAKAMURA, S. TSUDA, S. NAKANO, Y. KISHI and Y. KUWANO. *Interference–Free Determination of the Optical Absorption Coefficient and the Optical Gap of Amorphous Silicon Thin Films.* Japanese Journal of Applied Physics **30**(5) 1008 – 1014 (1991).

[63] J. TAUC, R. GRIGOROVICI and A. VANCU. *Optical Properties and Electronic Structure of Amorphous Germanium.* Physica Status Solidi **15** 627 – 637 (1966).

[64] O. KLUTH, A. LÖFFL, S. WIEDER, C. BENEKING, W. APPENZELLER, L. HOUBEN, B. RECH, H. WAGNER, S. HOFFMANN, R. WASER, J.A. ANNA SELVAN and H. KEPPNER. *Texture Etched Al-doped ZnO: a New Material for Enhanced Light Trapping in Thin Film Solar Cells.* In *Proceedings of the* 26^{th} *IEEE PVSC*, p. 715 – 718, Anaheim (1997).

[65] N. SACHER. *Herstellung und Charakterisierung von transparenten und leitfähigen Sputterschichten auf Basis von aluminiumdotiertem Zinkoxid.* Diploma thesis, FH München (1996).

[66] F. SIEBKE. *In-situ Bestimmung der elektronischen Oberflächen- und Volumendefektdichte von amorphem Silizium (a-Si:H) und verwandten Legierungen.* Dissertation, RWTH Aachen (1992). Bericht des Forschungszentrums Jülich 2643.

[67] M. WAGNER. Technical Report. (1992). Bericht des Forschungszentrums Jülich, ISSN 0366-0885.

[68] N. WYRSCH, F. FINGER, T.J. MCMAHON and M. VANECEK. *How to Reach More Precise Interpretation of Subgap Absorption Spectra of Deep Defect Density in a-Si:H.* Journal of Non–Cristalline Solids **137&138** 347 – 350 (1991).

[69] F. SIEBKE and H. STIEBIG. *The Interpretation of the Constant Photocurrent Method in Terms of Deep Defect Density of States in a–Si:H.* Material Research Society Symposium Proceedings **336** 371 – 376 (1994).

[70] J.M. BENNETT and L. MATTSSON. *Introduction to Surface Roughness and Scattering.* Optical Society of America, Washington D.C. (1989).

[71] K. HEIDLER. *Photovoltaische Messtechnik.* In *Solarzellen*, Meissner (ed.), p. 184. Vieweg, Braunschweig, Wiesbaden (1993).

[72] C. ULRICHS. *Dynamischer und spektraler Response amorpher Silizium- Solarzellen.* Diploma thesis, TU Braunschweig (1990).

[73] T. WITTCHEN, H.-C. HOLSTENBERG, D. HÜNERHOFF, Z.J. MIN and J. METZDORF. *Solar Cell Calibration and Characterization: Simplified DSR Apparatus.* In *Proceedings of the 20th IEEE PVSC*, p. 1251 – 1257, Las Vegas (1988).

[74] J. METZDORF. *Calibration of Solar Cells. 1: The Differential Spectral Responsivity Method.* Applied Optics **26**(9) 1701 – 1708 (1987).

[75] D. FISCHER. *Electric Field and Photocarrier Collection in Amorphous Silicon p-i-n Solar Cells. Effects of Light-Induced Degradation and of Low-Level i-layer Doping.* Dissertation, Université de Neuchâtel, Switzerland (1994).

[76] A. SCHÖNECKER. *Messung der spektralen Empfindlichkeit von Hochleistungszellen.* Dissertation, Universität Freiburg, Freiburg (1994).

[77] W. LUFT, B. STAFFORD and B. VON ROEDERN. *Stabilized Module Performance as a Goal for the Photovoltaic Amorphous Silicon Program in the United States.* AIP Conference Proceedings **234** 3 – 10 (1991).

[78] T. MINAMI, H. SATO, H. NANTO and S. TAKATA. *Heat Treatment in Hydrogen Gas and Plasma for Transparent Conductive Oxide Films such as ZnO, SnO_2, and Indium Tin Oxide.* Thin Solid Films **176** 277 – 282 (1989).

[79] A. CATALANO, M. BENNETT, J. NEWTON, L. YANG, Y.-M. LI, B. FIESELMANN, S. WIEDEMANN and R.V. D'AIELLO. *Progress Towards High Performance Low Cost a-Si:H Alloy Multijunction Modules.* AIP Conference Proceedings **286** 58 – 63 (1992).

[80] K. SATO, Y. MATSUI, K. ADACHI, Y. GOTOH, Y. HAYASHI and H. NISHIMURA. *Hydrogen Plasma Treatment of ZnO-coated TCO Films.* In *Proceedings of the 23rd IEEE PVSC*, p. 855 – 859, New York (1993).

[81] L. YANG, M. BENNETT, L. CHEN, K. JANSEN, J. KESSLER, Y. LI, J. NEWTON, K. RAJAN, F. WILLING, R. ARYA and D. CARLSON. *Technological Development for Commercialization of Amorphous Silicon Based Multijunction Modules.* Material Research Society Symposium Proceedings **420** 839 – 848 (1996).

[82] M. GOETZ, H. KEPPNER, P. PERNET, W. HOTZ and A. SHAH. *Contamination Problems of Amorphous Silicon n-i-p Solar Cells on Metal Substrates.* Material Research Society Symposium Proceedings **426** 89 – 94 (1996).

[83] T. MINAMI, H. NANTO and S. TAKATA. *Highly conductive and Transparent Aluminum Doped Zinc Oxide Films Prepared by RF Magnetron Sputtering.* Japanese Journal of Applied Physics **23**(5) L280 – L282 (1984).

[84] T. NAKADA, Y. OHKUBO and A. KUNIOKA. *Textured ZnO:Al Films for Solar Cells by DC-Magnetron Sputtering in Water Vapor Plasma.* In *Proceedings of the 22nd IEEE PVSC*, p. 1389 – 1392, Las Vegas (1991).

[85] O. KLUTH, C. BENEKING, B. RECH, W. APPENZELLER, H. WAGNER, R. WASER and S. HOFFMANN. *Nucleation and Growth of Textured Al-Doped ZnO Films for a-Si:H Solar Cells Analyzed by High Resolution SEM.* In *Technical Digest of the International PVSEC-9*, p. 357 – 358, Miyasaki (Japan) (1996).

[86] J.A. ANNA SELVAN, H. KEPPNER and A. SHAH. *The Growth of Textured Aluminium Doped ZnO Films for a-Si Solar Cells by RF Magnetron Sputtering at Low Temperature.* Material Research Society Symposium Proceedings **426** 497 – 502 (1996).

[87] O. KLUTH, B. RECH, L. HOUBEN, S. WIEDER, G. SCHÖPE, C. BENEKING, H. WAGNER, A. LÖFFL and H.W. SCHOCK. *Texture Etched ZnO:Al Coated Glass Substrates for Silicon Based Thin Film Solar Cells.* Thin Solid Films (1998). in print.

[88] K. PRASAD. *Microcrystalline Silicon (μc-Si:H) Prepared With Very High Frequency Glow Discharge (VHF-GD) Process.* Dissertation, Université de Neuchâtel (1992).

[89] F. FINGER, P. HAPKE, M. LUYSBERG, R. CARIUS, H. WAGNER and M. SCHEIB. *Improvement of Grain Size and Deposition Rate of Microcrystalline Silicon by use of Very High Frequency Glow Discharge.* Applied Physics Letters (1994).

[90] M. KUBON. *Präparation und Eigenschaften der p–seitigen Grenzflächen in Solarzellen aus amorphem Silizium.* Dissertation, RWTH Aachen (1995).

[91] R. FLÜCKIGER, J. MEIER, A. SHAH, J. PHOL, M. TZOLOV and R. CARIUS. *Structural, Optical and Electrical Properties of <p> μc-Si:H Thin Films Deposited by the VHF-GD.* Material Research Society Symposium Proceedings **xy** 793 – 798 (1994).

[92] P. SICHNUGRIST, T. SASAKI, A. ASANO, I. ICHIKAWA and H. SAKAI. *Amorphous Silicon Oxide and its Application to Metal/n-i-p/ITO Type a-Si Solar Cells.* Solar Energy Materials and Solar Cells **34** 415 – 422 (1994).

[93] N. PELLATON VAUCHER, B. RECH, D. FISCHER, S. DUBAIL, M. GOETZ, H. KEPPNER, C. BENEKING, O. HADJADJ, V. SHKLOVER and A. SHAH. *Controlled Nucleation of Thin Microcrystalline Layers for the Recombination Junction in a-Si Stacked Cells.* Solar Energy Materials and Solar Cells **49** 27 – 33 (1997).

[94] T. ROSCHEK. Diploma thesis, Forschungszentrum Jülich, to be published.

[95] R.S. FLÜCKIGER. *Microcrystalline Silicon Thin Films Deposited by VHF Plasmas for Solar Cell Applications.* Dissertation, Université de Neuchâtel, Switzerland (1994). ISBN 3-89191-965-4.

[96] S. WIEDER. *Zum Einfluß der intrinsischen Absorberschicht auf Eigenschaften und Stabilität von Solarzellen aus amorphem Silizium.* Diploma thesis, RWTH Aachen (1996).

[97] B. RECH, S. WIEDER, F. SIEBKE, C. BENEKING and H. WAGNER. *Material Basis of Highly Stable a-Si:H Solar Cells.* Material Research Society Symposium Proceedings **420** 33 – 38 (1996).

[98] M. NISHIKUNI, T. TAKAHAMA, S. OKAMOTO, K. NINOMIYA, H. NISHIWAKI, S. TSUDA, A. TAKEOKA, M. OHNISHI, S. NAKANO and Y. KUWANO. *Characteristics of a-Si Solar Cells Prepared by the Super Chamber at a High Substrate Temperature.* Progress in Photovoltaics: Research and Applications **2** 211 – 219 (1994).

[99] G. GANGULY and A. MATSUDA. *Defect Formation Process During Growth of Hydrogenated Amorphous Silicon at High Temperatures.* Japanese Journal of Applied Physics **31**(Part 2, 9A) L1269–L1271 (1991).

[100] T. TAKAHAMA, S. OKAMOTO, K. NINOMIYA, M. NISHIKUNI, N. NAKAMURA, S. TSUDA, M. OHNISHI, S. NAKANO and Y. KUWANO. *Application of High Temperature Deposition to a–Si:H Solar Cells.* In *Technical Digest of the International PVSEC–5*, p. 375 – 378, Kyoto (1990).

[101] Y. HISHIKAWA, M. SASAKI, S. TSUGE and S. TSUDA. *Effect of Heating SiH_4 on the Plasma Chemical Vapor Deposition of Hydrogenated Amorphous Silicon.* Japanese Journal of Applied Physics **33** 4373 – 4376 (1994). Part 1, No.7B.

[102] M. KAWASAKI, M. SUMIYA and H. KOINUMA. *Piezoelectric Effect on Plasma Chemical Vapor Deposition of Hydrogenated Amorphous Silicon Films.* Material Research Society Symposium Proceedings **297** 139 – 144 (1993).

[103] A. SUZUKI, Y. TOYOSHIMA, P.J. MCELHENY and A. MATSUDA. *In Situ Ultraviolet Laser Treatment during Plasma Deposition for the Improvement of Film Qualities in Hydrogenated Amorphous Silicon.* Japanese Journal of Applied Physics **30**(5A) L790 – L792 (1991).

[104] G. GANGULY and A. MATSUDA. *Defect Formation During Growth of Hydrogenated Amorphous Silicon.* Physical Review B **47**(7) 3661–3670 (1993).

[105] H. NISHIO, G. GANGULY and A. MATSUDA. *Reduction of the Defect Density in a–Si:H Deposited at $\leq$ 250 °C.* Material Research Society Symposium Proceedings **297** 91–96 (1993).

[106] S. RAY, S. HAZRA, A.R. MIDDYA and A.K. BARUA. *Low Bandgap a–Si:H Film with Better Stability Prepared by RF PECVD Method using Helium Dilution.* In *Proceedings of the 1st IEEE WCPEC*, p. 551–554, Hawaii (1994).

[107] Y. NAKAMURA, T. YAMAGUCHI and A. OKAGAWA. *Formation of a-Si:H Film by p–CVD Method with SiH_4–He Mixtures and its Opto–Electronic Properties.* Material Research Society Symposium Proceedings **377** 21–26 (1995).

[108] J.C. KNIGHTS, R.A. LUJAN, M.P. ROSENBLUM, R.A. STREET, D.K. BIEGLESEN and J.A. REIMER. *Effects of Inert Gas Dilution of Silane on Plasma–Deposited a–Si:H Films.* Applied Physics Letters **38**(5) 331–333 (1980).

[109] R. MEAUDRE, M. MEAUDRE, P. ROCA I CABARROCAS, S. TANIDI, Y. BOUZIEM and M.L. THEYE. *Absence of Thermal Quenching Effects in Undoped Amorphous Silicon Deposited by the PECVD of He-Diluted Silane.* Journal of Non-Crystalline Solids **137&138** 171–174 (1991).

[110] J.E. POTTS, E.M. PETERSON and J.A. MCMILLAN. *Effects of RF Power and Reactant Gas Pressure on Plasma on Plasma Deposited Amorphous Hydrogenated Silicon.* Journal of Applied Physics **52**(11) 6665–6672 (1981).

[111] K.C. PARK, T.G. KIM, S.K. KIM, S.C. KIM, M.H. HWANG, J.M. JUN and J. JANG. *Improved Amorphous Silicon Solar Cells Using RPCVD.* Material Research Society Symposium Proceedings **297** 767–778 (1993).

[112] A. MATSUDA. *Control of Plasma and Surface Conditions for Low Defect Density a–Si:H at High Growth Rates.* In *Proceedings of the* 25^{th} *IEEE PVSC*, p. 1029 – 1034, Washington (1996).

[113] H. SHIRAI, J. HANNA and I. SHIMIZU. *Very Stable a–Si:H Prepared by "Chemical Annealing".* Japanese Journal of Applied Physics **30**(5B) L881–L884 (1991).

[114] J.N. BULLOCK, K. RIM and S. WAGNER. *Hydrogen Content of a–Si:H and a–Si:H,F as a Function of Chemical Annealing.* Material Research Society Symposium Proceedings **297** 133–138 (1993).

[115] L. ZANZIG. *Einsatz alternativer Depositionsmethoden zur Herstellung amorpher Siliziumlegierungen.* Dissertation, TU Berlin (1995). Bericht des Forschungszentrums Jülich, ISSN 0944–2952.

[116] H. WAGNER and W. BEYER. *Reinterpretation of the Silicon–Hydrogen Stretch Frequencies in Amorphous Silicon.* Solid State Communications **48**(7) 585 – 587 (1983).

[117] W. BEYER. *Hydrogen Incorporation in Amorphous Silicon.* In *Tetrahedally–Bonded Amorphous Semiconductors*, D. Adler and H. Fritzsche (ed.), p. 129 – 146. Academic Press, New York (1985).

[118] R.V. KRUZELECKY, D. RACANSKY, S. ZUKOTYNSKI and J.P. PERZ. *Dependance of Optical Gap in a–Si:H on Bonded Hydrogen Concentration.* Journal of Non–Crystalline Solids **99** 89 – 96 (1988).

[119] M. GOETZ. *Solarzellen aus amorphem Silizium auf Aluminium: drei Wege, den Substrateinfluss zu beschreiben.* Dissertation, Université Neuchâtel, Switzerland (1997). Thèse N° 1637.

[120] B. RECH, S. WIEDER, C. BENEKING, A. LÖFFL, O. KLUTH, W. REETZ and H. WAGNER. *Texture Etched ZnO:Al Films as Front Contact and Back Reflector in Amorphous Silicon p-i-n and n-i-p Solar Cells.* In *Proceedings of the* 26^{th} *IEEE PVSEC*, p. 619 – 622, Anaheim (1997).

[121] S. WIEDER, B. RECH, O. KLUTH, O. VETTERL, W. REETZ, C. BENEKING and H. WAGNER. *Optimization of the i-p-TCO-Region in Amorphous Silicon n-i-p Solar Cells.* In *Proceedings of the* 2^{nd} *WCPEC*, p. 952 – 955, Vienna (1998).

[122] R. FLÜCKIGER, J. MEIER, A. SHAH, A. CATANA, M. BRUNEL, H.V. NGUYEN, R.W. COLLINS and R. CARIUS. *Structural, Optical and Electrical Properties of <p> μc-Si:H Very Thin Films Deposited by the VHF-GD Technique.* Material Research Society Symposium Proceedings **336** 511 – 516 (1994).

[123] S. HAMMA, P. ST'AHEL and P. ROCA I CABARROCAS. *Optimum Crystalline Fracion in p-(μc-Si:H) Layers for PIN Solar Cells: In-Situ Study by Ellipsometry and Kelvin Probe.* In *Proceedings of the* 2^{nd} *WCPEC*, p. 833 – 856, Vienna (1998).

[124] O. KLUTH, O. VETTERL, R. CARIUS, F. FINGER, S. WIEDER, B. RECH and H. WAGNER. *Investigations of Textured Back Reflectors for Microcrystalline Silicon Based Solar Cells.* Material Research Society Symposium Proceedings (1999). in print.

[125] F. KARG, H. CALWER, J. RIMMASCH, V. PROBST, W. RIEDL, W. STETTER, H. VOGT and M. LAMPERT. *Development of Stable Thin film Solar Modules Based on* $CuInSe_2$. In *Proceedings of the* 11^{th} *International Conference on Ternary and Multinary Compounds*, p. 909 – 913, Salford (1997).

[126] J. WENNERBERG, J. KESSLER, M. BODEGÅRD and L. STOLT. *Damp Heat Testing of High Performance CIGS Thin Film Solar Cells.* In *Proceedings of the* 2^{nd} *WCPEC*, p. 1161 – 1164, Vienna (1998).

[127] X. DENG, K.L. NARASIMHAN, J. EVANS, M. IZU and S. R. OVSHINSKY. *Dependence of a-Si Solar Cell* V_{oc} *on Deposition Temperature.* In *Proceedings of the* 1^{st} *WCPEC*, p. 678 – 681, Hawaii (1994).

[128] M. KUBON, N. SCHULTZ, M. KOLTER, C. BENEKING and H. WAGNER. *Modification of TCO–p Interface in a-Si:H Solar Cells by Intermediate Layers and Plasma Treatments.* In *Proceedings of the* 12^{th} *EC PVSEC*, p. 1268 – 1271, Amsterdam (1994).

[129] M. IZU, X. DENG, A. KRISKO, R. YOUNG, H.C. OVSHINSKY, K.L. NARASIMHAN and S.R. OVSHINSKY. *Manufacturing of Triple Junction 4* ft^2 *a-Si Alloy PV Modules.* In *Proceedings of the* 23^{rd} *IEEE PVSC*, p. 919 – 925, Louisville (1993).

[130] B. RECH and H. WAGNER. *Potential of Amorphous Silicon for Solar Cells.* Applied Physics A **69** 155 – 167 (1999).

[131] S. GUHA, J. YANG, A. BANERJEE and S. SUGIYAMA. *Material Issues in the Commerzialization of Amorphous Silicon Alloy Thin-Film Photovoltaic Technology.* Material Research Society Symposium Proceedings **507** 99 – 105 (1998).

Danksagung

Ich bedanke mich bei:

- Prof. Dr. phil. Heinrich Kurz für sein Interesse an dieser Arbeit sowie die Übernahme der Begutachtung.
- Prof. Dr. Ing. Rik W. De Doncker für die freundliche Bereitschaft zur Begutachtung.
- Dr. Claus Beneking für die Betreuung dieser Arbeit.

Desweiteren möchte ich mich an dieser Stelle bei allen Mitarbeitern der Abteilung Photovoltaik des Instituts für Schicht- und Ionentechnik bedanken, die zum Gelingen dieser Arbeit und zu der angenehmen Arbeitsatmosphäre beigetragen haben; erst dadurch hat mir die Arbeit so viel Spaß gemacht. Insbesondere bedanke ich mich bei:

- Prof. Heribert Wagner für die Möglichkeit, diese Arbeit in seiner Abteilung durchzuführen.
- Dr. Bernd Rech für sein unermüdliches Engagement und Interesse an dieser Arbeit. Seine ständige Bereitschaft für fachliche Ratschläge und Diskussionen haben mich immer sehr motiviert.
- Dipl.-Phys. Lothar Houben und Dr. Joachim Müller für das sorgfältige Korrekturlesen der Arbeit.

Selbstverständlich ist eine experimentelle Doktorarbeit nicht ohne die dauernde Hilfe der Kollegen im Bereich Meßtechnik und technische Unterstützung möglich; hierfür geht mein spezieller Dank an Wolfgang Appenzeller, Franz Birmans, Willi Hilgers, Resi Nieveler, Wilfried Reetz, Ralf Schmitz, Hilde Siekmann, Uwe Zastrow. Mein Danke gilt auch Andrea Mühlheims, die mir in Sachen Verwaltungsangelegenheiten immer weiterhelfen konnte.

Desweiteren möchte ich mich bei allen Menschen bedanken, die mich immer wieder daran erinnert haben, daß es außer Photovoltaik auch noch andere wichtige Dinge im Leben gibt.

Forschungszentrum Jülich

Jül-3721
December 1999
ISSN 0944-2952